AERODYNAMIC CHARACTERISTICS OF SCAFFOLDING WITH NONPOROUS CLADDING

A dissertation

Submitted to the Graduate School of Engineering of
Tokyo Polytechnic University in Partial Fulfillment
of the Requirements for the Degree of

Doctor of Philosophy

By
Feng Wang

Under the Supervision of
Prof. Yukio Tamura, Director

School of Architecture, Graduate School of Engineering
Tokyo Polytechnic University, Japan
September 2013

This Page Intentionally Left Blank

ACKNOWLEDGMENT

First of all, I would like to express my sincere gratitude to my supervisor, Prof. Yukio Tamura, who provided me the opportunity to study in Japan three years ago and continuous support, patience and encouragement during the last three years. Although he is always busy walking at the top of the world wind engineering field, his patience and considerate nature made him accessible whenever I needed his assistance. I was deeply moved because he served as not only an academic supervisor but also a mental mentor inspiring young generations.

I am grateful to Assoc. Prof. Akihito Yoshida for his support in conducting wind tunnel experiments during this study; I would like to thank Prof. Masahiro Matsui, Prof. Takeshi Ohkuma, Prof. Masaaki Ohba and Prof. Ryuichiro Yoshie for their suggestions and comments for improving this dissertation.

Special thanks go out to Dr. Rei Okada and Ms. Nozomi Kodama for help in conducting wind tunnel experiments. Thank my colleagues, GCOE researchers and students at Wind Engineering Research Center of Tokyo Polytechnic University, for the cooperation during research, for their help in everyday work and friendship, and GCOE secretaries Ms. Aya Saito and Ms. Kazuko Ando for their kind help and assistance.

Last but not least, I would like to thank my parents and my sister who gave their love and support throughout my life.

The financial support, provided by the Ministry of Education, Culture, Sports, Science and Technology, Japan, through the Global Center of Excellence Program, 2008-2012, is gratefully acknowledged.

Feng Wang

September, 2013

ABSTRACT

Safety is the most important issue in civil engineering construction. Cladding may cause severe wind loads acting on scaffolding, especially when it is nonporous. Existing design recommendations provide limited information on wind loads for scaffolding. This study aims to investigate aerodynamic characteristics on clad scaffolding.

From the literature, scaffolding geometries and building openings may have significant effects on wind loads acting on clad scaffolding. Wind tunnel experiments were carried out based on a prototype of scaffolding with nonporous cladding. A medium height building with rectangular cross-section was selected as the principal building. Practical building openings and scaffolding geometries were considered. Various wind directions were tested. A systematic study on wind load characteristics on clad scaffolding was conducted. Wind loads on structures in real environments can be quite different from those measured on isolated structures in wind tunnels. Previous research only focused on scaffolding for an isolated building. However, this paper studies interference effects of neighboring building on aerodynamics of clad scaffolding. Parameters of neighboring building location, neighboring building height ratio and principal building opening ratio were investigated.

Local peak pressures acting on scaffolding and unfavorable wind directions for the largest local peak pressures were studied. Most design recommendations provide an aerodynamic force coefficient or wind force coefficient for scaffolding for wind load calculation. Mean panel force coefficients were determined based on experimental data. Comparisons were made with current related design recommendations. Tie members

mainly contribute to the horizontal stability of scaffolding and prevent scaffolding from collapse. The tensile forces in tie members induced by wind loads imperil the horizontal stability of scaffolding. Wind loads acting on scaffolding tie members were calculated. In order to supply designers and engineers with more information on wind loads acting on scaffolding, wind-resistant design considerations for scaffolding are proposed.

TABLE OF CONTENTS

LIST OF FIGURES

LIST OF TABLES

NOMENCLATURE

z	Height
z_{ref}	Reference height
α	Power law exponent
Φ_B	Building opening ratio
θ	Wind direction
$C_{p\text{-}outer}$	Wind direction
$C_{p\text{-}inner}$	Wind pressure coefficient on the outer surface of scaffolding
$C_{p\text{-}inner}$	Wind pressure coefficient on the inner surface of scaffolding
P_0	Static reference pressure
ρ	Air density
U_H	Mean longitudinal wind speed at the reference height
$C_{p\text{-}net}$	Wind net pressure coefficient
τ	Averaging time
L	The length of the diagonal for a typical door-type tubular steel scaffold unit
$\hat{C}_{p-net}$	Peak net pressure coefficient
$U_{\hat{C}_{p-net}}$	Mode of the extreme distribution of net pressure coefficient
$a_{\hat{C}_{p-net}}$	Dispersion of the extreme distribution of net pressure coefficient
a_k	BLUE coefficient
b_k	BLUE coefficient
$C_{p\text{-}netk}$	The kth value of the ascending array of maximum values of 10 samples of peak net pressures
$\hat{C}_{p-net}(i,\theta,\Phi_B)$	Positive local peak net pressure coefficient at measurement point i, along wind direction θ, and with building opening ratio Φ_B.
$\check{C}_{p-net}(i,\theta,\Phi_B)$	Negative local peak net pressure coefficient at measurement point i, along wind direction θ, and with building opening ratio Φ_B.

$\hat{C}_{p-net}(i,\Phi_B)$	Largest positive local peak net pressure coefficient at measurement point *i* with building opening ratio Φ_B, and for all wind directions.
$\check{C}_{p-net}(i,\Phi_B)$	Largest negative local peak net pressure coefficient at measurement point *i* with building opening ratio Φ_B, and for all wind directions.
$\hat{C}_{p-net}(\theta,\Phi_B)$	Largest positive local peak net pressure coefficient along wind direction θ, with building opening ratio Φ_B, and for all measurement points.
$\check{C}_{p-net}(\theta,\Phi_B)$	Largest negative local peak net pressure coefficient along wind direction θ, with building opening ratio Φ_B, and for all measurement points.
$\hat{C}_{p-net}(\Phi_B)$	Largest positive local peak net pressure coefficient with building opening ratio Φ_B, for all measurement points and all wind directions.
$\check{C}_{p-net}(\Phi_B)$	Largest negative local peak net pressure coefficient with building opening ratio Φ_B, for all measurement points and all wind directions.
$\hat{C}_{p-net}$	Largest positive local peak net pressure coefficient for all building opening ratios, all measurement points and all wind directions.
$\check{C}_{p-net}$	Largest negative local peak net pressure coefficient for all building opening ratios, all measurement points and all wind directions.
$\overline{C}_f(\theta,\Phi_B)$	Mean panel force coefficient along wind direction θ with building opening ratio.
$\overline{C}_{f,max}(\Phi_B)$	Largest positive mean panel force coefficient with building opening ratio Φ_B for all wind directions.
$\overline{C}_{f,min}(\Phi_B)$	Largest negative mean panel force coefficient with building opening ratio Φ_B for all wind directions.
$\overline{C}_{f,max}$	Largest positive mean panel force coefficient for all wind directions and all building opening ratios.
$\overline{C}_{f,min}$	Largest negative mean panel force coefficient for all wind directions and all building opening ratios.
$\overline{C}_{ft,max}$	Largest positive area-averaged force coefficient for top zone for all wind directions and all building opening ratios.
$\overline{C}_{ft,min}$	Largest negative area-averaged force coefficient for top zone for all wind directions and all building opening ratios.

$\overline{C}_{fs,max}$	Largest positive area-averaged force coefficient for side zone for all wind directions and all building opening ratios.
$\overline{C}_{fs,min}$	Largest negative area-averaged force coefficient for side zone for all wind directions and all building opening ratios.
$\overline{C}_{fm,max}$	Largest positive area-averaged force coefficient for middle zone for all wind directions and all building opening ratios.
$\overline{C}_{fm,min}$	Largest negative area-averaged force coefficient for middle zone for all wind directions and all building opening ratios.
D	Building depth
B	Building breadth
Hr	Neighboring building height ratio
$p_i(t)$	Wind pressure time history
A_i	A finite area
$F(t)$	Wind force time history
$\hat{F}(\Phi_B)$	Largest peak tensile force with building opening ratio Φ_B for all wind directions.
$\hat{F}$	Largest peak tensile force for all wind directions and all building opening ratios.
IF	Interference factor
W	Equivalent static wind load
G	Gust loading factor
q_H	Velocity pressure at a reference height H
A	Reference area

CHAPTER I : INTRODUCTION

1.1 Background

Scaffolding is a temporary structure used to support people and material during construction or maintenance of buildings and other large structures. It provides a safe work place with safe access suitable for the work being done. Such temporary support systems are widely used because they are economical, convenient and have a wide range of adaptability.

Safety is the most important issue in civil engineering construction. Ohdo (1999, 2002, 2005) investigated scaffolding collapse accidents and found that about 10% of severe collapse accidents were due to wind. Thus, wind loads on scaffolding have become an important issue in scaffolding design. For safety, and environmental and noise considerations, clad scaffolding is becoming more commonly used, thus increasing the solidity ratio, leading to larger wind loads on the scaffolding.

In general, the lifetime of a structure can be divided into three phases: the construction period; the period of normal use; and the period of wear-out and repair. Engineers are accustomed to designing the structure for the period of normal use corresponding to the service-life of the facility. Considerable efforts have focused on design for safety and performance during this period. However, relatively few design documents exist pertaining specifically to the construction period, during which there exists a significant amount of uncertainty. None has been focused on the wear-out and

repair period (J. L. Peng, 1996).

Source:
http://www.geograph.org.uk/photo/1673878
http://www.yomiuri.co.jp/feature/graph/201012wind/garticle.htm?ge=863&gr=3122&id=94211
http://www.jiaodong.net/news/system/2011/07/16/011339933.shtml
http://www.zj.xinhuanet.com/newscenter/2007-01/23/content_8958363.htm

Fig. 1.1 Scaffolding collapse accidents.

Scaffolding as temporary structural system, its importance is often overlooked by design engineers. Furthermore, existing design standards and recommendations provide limited assistance to engineers for the design of temporary structure systems during construction. Designers also have little information describing the actual cases of wind induced scaffolding collapse. Often, construction engineers rely on their own experience in view of the lack of guidelines. The collapse of scaffolding not only leads to work delays and property loss, but has also been responsible for numerous worker

injuries and deaths.

1.2 Literature survey on wind loads on scaffolding

1.2.1 Field measurements

Ohdo (2005) investigated transferred forces in ties from field measurement. The loads acting on the ties due to strong wind varied and concentrated on only some specific ties, especially the ties at the upper part of the scaffolds in this experiment. Furthermore, from the results, the measured values were higher than the design values on some ties. Therefore, it can be concluded that the design load acting on the ties should be increased or the allowable strength of the ties should be decreased in the design stage for the scaffolds to the wind loads.

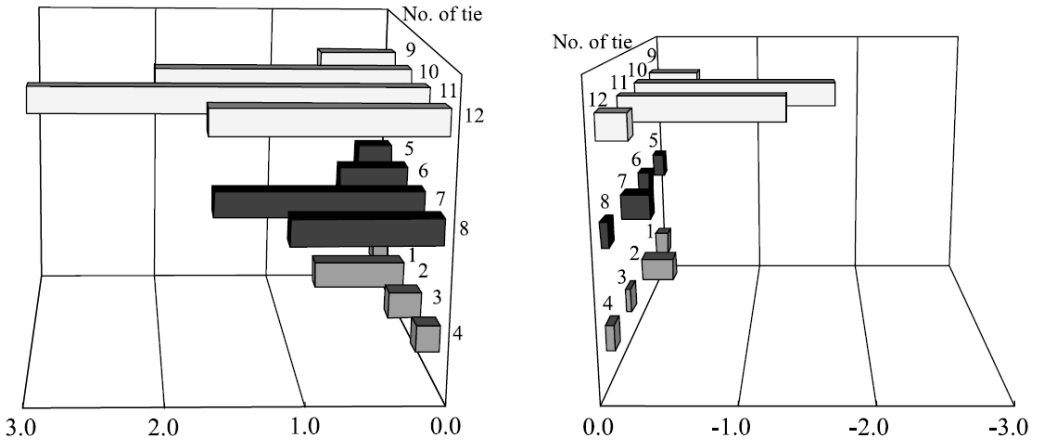

Fig. 1.2 Distribution of wind loads acting on the ties obtained from the measurement of Ohdo's study.

1.2.2 Wind tunnel experiments

Yue et al (2001, 2004, 2005) conducted wind tunnel experiments in which a practical design of typical integral-lift scaffolding was taken as a prototype. Four building opening ratios and thirteen scaffolding solidity ratios were tested. The wind loads on the scaffolding were measured by a five-component strain scale. The results

showed that the drag force coefficient of scaffolding increased almost linearly with increase in scaffolding solidity ratio, as shown in Fig. 1.3. For the same condition, the greatest wind loads acting on the scaffolding occurred when the wall opening ratio of the building structure was the largest. However, only one scaffolding geometry with scaffolding completely enclosing the principal building was tested.

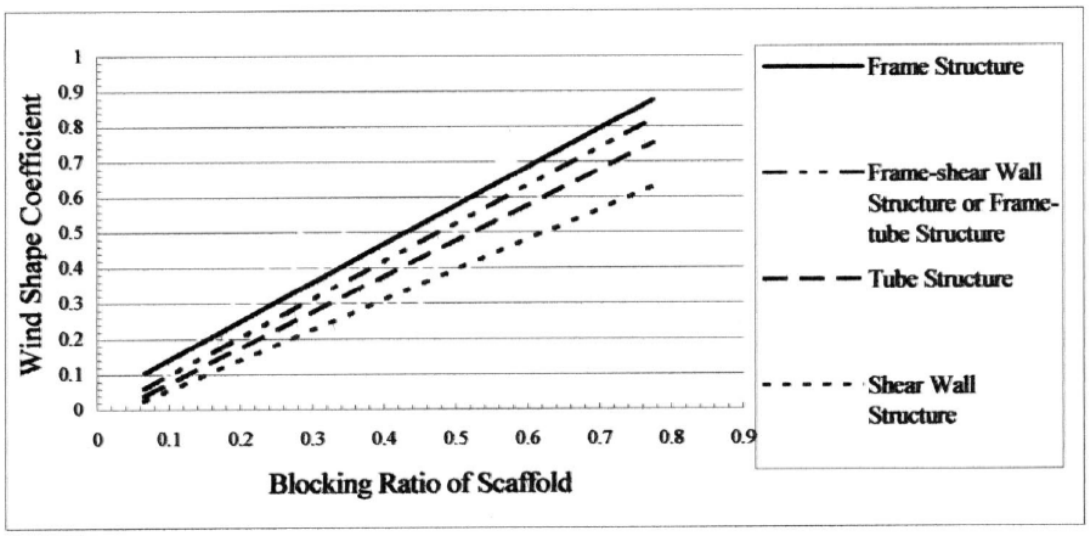

Fig. 1.3 Suggested shape coefficient of wind loading of scaffolds for use of Yue's study.

Cladding increases wind loads on scaffolding, and nonporous cladding increases them the most. It is very difficult to maintain the stiffness of scaled scaffolding pipes. It is also very difficult to fix pressure taps on scaled scaffolding tubes and on cladding. Some researchers have studied wind pressures on nonporous clad scaffolding by using very thin panel models on which it was easier to fix pressure taps. Charuvisit et al (2002, 2007) studied the characteristics of wind pressure on clad scaffolding. Five different scaffolding geometries were considered, but building openings were not considered. The magnitude of the maximum wind pressure coefficient was found to be larger when the scaffolding width was smaller. Besides, wind pressures on the principal scaffolding were significantly affected by scaffolding arranged along another building side.

Hino et al (2002, 2005) carried out a series of wind tunnel experiments on a prototype of a square section building for four building openings and four scaffolding

geometries. The fundamental characteristics of wind pressures acting on scaffolding were investigated. When wind flowed into the gap between the scaffolding and the building surface, wind pressures on the inner surface of the scaffolding increased. In most cases, the wind pressures on the outer surface of the scaffolding were not greatly affected by the building openings.

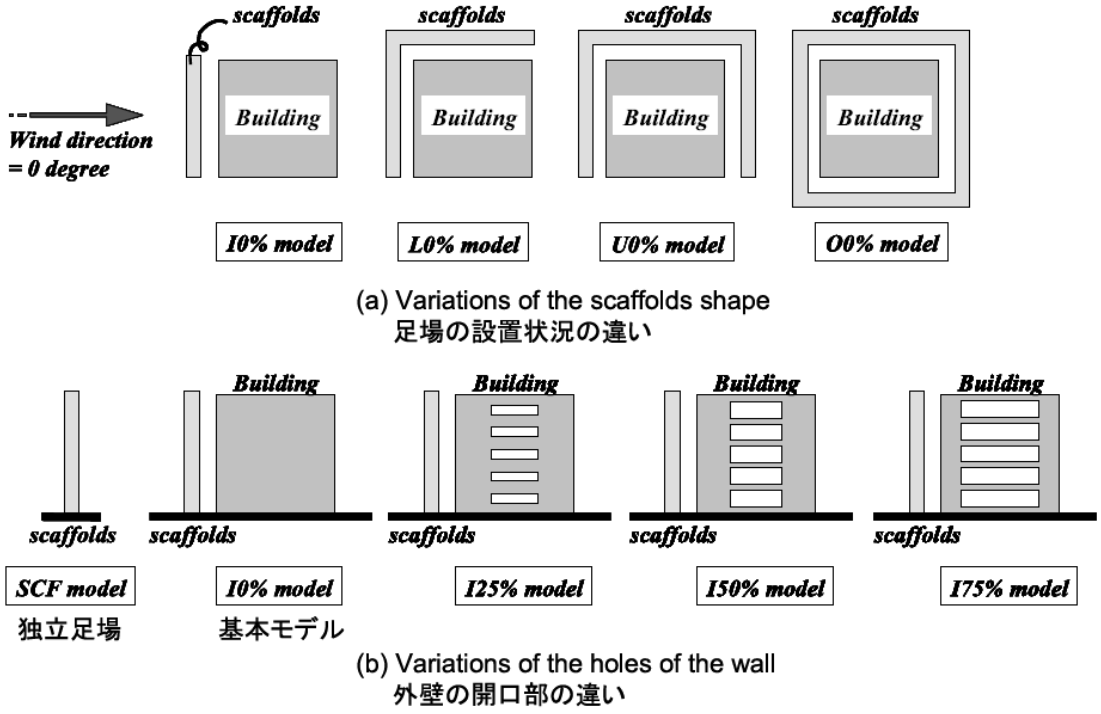

Fig. 1.4 Experimental models of Hino's study.

Irtaza et al (2012) investigated models of sheet-clad and elevated sheet-clad scaffolding surrounding a cubic building. Experimental data and code recommendations were compared. Irtaza concluded that the Eurocode provisions for sheet-clad scaffolding were appropriate for the pressure coefficients on the windward and side faces, but recommended that the leeward side be designed to have a pressure coefficient of 0.25.

1.2.3 Current related design recommendations

In most wind load recommendations, wind loads on scaffolding are calculated by

an equation including three main components: velocity pressure, reference area and mean wind force coefficient.

For clad scaffolding, BS EN 12811 (British Standards Institution, 2003) states that the aerodynamic force coefficient for the cladding shall be assumed as 1.3 and 0.1 for perpendicular direction and parallel direction, respectively. However, this method may not be applied to scaffolding that completely encloses a building.

JGJ 128 (The Ministry of Construction of People's Republic of China, 2000) uses the shape coefficient of wind load to represent aerodynamic force coefficient. For clad scaffolding, JGJ 128 provides a shape coefficient of wind load by considering a solidity ratio of cladding and principal building openings. If the principal building has wall openings, the shape coefficient of wind load shall be 1.3φ, where φ is the solidity ratio of the scaffolding. If the principal building does not have openings, the shape coefficient of wind load shall be 1.0φ.

SCEA recommendations (Scaffolding and Construction Equipment Association of Japan, 1999) suggests a shape compensation factor and a position compensation factor for mean wind force coefficient for clad scaffolding. The shape compensation factor is related to the aspect ratio of the cladding, and distinguishes between elevated scaffolding and scaffolding on the ground. The position compensation factor supplies positive and negative factors for positive and negative wind loads. Scaffolding is divided into three main zones: top two-storey scaffolds, side two-bay scaffolds and middle part, each zone having a different position compensation factor. Furthermore, the position compensation factor for side zone is distinguished by whether or not it is connected to adjacent side scaffolding.

1.3 Literature survey on interference effects on wind loads

Past research on wind loads acting on scaffolding have mainly focused on the

isolated building condition. However, wind loads on structures in real environments can be quite different from those measured on isolated structures in wind tunnels. Surroundings can significantly increase or decrease the wind forces on the interfered structures. Orlando (2001) carried out wind tunnel experiments on a rigid model of two adjacent cooling towers. Pressures measured on the two towers were compared with those registered on an isolated tower. Gu and Xie (2007) studied base-bending moment (BBM) response and the mean BBM of grouped high-rise buildings by a series of wind tunnel tests on typical tall building models using the high-frequency force balance technique. Lam et al (2008) investigated interference effects on a row of square-plan tall buildings arranged in close proximity. Wind forces and moments on each building in the row are measured with the base balance under different wind incidence angles and different separation distances between buildings. Kim et al (2011) and Hui et al (2012) discussed interference effects on local peak pressures on a principal building with various configurations and different height ratios of a neighboring building. Interference factor was defined and discussed. The largest interference factor is greater than 1.5 for some cases, which means the absolute value of the largest negative peak pressure coefficient becomes 50% higher than the design value of the isolated building situation. Many studies have been done on interference effects on wind loads on buildings and other structures, which showed that a neighboring building may cause significant interference effects under some conditions.

1.4 Research scope, objectives and contents

This study aims to investigate aerodynamic characteristics on clad scaffolding. As described in the literature, clad scaffolding may suffer more severe wind loads because of the cladding, especially when it is nonporous. Scaffolding geometries and building openings may have significant effects on wind loads acting on clad scaffolding. In this

study, wind tunnel experiments were carried out based on a prototype of nonporous sheet-clad scaffolding. A medium height building with rectangular cross-section was selected as the principal building. Practical building openings and scaffolding geometries were considered. A systemic study on wind loads on clad scaffolding was conducted. Effects of building openings, scaffolding geometries and wind directions are presented, and the experimental data are compared with relevant current design recommendations.

Many studies have been done on interference effects on wind loads on buildings and other structures, which showed that a neighboring building may cause significant interference effects under some conditions. Interference effects of neighboring building on wind loads on scaffolding are also investigated in this study. Effects of neighboring building locations, neighboring building height ratios and principal building opening ratios are discussed. It is the first time to study interference effects on wind loads on scaffolding.

Tie member is the one of the most important components of scaffolding. Tie members are mainly contributing to the horizontal stability of scaffolding and preventing scaffolding from collapse. Wind loads acting on tie members imperil the horizontal stability of scaffolding strongly. The failure of tie member may cause severe casualties and losses. Wind loads acting on scaffolding tie members are calculated by a pressure integration method. Effects of scaffolding geometry, building openings and turbulence intensity on tie forces are studied. Interference effects of neighboring building on wind loads acting on tie members are also discussed. Interference factor is adopted to indicate the intensity of interference effect on the largest peak tensile force acting on tie members.

This study is going to supply designers and engineers with more information on wind loads acting on scaffolding. Therefore, equivalent static wind loads for

scaffolding are proposed. Fig. 1.4 shows the framework of the study.

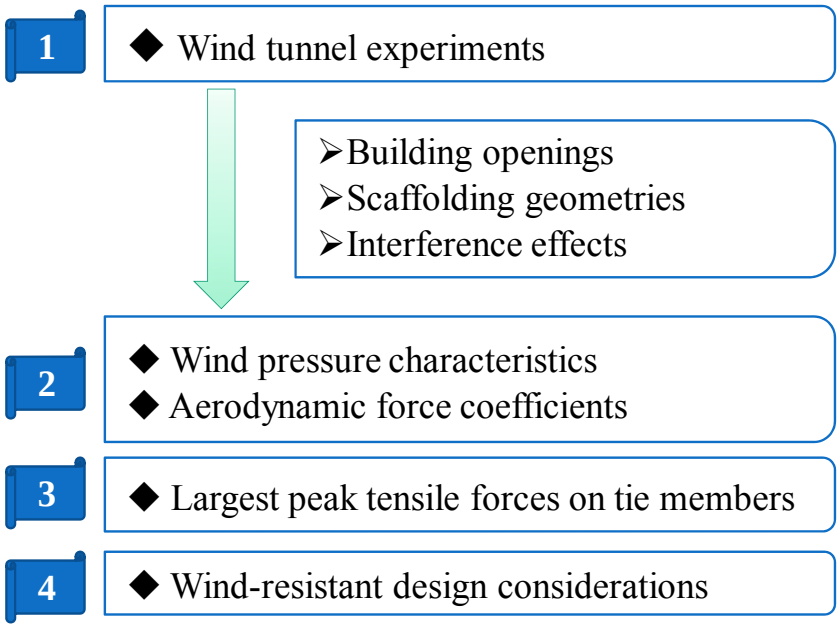

Fig. 1.5 Framework of the study.

The thesis consists of eight chapters as following:

Chapter I Introduction

Chapter II Effects of building openings on wind loads on scaffolding

Chapter III Effects of scaffolding geometries on wind loads on scaffolding

Chapter IV Interference Effects of neighboring building on wind loads on scaffolding

Chapter V Peak tensile forces in tie members

Chapter VI Interference effects of neighboring building on peak tensile forces in tie members

Chapter VII Wind-resistant design recommendations

Chapter VIII Conclusions

CHAPTER II : EFFECTS OF BUILDING OPENINGS ON WIND LOADS ON SCAFFOLDING

For different structural types and different construction sequences, buildings have different kinds of wall openings during construction stages, which may affect wind loads on scaffolding. Yue et al (2005) conducted wind tunnel experiments in which a practical design of typical integral-lift scaffolding was taken as a prototype. Four building opening ratios were tested. The wind loads on the scaffolding were measured by a five-component strain scale. The results showed that the greatest wind loads acting on the scaffolding occurred when the wall opening ratio of the building structure was the largest. Hino et al (2005) carried out a series of wind tunnel experiments on a prototype of a square section building for four building openings and four scaffolding geometries. In most cases, the wind pressures on the outer surface of the scaffolding were not greatly affected by the building openings. However, there was only one hole on each side in each floor of the building model to simulate the openings, which was not very similar to real buildings. Thus, the influence of building opening ratios should be considered in the design stage when estimating wind loads acting on scaffolding.

In this chapter, effects of building openings on wind loads on scaffolding were studied. Partial covered buildings were also investigated.

2.1 Experimental setup

2.1.1 Wind speed and turbulent intensity profiles

Wind tunnel experiments were carried out in a Boundary Layer Wind Tunnel in Tokyo Polytechnic University, Japan. The test section was 2.2m wide and 1.8m high. The atmospheric boundary layer was simulated as a geometrical scale of 1:75. Two kinds of terrain characteristics were simulated and same velocity scale of 1:2.5 was adopted. The power law exponents α of mean wind speed were 0.2 and 0.27 (AIJ 2004 category 3 and 4), which represent residential area and urban area, respectively. The mean wind speeds at the reference height z_{ref} (top of the principal building which is 318mm above the bottom of the tunnel) were the same around 8.6m/s, the corresponding turbulence intensity were approximately 21% and 29%, as shown in Fig.2.1.

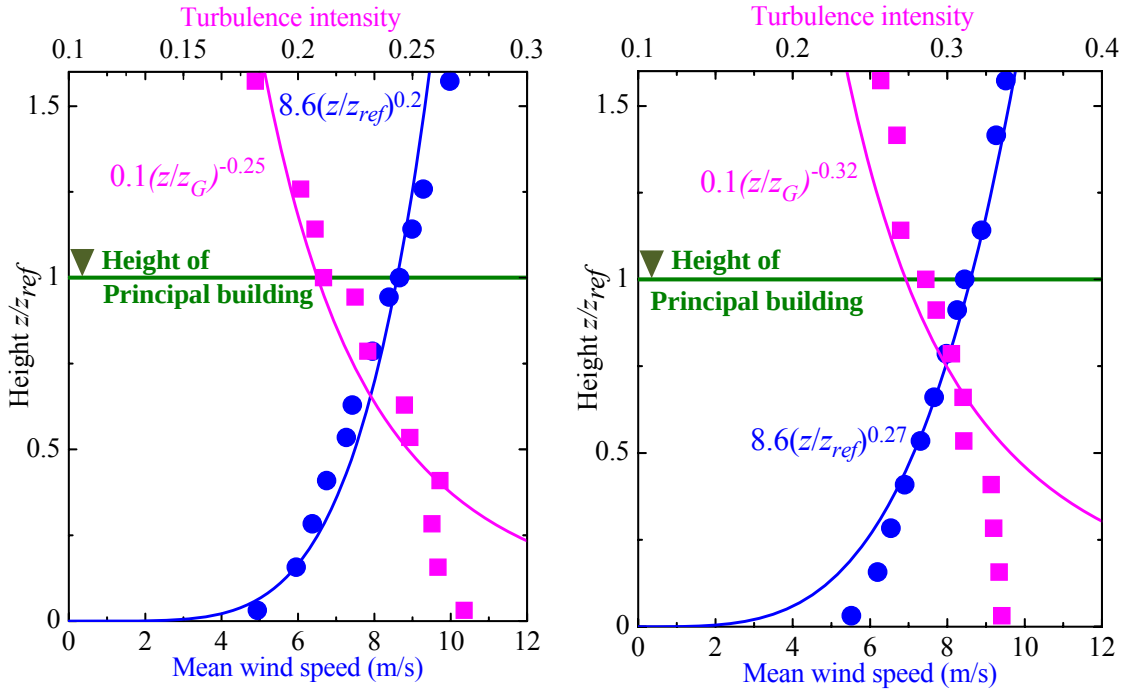

(a) AIJ 2004 category 3 (α=0.2) (b) AIJ 2004 category 4 (α=0.27)

Fig. 2.1 Mean wind speed and turbulence intensity profile.

2.1.2 Experimental models

The prototype dimensions of the building were 19.2m×12m in plan and 23.8m in height. The building comprised seven stories 3.4m high. The scaffolding was assembled by using typical door-type tubular-steel scaffold units 1.7m high, 0.9m wide and 1.8m in span (one-bay). The prototype scaffolding was 27.2m high, and comprised sixteen stories. The scaffolding was 3.4m (two-stories) higher than the principal building. The distance between the building surface and the cladding of scaffolding was 1.2m in full scale. There were four scaffolding models for the four sides of the principal building. Two were pressure-measured models and the other two were dummy models. Nonporous acryl models 5mm thick were made to simulate the nonporous clad scaffolding (scaffolding pipes were ignored). Pressure taps were fixed symmetrically on both the outer and inner surfaces of the scaffolding models. 188 pressure taps were fixed on scaffolding model L, which was arranged along the long side of the building. 116 pressure taps were fixed on scaffolding model S, which was arranged along the short side of the building, as shown in Fig. 2.2. In this study, twelve scaffolding geometries were tested, and there was only one measured scaffolding model for each geometry, as shown in Fig. 2.3. The last letters of the geometry definitions stand for the measured model.

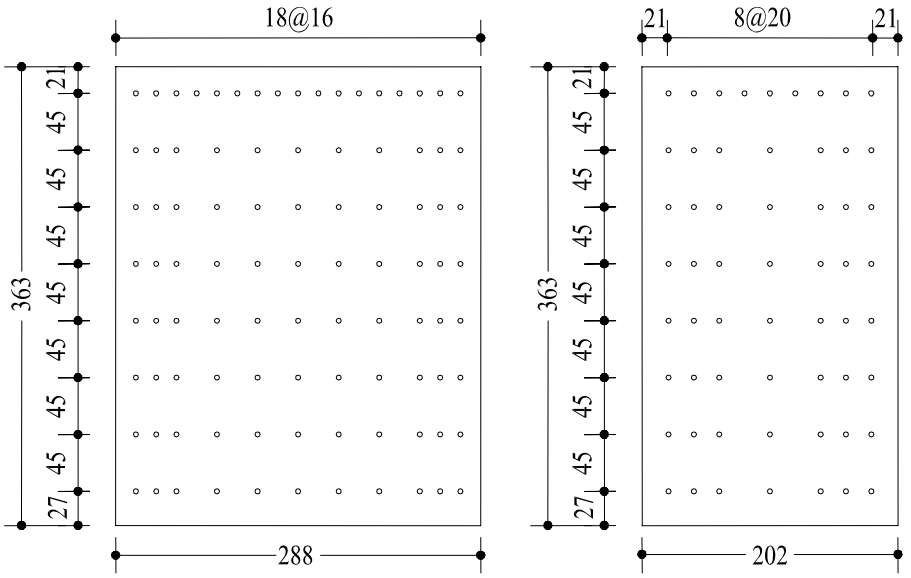

(a) Model L (b) Model S.

Fig. 2.2 Pressure tap positions on measured scaffolding models (unit: mm).

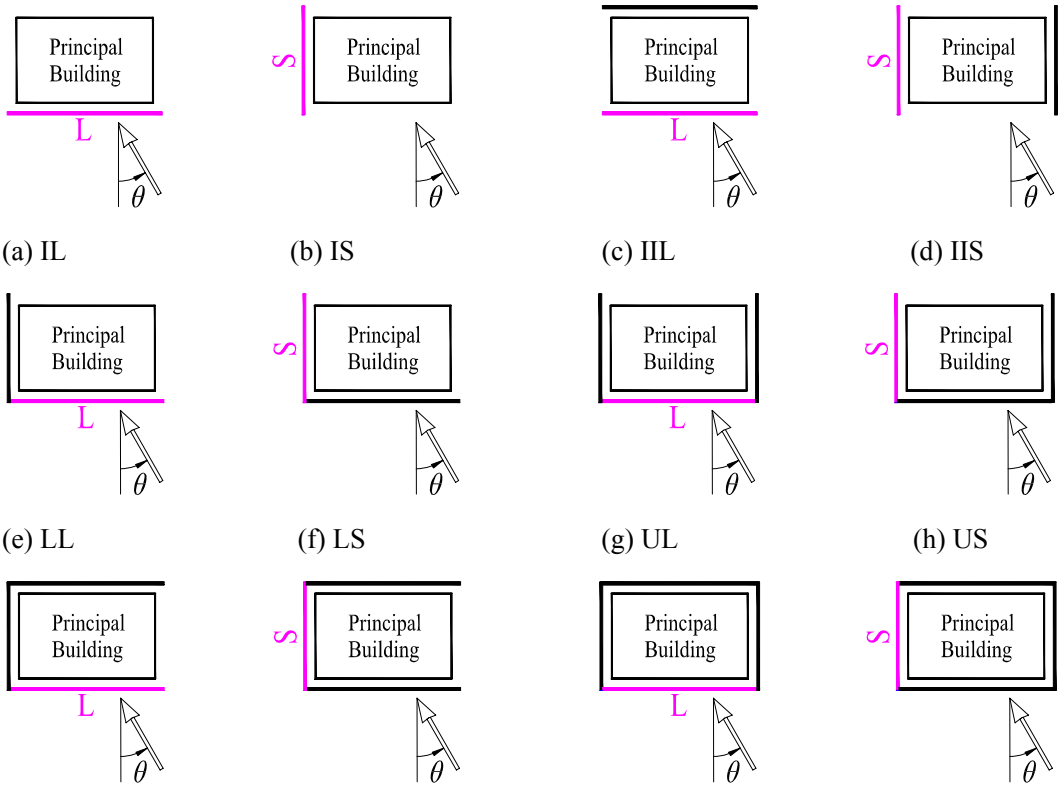

(a) IL (b) IS (c) IIL (d) IIS

(e) LL (f) LS (g) UL (h) US

(i) CL (j) CS (k) OL (l) OS

Fig. 2.3 Definitions for angle and scaffolding geometries (top view).

The experimental principal buildings were made from organic glass. To simulate the internal wind environment of the building under construction, floor slabs and pillars

were considered, and each floor slab had a hole as the stairwell. All the building models had the same height, breadth and depth.

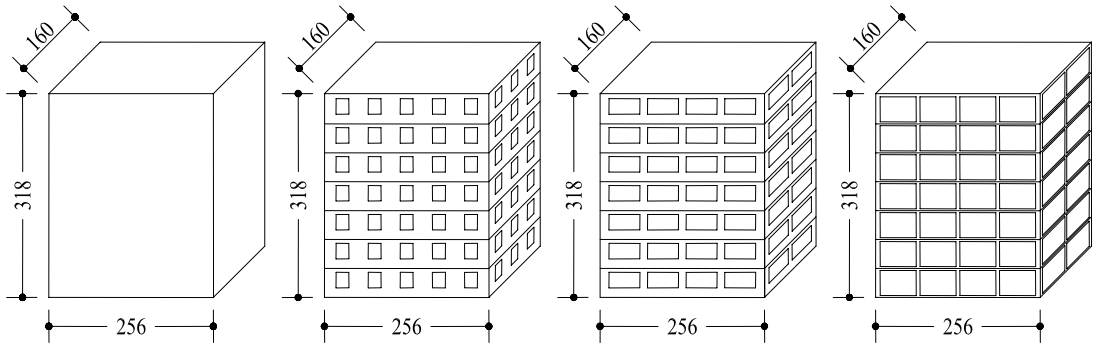

(a) Building opening ratio (Φ_B) 0% (b) Building opening ratio (Φ_B) 20% (c) Building opening ratio (Φ_B) 40% (d) Building opening ratio (Φ_B) 80%

Fig. 2.4 Building models with uniform opening ratio (unit: mm).

There were two kinds of opened building models in this study: uniform opened building and partial covered building. Building opening ratios for the uniform opened building (Φ_B) were 0%, 20%, 40%, 80%, as shown in Fig 2.4.

Five partial covered building models were investigated in this study, the dimensions of the building models were the same, as Fig. 2.5 shown. 7/7 covered building model was the building seven floors totally covered, and same as the building model whose opening ratio was 0%. Namely, 0/7 covered building is corresponding to building opening ratio 80%. Thus, 1/7 covered, 3/7 covered and 5/7 covered buildings represent two seventh, four seventh and six seventh floors covered.

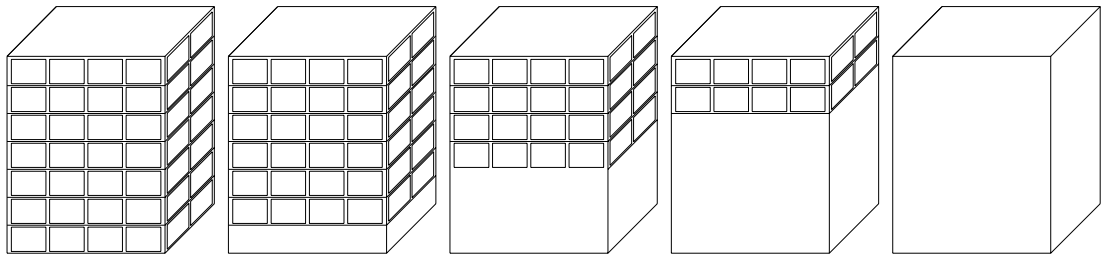

(a)0/7 coverage (b)1/7 coverage (c)3/7 coverage (d)5/7 coverage (e)7/7 coverage

Fig. 2.5 Partial coverage ratio of buildings.

Wind tunnel setup and experimental models are shown in Fig.2.6.

(a) Geometry UL, building opening ratio 40% (b) Geometry IL, 3/7 coverage

Fig. 2.6 Wind tunnel setup and models in experiments.

2.1.3 Experimental arrangements and procedure

Pressure coefficients were obtained at a sampling frequency of 781Hz using a multi-channel simultaneous-scanning pressure measurement system. For each case, ten 20s-long samples were collected, which corresponded to 26Hz and ten 10min-long samples in full scale. Wind direction (θ) was changed at intervals of 5° for each case. The tubing effects were compensated by the gain and phase-shift characteristics of the pressure measuring system (Irwin et al., 1979). Table 1 shows the experimental cases.

Table 2.1 Experimental cases

(1) AIJ 2004 category 3 (α=0.2)		
Scaffolding geometry	Building openings	Wind direction
IL IILLL UL CL OL IS IIS LS US CS OS	Building opening ratio (Φ_B) 0%, 20%, 40%, 80%	0°~360° (interval 5 º)
IL LL	Partial coverage ratio: 0/7, 1/7, 3/7, 5/7, 7/7	0°~360°(interval 15 º)
(2) AIJ 2004 category 4 (α=0.27)		
Scaffolding geometry	Building openings	Wind direction
IL IIL LL OL IS IIS LS OS	Building opening ratio (Φ_B) 0% ,80%	0°~360°(interval 15 º)

2.2 Data processing method

Wind pressures on the models are expressed in the form of a non-dimensional pressure coefficient, defined as:

$$C_{p\text{-}outer}(i,t)=\frac{P_{outer}(i,t)-P_0}{0.5\rho U_H^2} \qquad C_{p\text{-}inner}=\frac{P_{inner}(i,t)-P_0}{0.5\rho U_H^2} \tag{2.1}$$

where $C_{p\text{-}outer}(i,t)$ and $C_{p\text{-}inner}(i,t)$ are the wind pressure coefficients at tap i and time t on the outer and inner surfaces of the models, respectively, P_0 is the static reference pressure, U_H is the mean longitudinal wind speed at the reference height (model top) and ρ is air density. Wind net pressure coefficient:

$$C_{p\text{-}net}(i,t)=C_{p\text{-}outer}(i,t)-C_{p\text{-}inner}(i,t) \tag{2.2}$$

The positive wind net pressure coefficient direction is from the outer surface to the inner surface, namely, from the scaffolding toward the building.

An "Equivalent time averaging" method was used to determine the wind load acting on a finite area from point pressure. With this approach, the times from point pressures were filtered by means of a moving average filter (Holmes, 1997). The equivalent time was calculated as:

$$\tau=1.0\times L/U_H \tag{2.3}$$

where τ is averaging time and L is the length of the diagonal for a typical door-type tubular steel scaffold unit of principal scaffolding in full scale. The dimensions of a scaffold unit were 1.7m×1.8m in windward, making L = 2.5m. In this study, 0.0039s corresponding to 0.12s in full scale was used for time averaging. The peak net pressure coefficients were calculated by the "Cook-Mayne method" (Cook and Mayne, 1979) using the equation:

$$\hat{C}_{p\text{-}net}=U_{\hat{C}_{p\text{-}net}}+1.4/a_{\hat{C}_{p\text{-}net}} \tag{2.4}$$

where $U_{\hat{C}_{p\text{-}net}}$ and $1/a_{\hat{C}_{p\text{-}net}}$ are the mode and dispersion of the extreme distribution

of net pressure coefficients, respectively, which can be calculated by the Best Linear Unbiased Estimators (BLUE) as:

$$U_{\hat{C}_{p\text{-}net}} = \sum_{k=1}^{10} a_k \hat{C}_{p\text{-}netk} \qquad 1/a_{\hat{C}_{p\text{-}net}} = \sum_{k=1}^{10} b_k \hat{C}_{p\text{-}netk} \tag{2.5}$$

where, $\hat{C}_{p\text{-}netk}$ is the kth value of the ascending array of maximum values of 10 samples of peak net pressures and a_k and b_k are the BLUE coefficients.

2.3 Results and discussions

2.3.1 Mean pressure coefficient distribution

2.3.1.1 Uniform building opening ratio for entire building

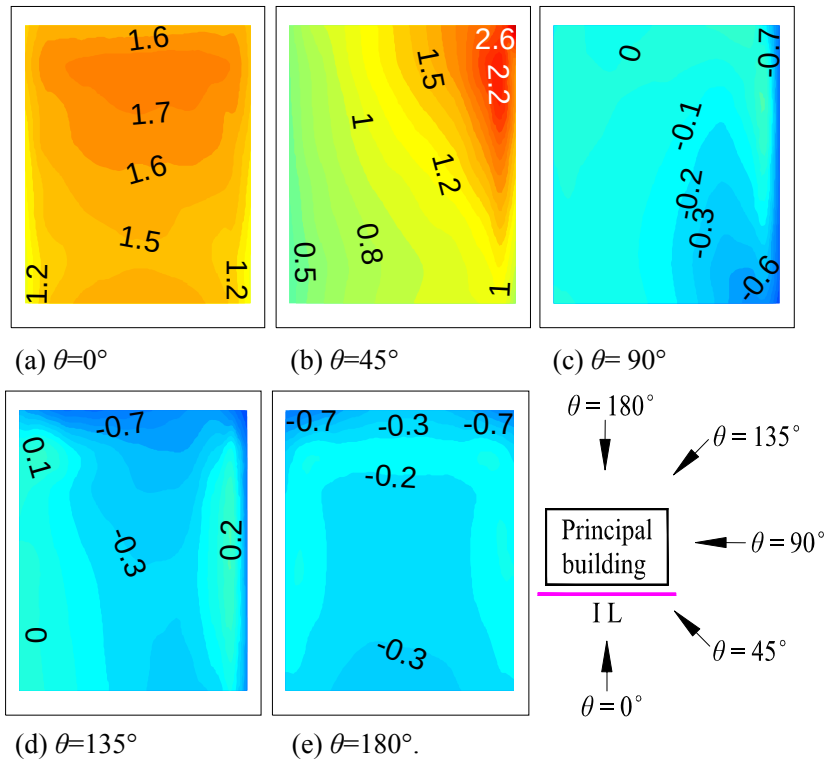

(a) θ=0° (b) θ=45° (c) θ= 90°

(d) θ=135° (e) θ=180°.

Fig. 2.7 Mean net pressure coefficient distributions for different wind directions, geometry IL, building opening ratio 0%.

Fig. 2.7 shows the mean net pressure coefficient distributions on scaffolding for geometry IL for different wind directions. When wind direction is 45°, the largest positive net pressure coefficient among all wind directions is found, which is at the top corner of the scaffolding model. For wind directions 90°, 135° and 180°, the net

pressure coefficients are negative due to the effect of the principal building.

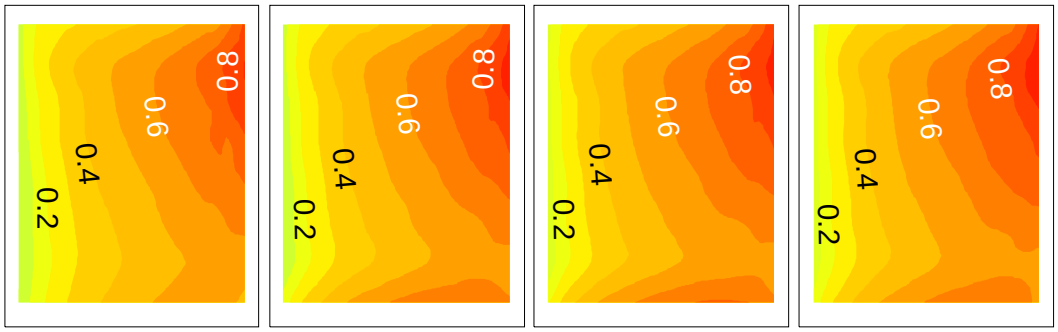

(a) Outer surface, building opening ratio 0%

(b) Outer surface, building opening ratio 20%

(c) Outer surface, building opening ratio 40%

(d) Outer surface, building opening ratio 80%

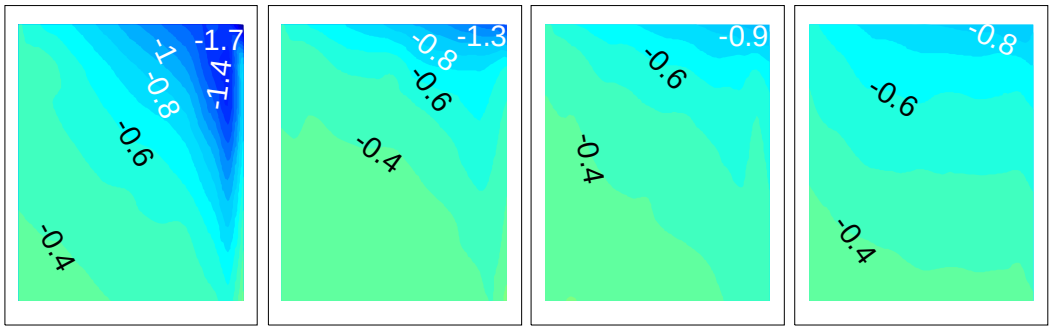

(e) Inner surface, building opening ratio 0%

(f) Inner surface, building opening ratio 20%

(g) Inner surface, building opening ratio 40%

(h) Inner surface, building opening ratio 80%

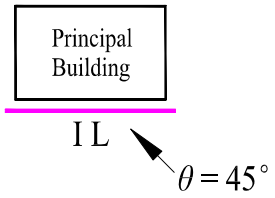

Fig. 2.8 Mean pressure coefficient distributions for different building opening ratios, geometry IL, θ=45°.

Fig. 2.8 shows mean pressure coefficient distributions on the outer and inner surfaces of scaffolding for geometry IL for different building opening ratios for θ=45º. Fig. 2.8 (a), (b), (c) and (d) show pressure distributions on the outer surface of the scaffolding for building opening ratios of 0%, 20%, 40% and 80%, respectively. When the building opening ratio varies from 0% to 80%, both the distributions and magnitudes of pressures on the outer surface are almost the same. Thus, building

openings do not affect mean pressures on the outer surface of scaffolding. Fig. 2.8 (e), (f), (g) and (h) show pressure distributions on the inner surface of scaffolding for building opening ratios of 0%, 20%, 40% and 80%, respectively. The pressure distributions show that all the largest negative pressure coefficients always occur at the top corner of scaffolding. Moreover, negative pressures on the inner surface become larger as building opening ratio increases. When the building opening ratio is 0%, wind speeds up as it flows into the gap between scaffolding cladding and building surface, leading to larger negative pressures. For other building opening ratios, wind flow inside the gap probably leaks out through the wall openings, resulting in smaller negative pressure. According to the experimental data, for wind direction 135°, positive pressures are found on the inner surface of scaffolding and tend to increase as building opening ratio increases.

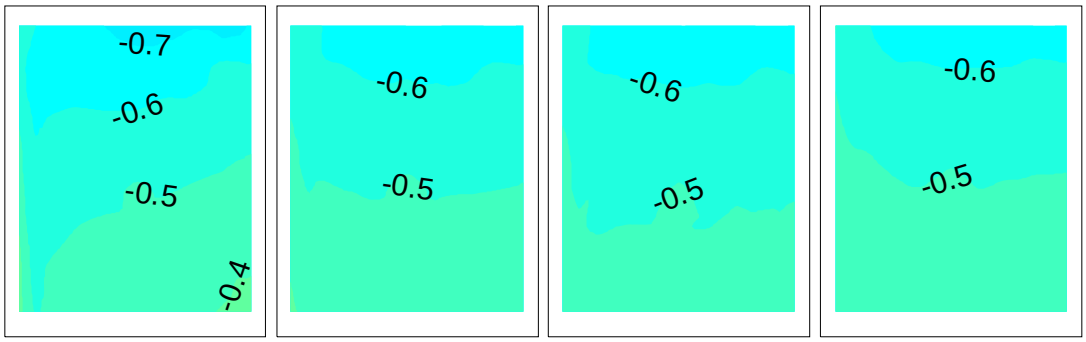

(a) Building opening ratio 0% (b) Building opening ratio 20% (c) Building opening ratio 40% (d) Building opening ratio 80%

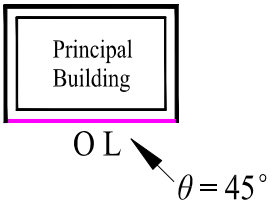

Fig. 2.9 Mean pressure coefficient distributions on the inner surface of scaffolding for different building opening ratios, geometry OL, θ=45°.

It is found that pressure coefficients on the outer surface of scaffolding always keep the same distribution and magnitude for different building opening ratios.

Furthermore, based on the experimental data, pressures on the outer surface of scaffolding for different scaffolding geometries are also almost the same. Hence, wind pressures on the inner surface of scaffolding play an important role in the investigation of pressure characteristics on clad scaffolding.

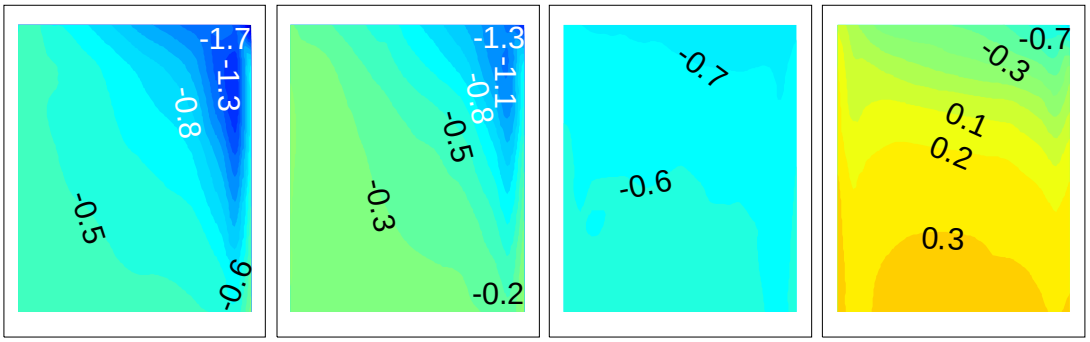

(a) Building opening ratio 0%, geometry IIL (b) Building opening ratio 0%, geometry LL (c) Building opening ratio 0%, geometry UL (d) Building opening ratio 0%, geometry CL

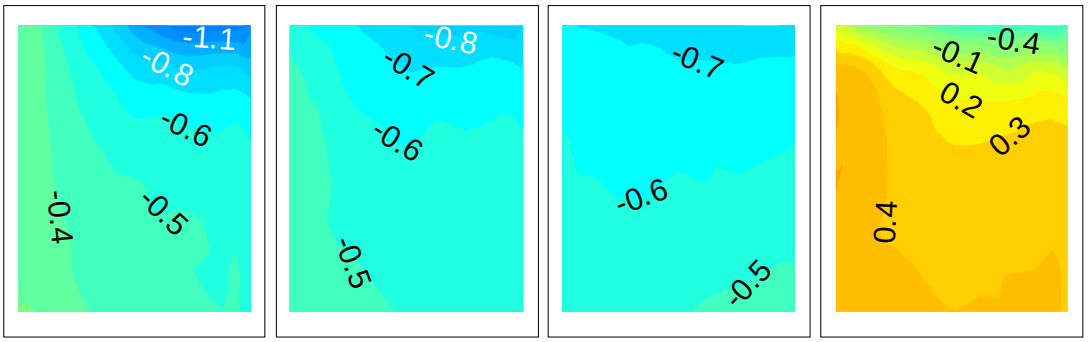

(e) Building opening ratio 80%, geometry IIL (f) Building opening ratio 80%, geometry LL (g) Building opening ratio 80%, geometry UL (h) Building opening ratio 80%, geometry CL

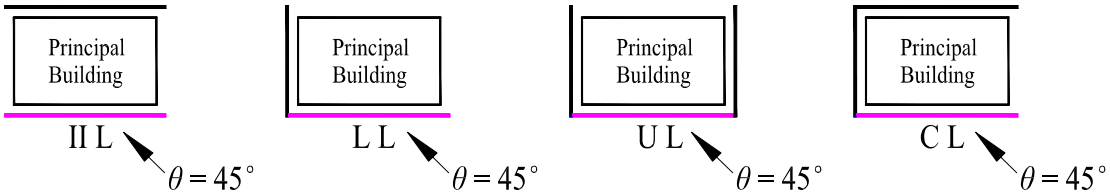

Fig. 2.10 Mean pressure coefficient distributions on the inner surface of scaffolding for different building opening ratios and scaffolding geometries, θ=45°.

Fig. 2.9 shows the mean pressure coefficient distributions on the inner surface of the scaffolding for geometry OL for different building opening ratios for θ=45º. For different building opening ratios, there is little change of pressure coefficients. For geometry IL, in which scaffolding is located on only one building side, wind easily flows into the gap between scaffolding and building. Thus, building openings can significantly affect pressure coefficients on the inner surface. But for geometry OL, scaffolding completely encloses the principal building, so that wind can not easily flow into the gap. Thus, building openings have little effect on pressures on the inner surface of the scaffolding.

Fig. 2.10 shows mean pressure coefficient distributions on the inner surface of scaffolding for four scaffolding geometries and two building opening ratios for θ=45º. Fig. 2.10 (a), (b), (c) and (d) show pressure distributions for building opening ratio 0% for geometries IIL, LL, UL and CL, respectively. Fig. 2.10 (e), (f), (g) and (h) are for building opening ratio 80%. For geometries IIL and LL, scaffolding is placed on two building sides, and for geometries UL and CL scaffolding is placed on three building sides. When the building opening ratio changes from 0% to 80%, for geometries IIL and LL, pressures on the inner surface experience similar changes to geometry IL, in which negative pressures become smaller. The same tendency is also found for geometries UL and CL, but not as significantly as for geometries IL, IIL and LL. Therefore, negative pressures on the scaffolding inner surface tend to decrease when building opening ratio increases. Furthermore, the more building sides on which scaffolding is placed, the weaker the effect.

2.3.1.2 Partial covered building

Fig. 2.11 shows the mean pressure coefficient distributions on the outer surface of scaffolding for geometry IL for different partial covered buildings for θ=45º. Fig. 2.11 (a), (b), (c), (d), (e) represents zero, one, three, five and seven floors were covered, respectively (see Fig. 2.5). The results coincide with the previous discussion, and the building openings are barely affecting the wind pressures on the outer surface of scaffolding.

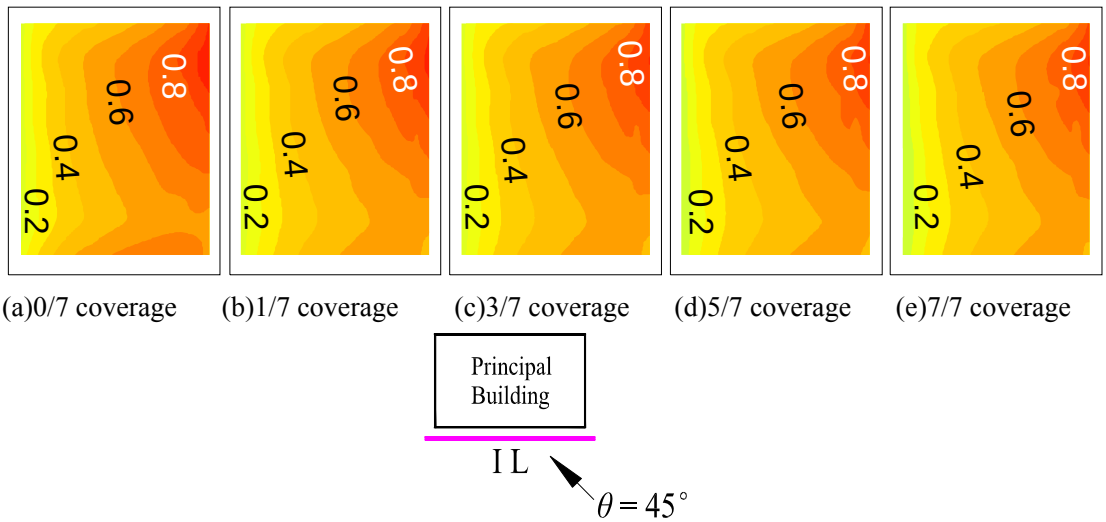

(a)0/7 coverage (b)1/7 coverage (c)3/7 coverage (d)5/7 coverage (e)7/7 coverage

Fig. 2.11 Mean pressure coefficient distributions on the outer surface of scaffolding for different partial covered buildings, geometry IL, θ=45°.

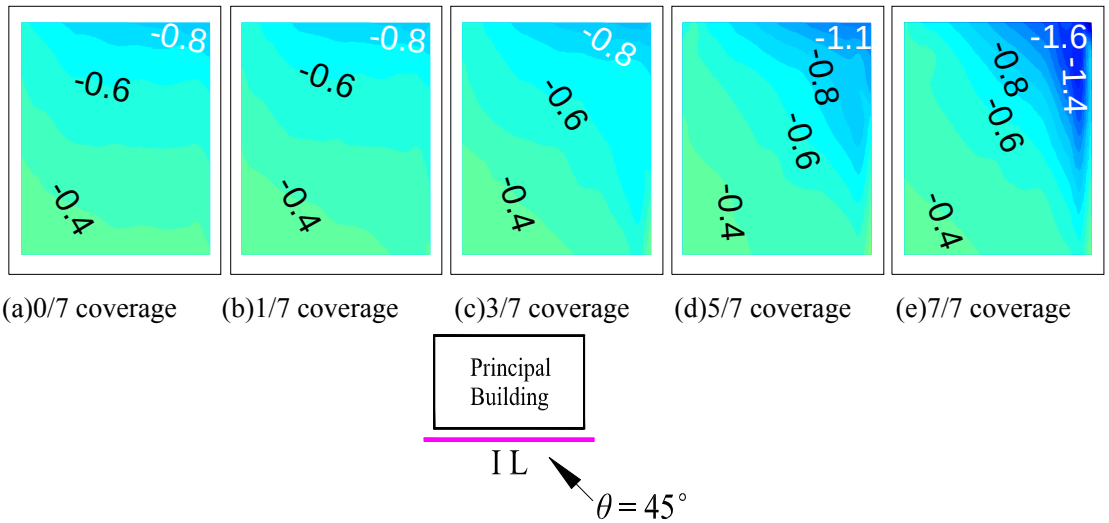

(a)0/7 coverage (b)1/7 coverage (c)3/7 coverage (d)5/7 coverage (e)7/7 coverage

Fig. 2.12 Mean pressure coefficient distributions on the inner surface of scaffolding for different partial covered buildings, geometry IL, θ=45°.

Fig. 2.12 shows the mean pressure coefficient distributions on the inner surface of scaffolding for geometry IL for different partial covered buildings for θ=45º. The principal buildings in Fig. 2.12 (a) and (e) are corresponding to the buildings with building opening ratios 80% and 0%, respectively. The largest negative pressure coefficients are always at the top corner of scaffolding, but the magnitudes are quite different. With the increment of covered floors, the largest negative pressure coefficient becomes larger. Base on the results of Fig. 2.11 and 2.12, when the wind direction is 45º, the net pressures on scaffolding are positive (outer surface minus inner surface), and the magnitudes tend to increase when the number of covered floors increasing.

When the wind direction is 105º, the net pressure coefficients on scaffolding for geometry LL are negative values. For different partial covered building, the more floors covered, the negative pressure coefficients are smaller, as shown in Fig. 2.13. This tendency is same as the results in section 2.3.1.1, the negative pressures are becoming smaller as the building opening ratio decreasing.

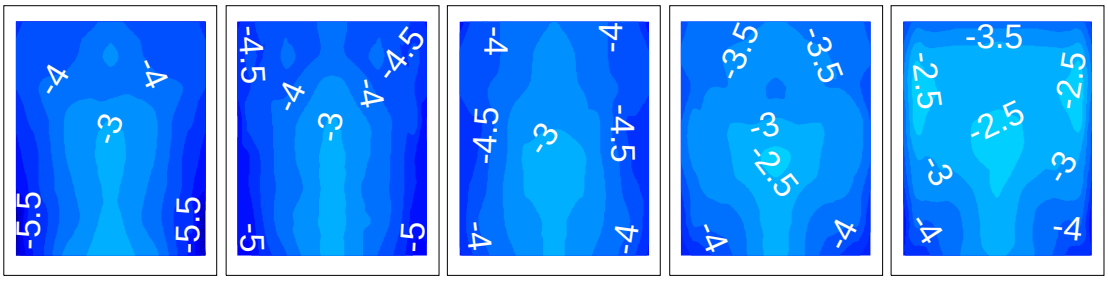

(a)0/7 coverage (b)1/7 coverage (c)3/7 coverage (d)5/7 coverage (e)7/7 coverage

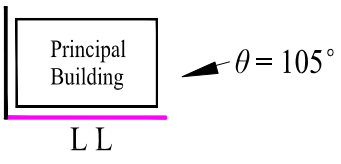

Fig. 2.13 Mean net pressure coefficient distributions for different partial covered buildings, geometry LL, θ=105°.

2.3.2 Local peak pressure coefficients

2.3.2.1 Uniform building opening ratio for entire building

Even if a part of scaffolding collapses due to wind, there may still be severe property loss and casualties. Study on local peak pressures can supply designers and engineers with more information on local wind loads on scaffolding. For each wind direction for each building opening ratio, one largest positive and one largest negative peak pressure coefficients ($\hat{C}_{p-net}(\theta,\Phi_B)$ and $\check{C}_{p-net}(\theta,\Phi_B)$) were chosen from among all the measurement points in Fig. 2.14 (a) and (b), respectively. Fig. 2.14 shows the experimental data for geometry IL. For positive peak net pressures, the largest peak value for building opening ratio 0% is around 20% larger than the value for building opening ratio 20%. The largest positive $\hat{C}_{p-net}(\theta,\Phi_B)$ becomes smaller when the building opening ratio increases from 0% to 80%, which agrees closely with previous discussion. When the building opening ratio increases, the negative pressures on the inner surface of the scaffolding become smaller and the pressures on the outer surface remain almost the same, which resulting in smaller positive peak net pressures. Furthermore, the largest positive $\hat{C}_{p-net}(\theta,\Phi_B)$ for building opening ratios 0%, 20%, 40% and 80% occur for wind directions 45º, 55º, 65º and 70º, respectively. This indicates that building openings not only affect the magnitude of peak net pressures, but also affect the wind directions causing the largest peak net pressures. Therefore, the largest peak pressures may occur for different wind directions when the building opening ratios are different.

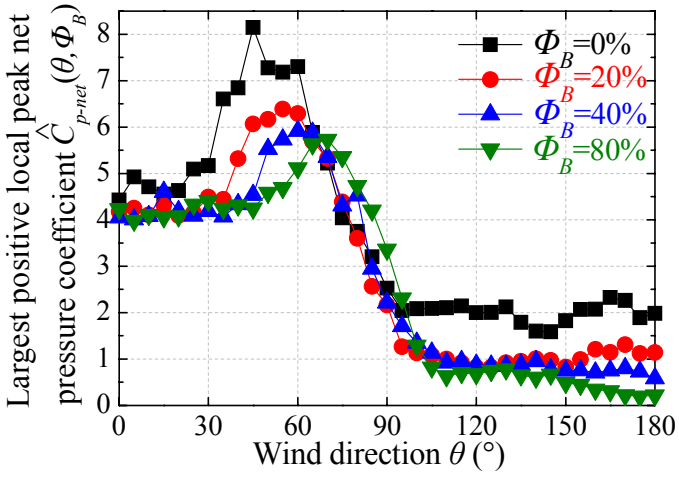

(a)Largest positive local peak net pressure coefficients ($\hat{C}_{p-net}(\theta,\Phi_B)$)

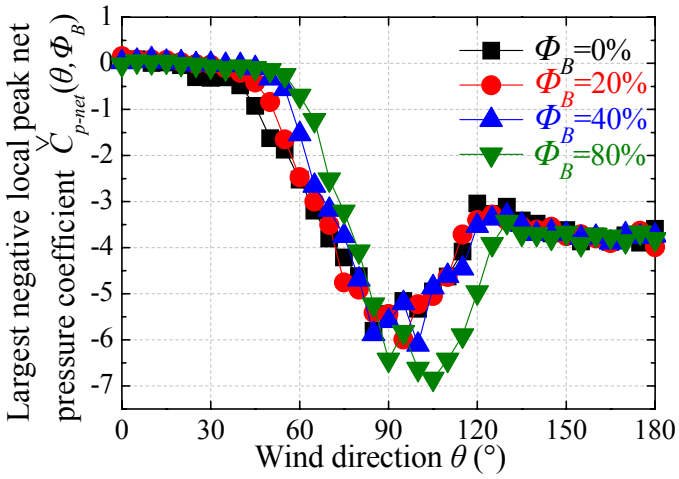

(b)Largest negative local peak net pressure coefficients ($\check{C}_{p-net}(\theta,\Phi_B)$)

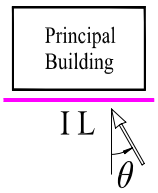

Fig. 2.14 Largest local peak net pressure coefficients for each wind direction, geometry IL.

In Fig. 2.14 (b), the largest negative $\check{C}_{p-net}(\theta,\Phi_B)$ occurs for wind directions from 85º to 105º for different building opening ratios. When the building opening ratio increases, $\check{C}_{p-net}(\theta,\Phi_B)$ become larger, this indicates that the positive pressure on the inner surface of the scaffolding becomes larger. As shown in Fig. 2.14 (a) and (b), when building opening ratios increase, $\hat{C}_{p-net}(\theta,\Phi_B)$ become smaller and $\check{C}_{p-net}(\theta,\Phi_B)$

become larger. Therefore, studying positive peak net pressures on scaffolding should focus on the cases when the building opening ratio is the smallest, and for negative ones should focus on the cases when the building opening ratio is the largest.

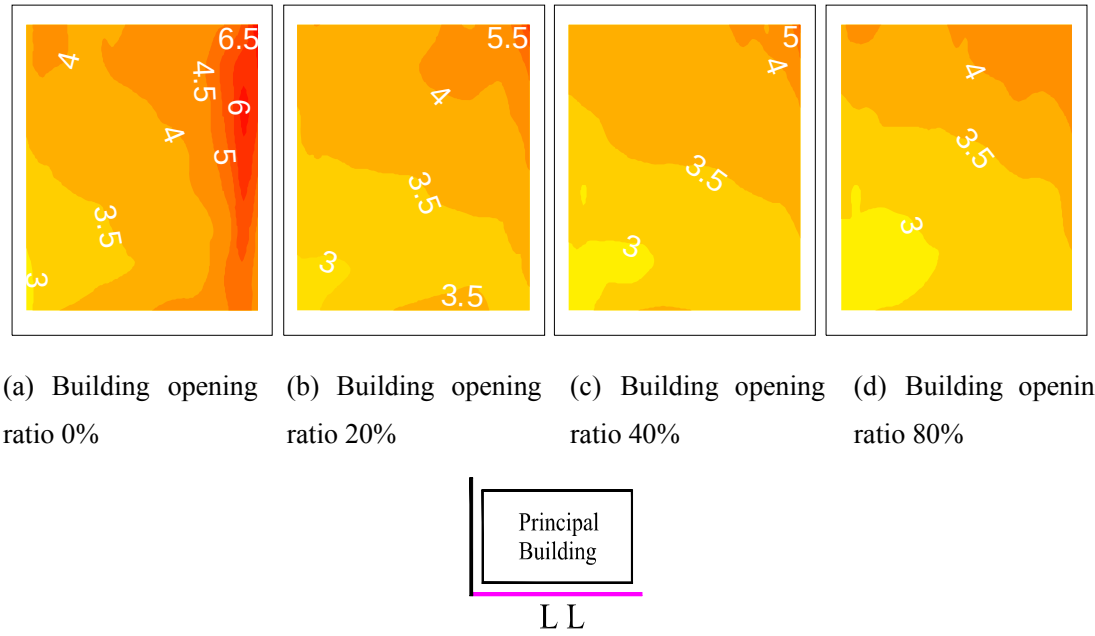

(a) Building opening ratio 0% (b) Building opening ratio 20% (c) Building opening ratio 40% (d) Building opening ratio 80%

Fig. 2.15 Largest positive local peak net pressure coefficient ($\hat{C}_{p-net}(i,\Phi_B)$) distributions for different building opening ratios for geometry LL.

Fig. 2.15 shows the largest positive peak net pressure coefficient ($\hat{C}_{p-net}(i,\Phi_B)$) distributions for different building opening ratios for geometry LL. For each measurement point, the largest positive value was chosen from all wind directions. For different building opening ratios, the largest positive $\hat{C}_{p-net}(i,\Phi_B)$ among all measurement points is always found near the top corner of scaffolding, and the smallest one is at the bottom corner of another side on scaffolding. When building opening ratio change from 0% to 80%, the largest $\hat{C}_{p-net}(i,\Phi_B)$ decrease from 6.5 to 4.

Fig. 2.16 shows the largest negative peak net pressure coefficient ($\check{C}_{p-net}(i,\Phi_B)$) distributions for different building opening ratios for geometry LL. For each building opening ratio, the largest negative $\check{C}_{p-net}(i,\Phi_B)$ among all measurement points occurs

at the side edge and lower part of the scaffolding and the magnitude tend to be larger as the building opening ratio increasing. The effects of building opening ratio on local peak net pressures and mean pressures on scaffolding are similar.

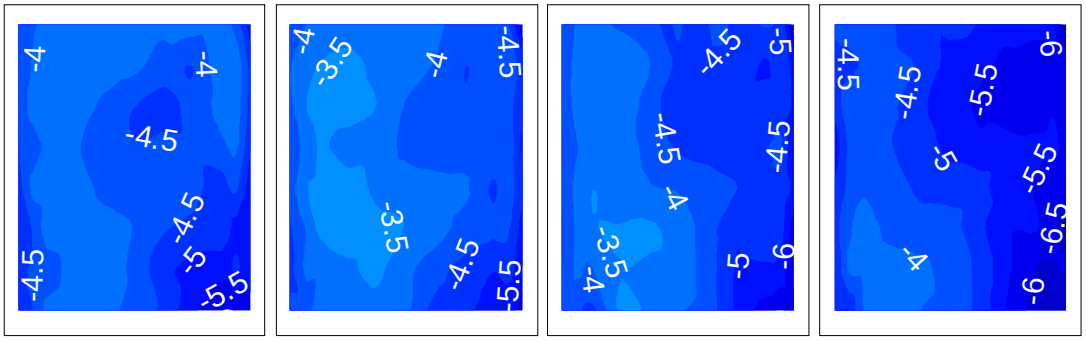

(a) Building opening ratio 0% (b) Building opening ratio 20% (c) Building opening ratio 40% (d) Building opening ratio 80%

Fig. 2.16 Largest negative local peak net pressure coefficient ($\check{C}_{p-net}(i,\Phi_B)$) distributions for different building opening ratios for geometry LL.

For each building opening ratio, the largest positive local peak net pressure coefficient ($\hat{C}_{p-net}(\Phi_B)$) was chosen from all measurement points and all wind directions, as shown in Fig. 2.17. When the building opening ratio increases, the largest positive local peak net pressure coefficient for each geometry tends to be smaller. As discussed before, the increase in building opening ratio leads to smaller negative pressures on the inner surface of the scaffolding, resulting in smaller positive net pressures. For model L, $\hat{C}_{p-net}(\Phi_B)$ for geometries IL, IIL and LL are larger than the values for geometries UL, CL and OL. The scaffolding placed on other sides of the principal building may affect and diminish the pressures on the measured scaffolding model. For model S, $\hat{C}_{p-net}(\Phi_B)$ for geometries IS, IIS and LS are also larger than

those for geometries US, CS and OS. The observation for geometry LS is not significant, but can still be seen when the building opening ratio is 0%.

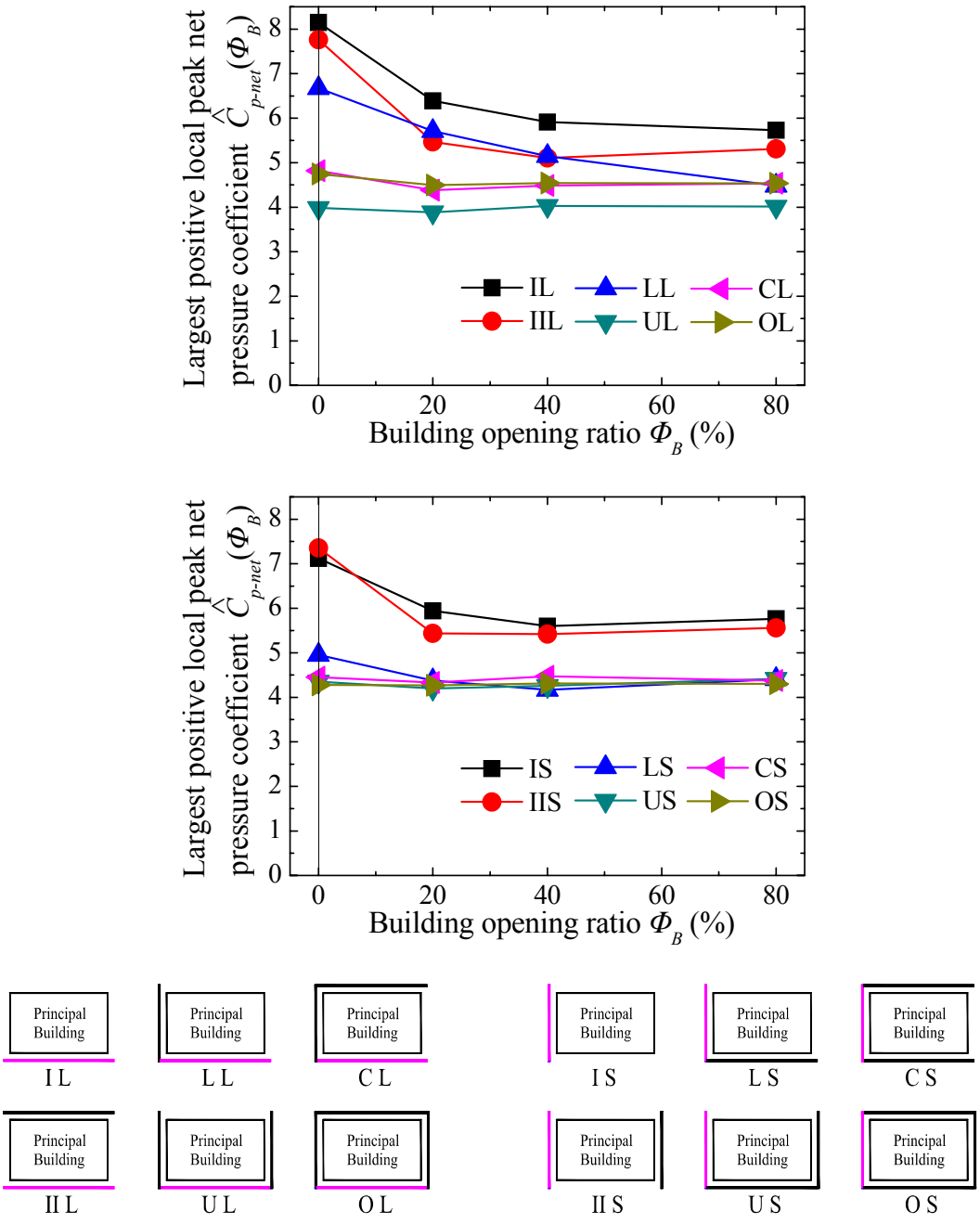

Fig. 2.17 Largest positive local peak net pressure coefficients ($\hat{C}_{p-net}(\Phi_B)$) for different building opening ratios.

For different building opening ratios, $\hat{C}_{p-net}(\Phi_B)$ for geometries IL, IS, IIL, IIS, LL and LS change more significantly than for other geometries. Therefore, the peak net

pressures for these geometries for which scaffolding is placed on only one or two sides of the principal building, are more sensitive to building openings.

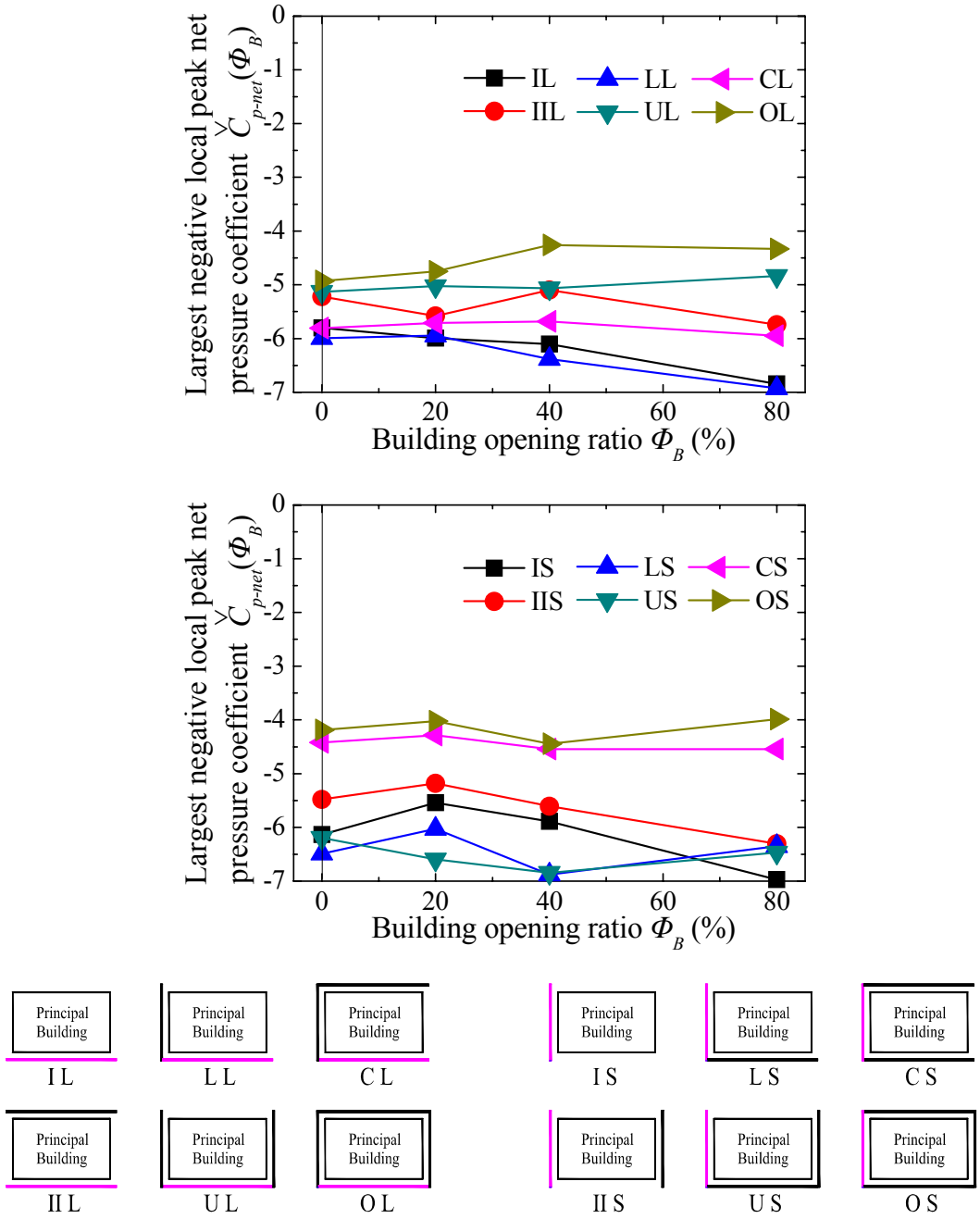

Fig. 2.18 Largest negative local peak net pressure coefficients ($\check{C}_{p-net}(\Phi_B)$) for different building opening ratios.

Fig. 2.18 shows the largest negative local peak net pressure coefficients ($\check{C}_{p-net}(\Phi_B)$) for different building opening ratios. For each building opening ratio, the largest negative local peak net pressure coefficient was chosen from all

measurement points and all wind directions. For geometries UL, CS, OL and OS, $\check{C}_{p-net}(\Phi_B)$ were smaller than for other geometries. Both side edges of the measured scaffolding model adjoin those scaffolding models placed on other sides of the principal building, which diminishes the pressures on the measured scaffolding model. When the building opening ratio becomes larger, $\check{C}_{p-net}(\Phi_B)$ tend to be larger for most geometries. However, for geometries OL and OS, in which scaffolding completely enclosed the principal building, the values have the inverse effect and become smaller.

2.3.2.2 Partial covered building

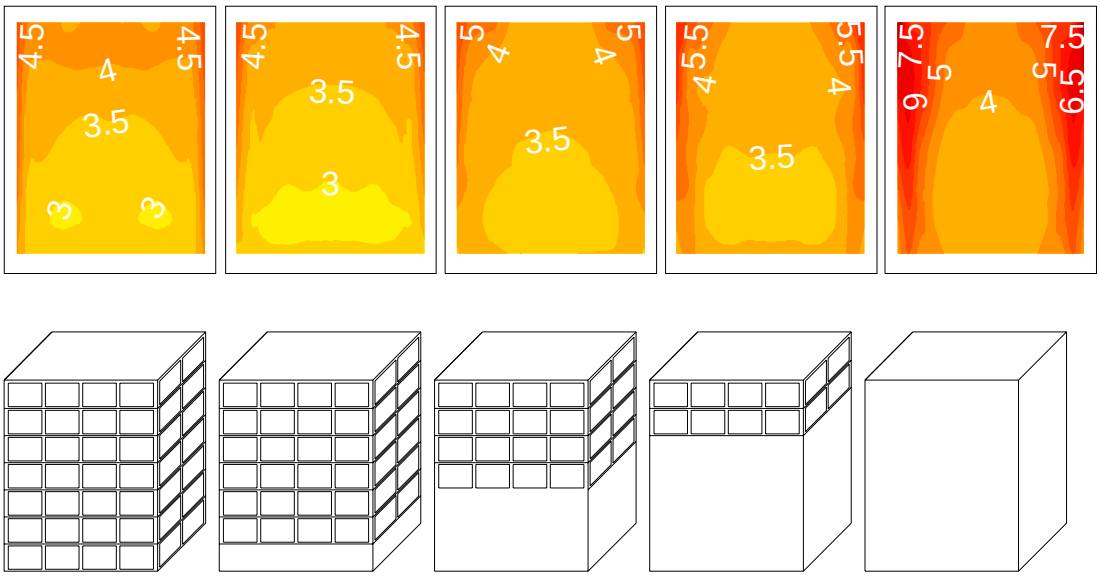

(a)0/7 coverage (b)1/7 coverage (c)3/7 coverage (d)5/7 coverage (e)7/7 coverage

Fig. 2.19 Largest positive local peak net pressure coefficient ($\hat{C}_{p-net}(i,\Phi_B)$) distributions for different partial covered buildings for geometry IL.

Fig. 2.19 and Fig. 2.20 show $\hat{C}_{p-net}(i,\Phi_B)$ and $\check{C}_{p-net}(i,\Phi_B)$ distributions for different partial covered buildings for geometry IL, respectively. For different partial covered buildings, the largest positive $\hat{C}_{p-net}(i,\Phi_B)$ among all measurement points are always found at the top corner of scaffolding, as Fig. 2.19 shown. The largest negative

$\check{C}_{p-net}(i,\Phi_B)$ among all measurement points occur at the side edges and lower part on scaffolding, as Fig.20 shown. When the partial coverage ratio increases, $\hat{C}_{p-net}(i,\Phi_B)$ tend to be larger and $\check{C}_{p-net}(i,\Phi_B)$ tend to be smaller.

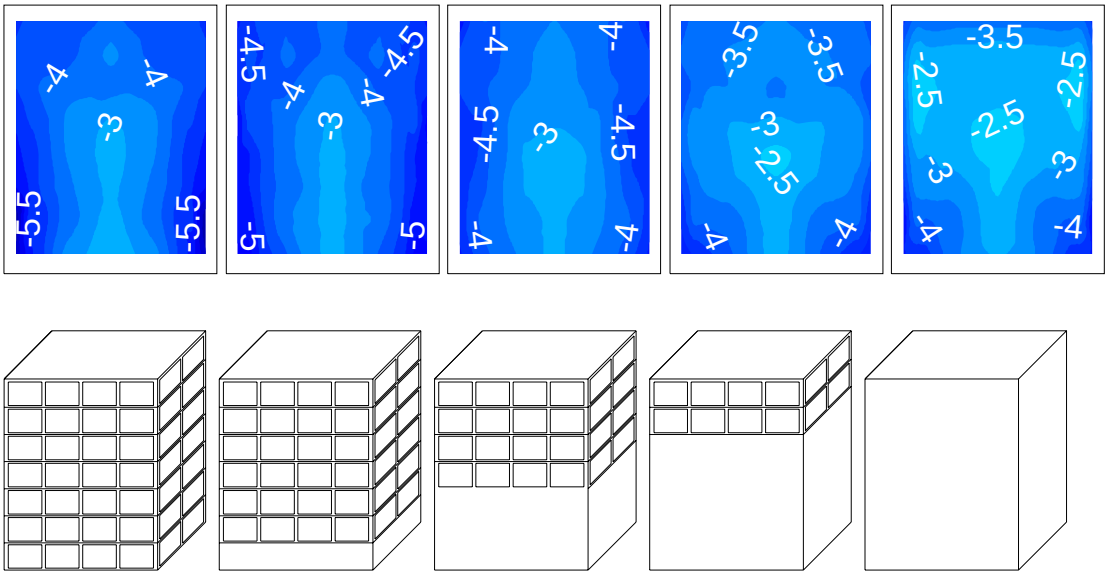

(a)0/7 coverage (b)1/7 coverage (c)3/7 coverage (d)5/7 coverage (e)7/7 coverage

Fig. 2.20 Largest negative local peak net pressure coefficient ($\check{C}_{p-net}(i,\Phi_B)$) distributions for different partial covered buildings for geometry IL.

2.3.2.3 Effects of turbulence intensity

There were two kind of flow conditions were studied, the mean wind speeds at the reference height z_{ref} (top of the principal building) were the same in this study. However, the turbulence intensities were quite different at the reference height. Fig. 2.21 shows the largest local peak net pressure coefficient distributions for different flow conditions for geometry LL. Fig. 2.21 (a) and (b) show the comparison of $\hat{C}_{p-net}(i,\Phi_B)$ distributions between the two turbulence intensities. For different turbulence intensities, the distributions of $\hat{C}_{p-net}(i,\Phi_B)$ and $\check{C}_{p-net}(i,\Phi_B)$ are similar, but both the largest

positive $\hat{C}_{p-net}(i,\Phi_B)$ and the largest negative $\check{C}_{p-net}(i,\Phi_B)$ are significant larger for I_H=29%. It is are mainly resulted from the larger turbulence intensity.

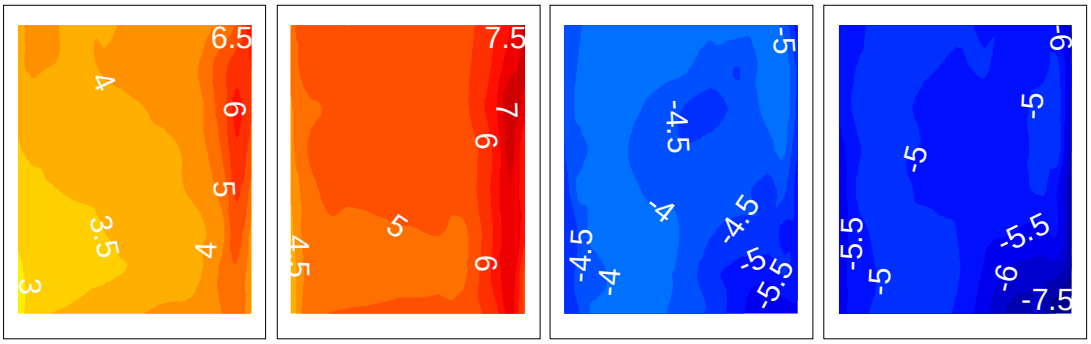

(a) Largest positive local peak net pressure coefficients $\hat{C}_{p-net}(i,\Phi_B)$ distributions (I_H=21%)

(b) Largest positive local peak net pressure coefficients $\hat{C}_{p-net}(i,\Phi_B)$ distributions (I_H=29%)

(c) Largest negative local peak net pressure coefficients $\check{C}_{p-net}(i,\Phi_B)$ distributions (I_H=21%)

(d) Largest negaive local peak net pressure coefficients $\check{C}_{p-net}(i,\Phi_B)$ distributions (I_H=29%)

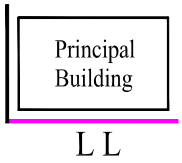

Fig. 2.21 Largest local peak net pressure coefficient distributions between different turbulence intensities, building opening ratio 0%, geometry LL.

Fig. 2.22 shows the comparison of $\hat{C}_{p-net}(\Phi_B)$ and $\check{C}_{p-net}(\Phi_B)$ between different flow conditions. For given building opening ratio and scaffolding geometry, when the turbulence intensity changes from I_H=21% to I_H=29%, $\hat{C}_{p-net}(\Phi_B)$ increase around 10%-40% and $\check{C}_{p-net}(\Phi_B)$ increase around 20% -60%. This results imply that the effects of turbulence intensity on $\check{C}_{p-net}(\Phi_B)$ are more remarkable than on $\hat{C}_{p-net}(\Phi_B)$. The turbulence intensities at the reference height (building top) were approximately 21% and 29% for this two flow conditions, respectively, which has around 40% increment.

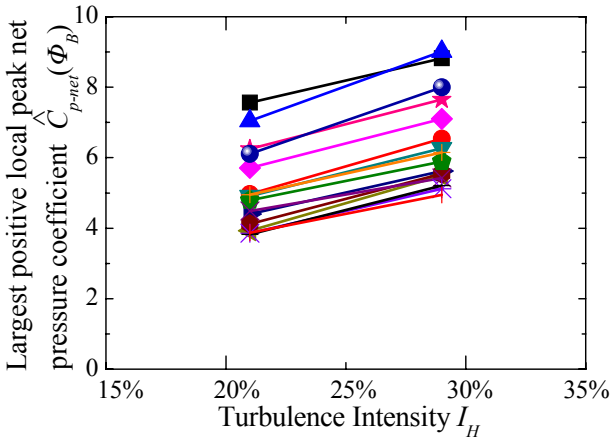

(a) Largest positive local peak net pressure coefficients $\hat{C}_{p-net}(\Phi_B)$

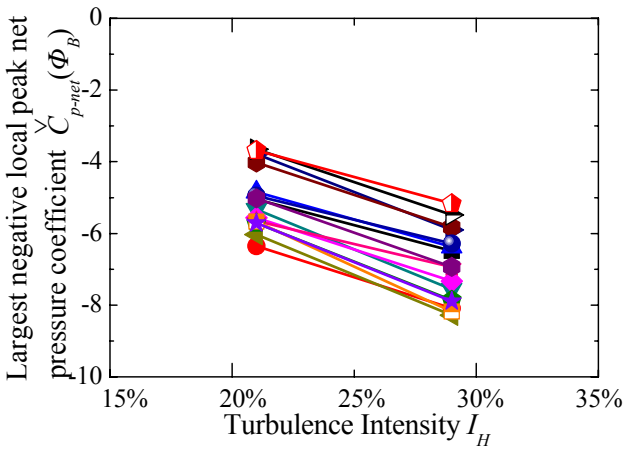

(b) Largest negative local peak net pressure coefficients $\check{C}_{p-net}(\Phi_B)$

Fig. 2.22 Comparison of largest local peak net pressure coefficients for different turbulence intensities.

2.3.3 Mean panel force coefficient

2.3.3.1 Uniform building opening ratio for entire building

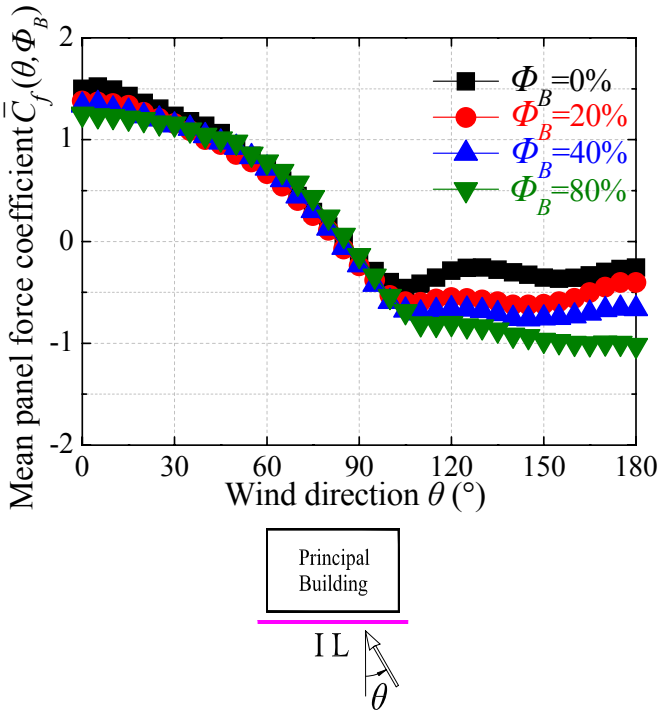

Fig. 2.23 Mean panel force coefficients ($\bar{C}_f(\theta,\Phi_B)$) for each wind direction, geometry IL.

Fig. 2.23 shows mean panel force coefficients ($\bar{C}_f(\theta,\Phi_B)$) for each wind direction for geometry IL. The largest positive $\bar{C}_f(\theta,\Phi_B)$ occurs for wind directions near 0º for each building opening ratio, and the values become smaller with increasing building opening ratio. As discussed in section 2.3.1.1, the negative pressures on the inner surface of the scaffolding tend to decrease as building opening ratio increases. The largest negative $\bar{C}_f(\theta,\Phi_B)$ tends to increase when the building opening ratio increases from 0% to 80%. This is because the positive pressures on the inner surface of the scaffolding increase as the building opening ratio increases. The wind direction for the largest negative mean panel force coefficient varies from 105º to 180º due to the building openings.

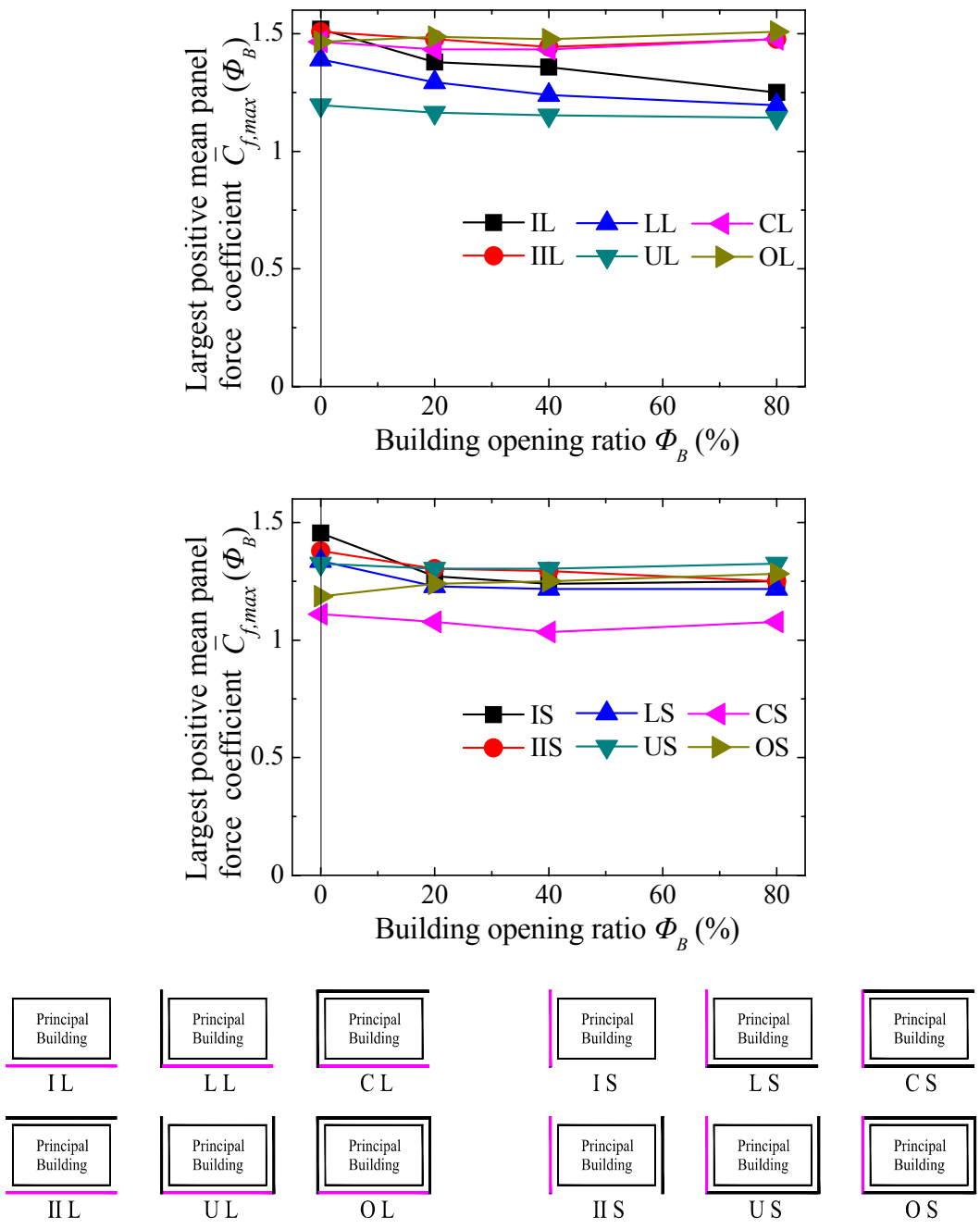

Fig. 2.24 Largest positive mean panel force coefficients ($\bar{C}_{f,max}(\Phi_B)$) for the entire scaffolding for different building opening ratios.

Fig. 2.24 and Fig. 2.25 show the largest positive and negative mean panel force coefficients ($\bar{C}_{f,max}(\Phi_B)$ and $\bar{C}_{f,min}(\Phi_B)$) for different building opening ratios. The force coefficients for model L and model S experience similar change tendencies as building opening ratio increases. For most scaffolding geometries, $\bar{C}_{f,max}(\Phi_B)$ tends

to be smaller and $\overline{C}_{f,min}(\Phi_B)$ tends to be larger when the building opening ratio increases from 0% to 80%. For geometries OL and OS, which represent scaffolding completely enclosing the principal building, there is an inverse effect. As discussed, model L for geometries IL, IIL, LL, IL, CL and OL correspond to model S for geometries IS, IIS, LS, US, CS and OS, respectively. For a given building opening ratio, the mean panel force coefficients of model L and model S are similar for corresponding geometries, and the difference is less than 0.3 in each case. For positive force coefficients, the values for different geometries are similar. Furthermore, the wind directions causing $\overline{C}_{f,max}(\Phi_B)$ are almost the same, and are perpendicular to the outer surface of the scaffolding.

However, the wind directions causing $\overline{C}_{f,min}(\Phi_B)$ for different geometries are quite different, which is due to the influence of the scaffolding placed on other sides of the building. Moreover, the magnitudes of $\overline{C}_{f,min}(\Phi_B)$ are also quite different for different geometries. $\overline{C}_{f,min}(\Phi_B)$ for geometries LL, CL, LS and US are greater than those for other geometries. Geometries LL, CL, LS and US have the common feature that one side of the measured scaffolding model adjoins an adjacent scaffolding model and the other side is free. When the wind comes from the free side of the measured scaffolding towards its inner surface, the adjacent scaffolding stops the flow and the positive pressures on the entire inner surface of the measured scaffolding become larger, thus, $\overline{C}_{f,min}(\Phi_B)$ increasing. $\overline{C}_{f,min}(\Phi_B)$ for geometries OL and OS are very small. For geometries OL and OS, because the scaffolding completely encloses the principal building, the pressures on the inner surface of the scaffolding are always negative for all wind directions, except the top two stories (higher than the principal

building). Thus, the negative net pressures and the negative mean panel force coefficients are small for geometries OL and OS.

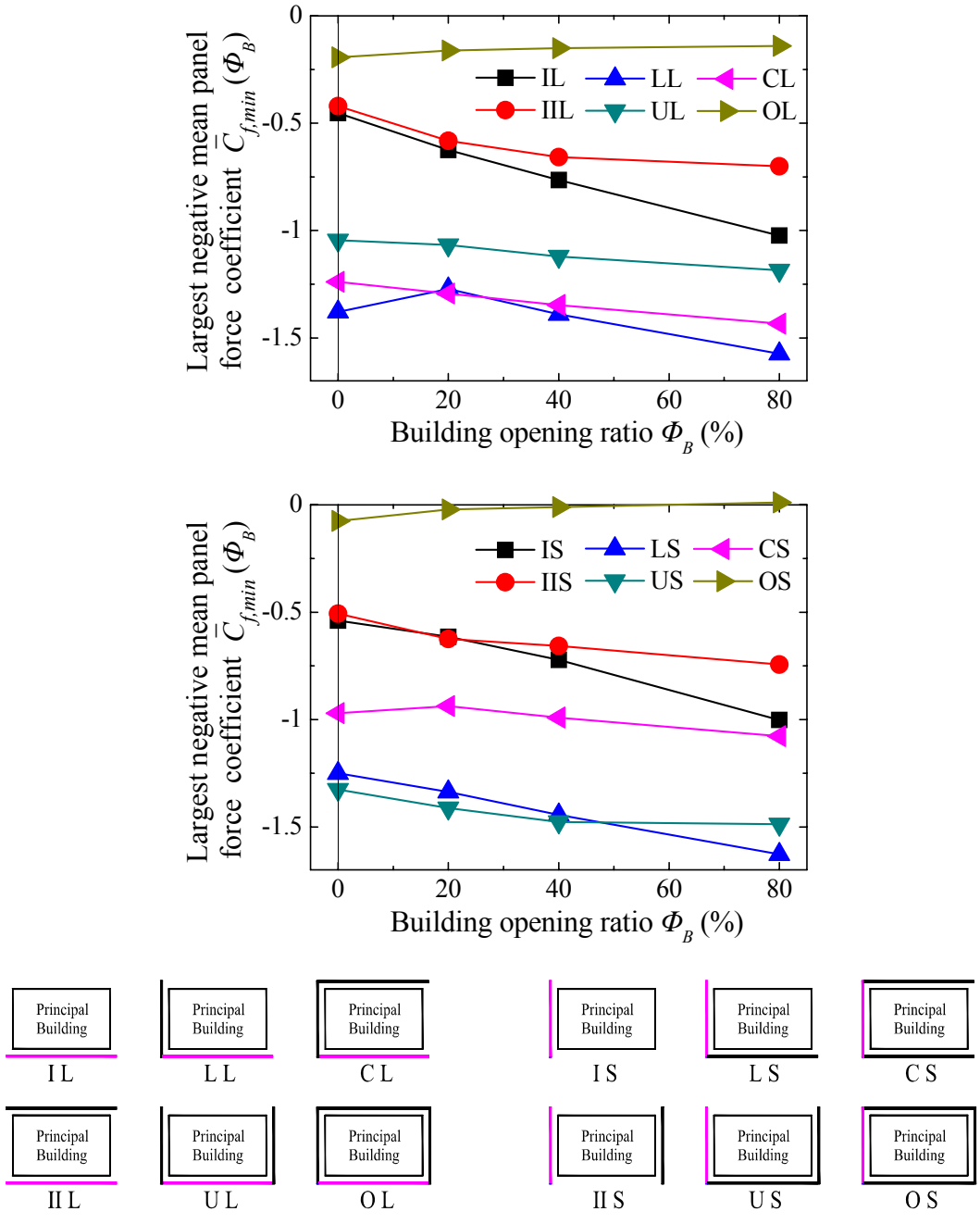

Fig. 2.25 Largest negative mean panel force coefficients ($\bar{C}_{f,min}(\Phi_B)$) for different building opening ratios.

2.3.3.2 Partial covered building

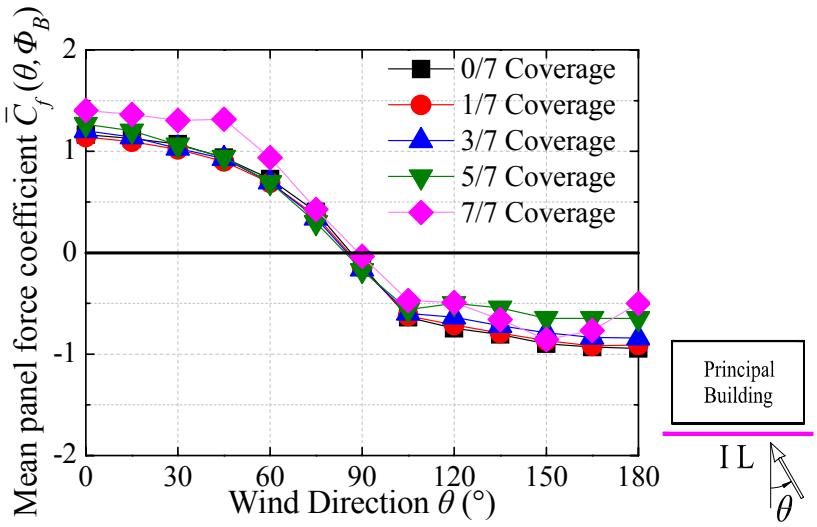

(a) Geometry IL

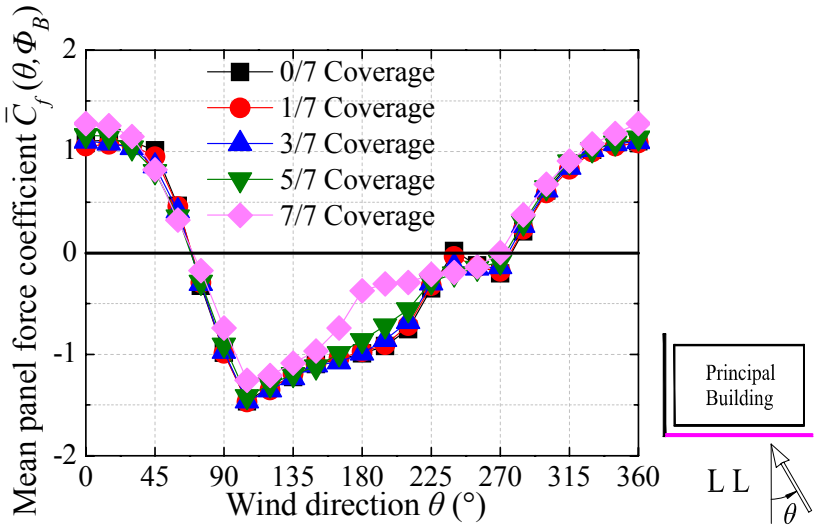

(b) Geometry LL

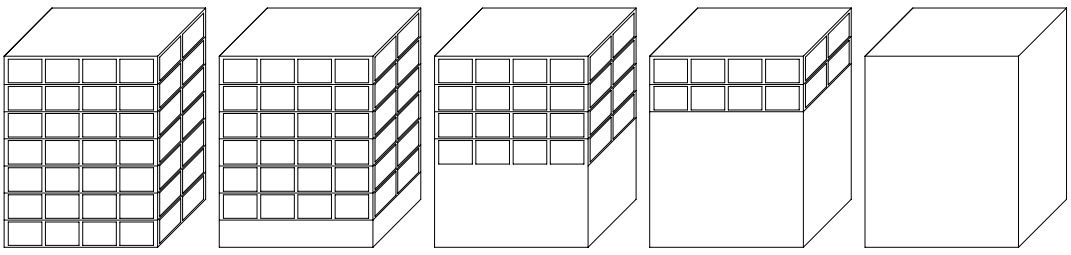

0/7 coverage 1/7 coverage 3/7 coverage 5/7 coverage 7/7 coverage

Fig. 2.26 Mean panel force coefficients ($\bar{C}_f(\theta, \Phi_B)$) for different partial covered building for each wind direction.

Fig. 2.26 shows $\overline{C}_f(\theta,\Phi_B)$ for different partial covered building. For both geometries IL and LL, $\overline{C}_f(\theta,\Phi_B)$ experience the same change tendency. When the coverage ratio increases, the largest positive $\overline{C}_f(\theta,\Phi_B)$ tends to be larger and the largest negative $\overline{C}_f(\theta,\Phi_B)$ tends to be smaller. This result agrees well with the previous discussion which on mean pressure coefficients and local peak pressure coefficients.

2.3.3.3 Effect of turbulence intensity

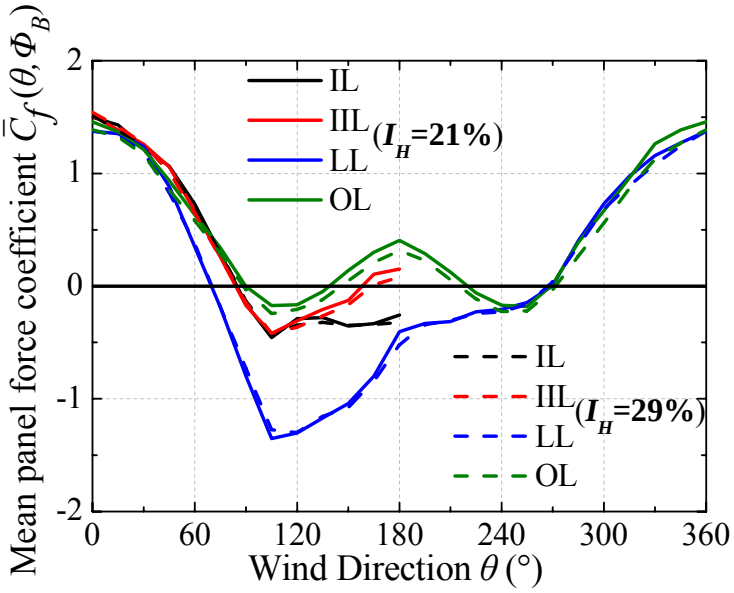

Fig. 2.27 Comparison of mean panel force coefficient ($\overline{C}_f(\theta,\Phi_B)$) between different turbulence intensities.

Fig. 2.27 shows ($\overline{C}_f(\theta,\Phi_B)$) for different turbulence intensities. From the study on local peak net pressure coefficients, the change of turbulence intensity leads to remarkable change on the magnitude of local pressures on scaffolding. However, the change of turbulence intensity does very little influence on $\overline{C}_f(\theta,\Phi_B)$, even the wind directions caused $\overline{C}_{f,max}(\Phi_B)$ and $\overline{C}_{f,min}(\Phi_B)$ are also not affected. Thus, turbulence intensity has significant effects on local peak pressures, but almost no effect on mean

panel force coefficient.

2.4 Summary

Building openings have almost no effect on pressures on the outer surfaces of scaffolding. However, wind pressures on the inner surfaces of scaffolding play an important role in wind loads on clad scaffolding.

For most scaffolding geometries, the largest positive local peak net pressures tend to become smaller and the largest negative local peak net pressures tend to become larger when building opening ratio increases. When scaffolding is placed on one or two sides of the building, local peak net pressures on the scaffolding are more sensitive to change of building openings.

For partial covered buildings, the largest positive local peak net pressures tend to become larger and the largest negative local peak net pressures tend to become smaller when coverage ratio increases.

For most scaffolding geometries, positive mean panel force coefficients tend to become smaller and negative mean panel force coefficients tend to become larger when the building opening ratio increases.

CHAPTER III : EFFECTS OF SCAFFOLDING GEOMETRY ON WIND LOADS ON SCAFFOLDING

3.1 Introduction

Effects of scaffolding geometry on wind loads on scaffolding are discussed in this chapter. Discussions will base on a part of the experimental data from the wind tunnel experiments introduced in chapter two (see Section 2.1). The experimental cases will be discussed in this chapter as Table 3.1 shown.

Table 3.1 Experimental cases

Scaffolding geometry	Building opening ratio (Φ_B)	Wind direction (interval 5 º)	Terrain category
IL IILLL UL CL OL IS IIS LS US CS OS	0%, 20%, 40%, 80%	0°~360°	AIJ 2004 category 3 (α=0.2, I_H=21%)

3.2 Data processing method

Wind pressures on the models are expressed in the form of a non-dimensional pressure coefficient, defined as:

$$C_{p\text{-}outer}(i,t) = \frac{P_{outer}(i,t) - P_0}{0.5\rho U_H^2} \qquad C_{p\text{-}inner} = \frac{P_{inner}(i,t) - P_0}{0.5\rho U_H^2} \tag{3.1}$$

where $C_{p\text{-}outer}(i,t)$ and $C_{p\text{-}inner}(i,t)$ are the wind pressure coefficients at tap i and time t on the outer and inner surfaces of the models, respectively, P_0 is the static reference

pressure, U_H is the mean longitudinal wind speed at the reference height (model top) and ρ is air density. Wind net pressure coefficient:

$$C_{p\text{-}net}(i,t) = C_{p\text{-}outer}(i,t) - C_{p\text{-}inner}(i,t) \tag{3.2}$$

The positive wind net pressure coefficient direction is from the outer surface to the inner surface, namely, from the scaffolding toward the building.

An "Equivalent time averaging" method was used to determine the wind load acting on a finite area from point pressure. With this approach, the times from point pressures were filtered by means of a moving average filter (Holmes, 1997). The equivalent time was calculated as:

$$\tau = 1.0 \times L / U_H \tag{3.3}$$

where τ is averaging time and L is the length of the diagonal for a typical door-type tubular steel scaffold unit of principal scaffolding in full scale. The dimensions of a scaffold unit were 1.7m×1.8m in windward, making L = 2.5m. In this study, 0.0039s corresponding to 0.12s in full scale was used for time averaging. The peak net pressure coefficients were calculated by the "Cook-Mayne method" using the equation:

$$\hat{C}_{p\text{-}net} = U_{\hat{C}_{p\text{-}net}} + 1.4 / a_{\hat{C}_{p\text{-}net}} \tag{3.4}$$

where $U_{\hat{C}_{p\text{-}net}}$ and $1/a_{\hat{C}_{p\text{-}net}}$ are the mode and dispersion of the extreme distribution of net pressure coefficients, respectively, which can be calculated by the Best Linear Unbiased Estimators (BLUE) as:

$$U_{\hat{C}_{p\text{-}net}} = \sum_{k=1}^{10} a_k \hat{C}_{p\text{-}netk} \qquad 1/a_{\hat{C}_{p\text{-}net}} = \sum_{k=1}^{10} b_k \hat{C}_{p\text{-}netk} \tag{3.5}$$

where, $\hat{C}_{p\text{-}netk}$ is the kth value of the ascending array of maximum values of 10 samples of peak net pressures and a_k and b_k are the BLUE coefficients.

3.3 Results and discussion

3.3.1 Mean pressure coefficient distributions

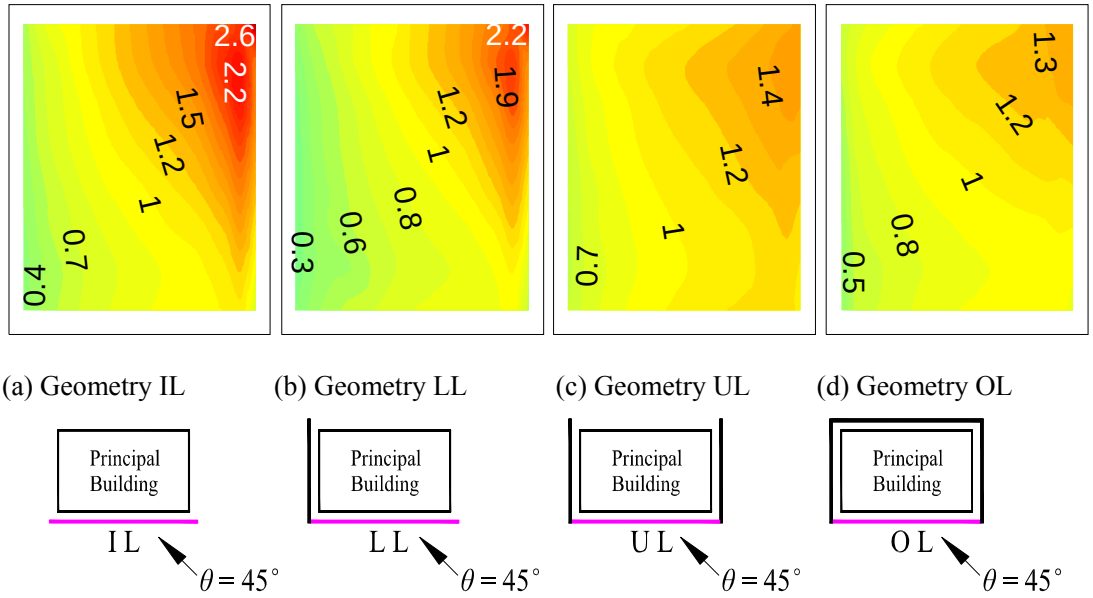

Fig. 3.1 Mean net pressure coefficient distributions for scaffolding geometries, building opening ratio 0%, θ=45°

Fig. 3.1 shows the mean net pressure coefficient distributions for building opening ratio 0% for different scaffolding geometries for θ=45º. Geometries IL, LL, UL and OL represent the scaffolding is placed on one, two, three and four building sides. When the geometry changes from IL to OL, the positive net pressure coefficients decrease sharply. As mentioned in chapter two, scaffolding geometry has very little effect on wind pressures on the outer surface of scaffolding. The scaffolding placing on the other sides of the building decrease the negative wind pressures on the inner surface of the measured scaffolding, which leads to the positive net pressure coefficients becoming smaller, as Fig. 3.1 shown.

When the wind direction is 110º, scaffolding experiences negative net pressures for all scaffolding geometries, as shown in Fig. 3.2. In Fig. 3.2 (b), scaffolding geometry is LL, the dummy scaffolding model which is placed in the adjacent side stops the wind flow in the leeward and increases the positive pressures on the inner surface of measured scaffolding. Comparing to geometry IL, geometry LL generates

larger negative net pressures at the side edge of scaffolding. In Fig. 3.2 (c), geometry UL has scaffolding in the windward what decreases the positive net pressures on the inner surface of scaffolding, as a result, the negative net pressures are smaller. For geometry OL, which scaffolding enclosed the building completely, quite small negative net pressure coefficients are found.

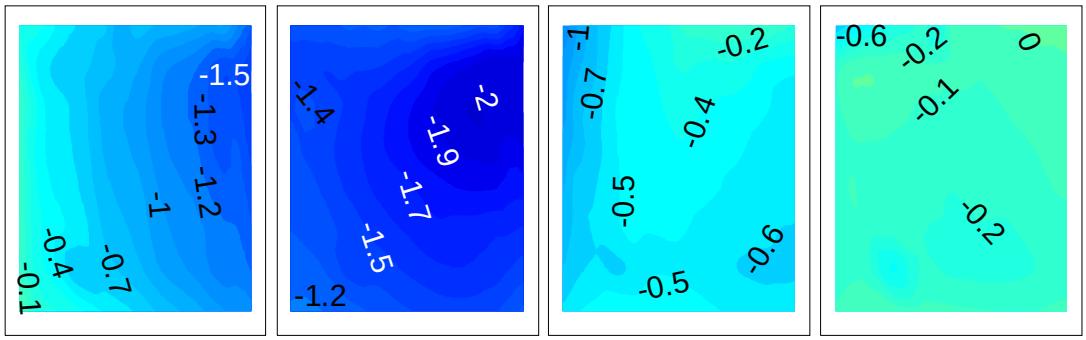

(a) Geometry IL (b) Geometry LL (c) Geometry UL (d) Geometry OL

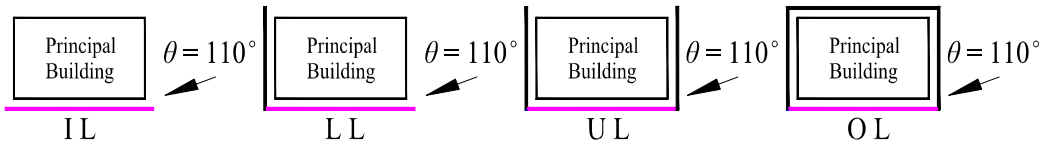

Fig. 3.2 Mean net pressure coefficient distributions for scaffolding geometries, building opening ratio 0%, θ=110°

When the net pressures on scaffolding are positive, the values seem to be smaller when the other scaffolding is placed. When the net pressures on scaffolding are negative, the distributions of net pressure coefficients are different and the values are quite small for geometry OL.

3.3.2 Local peak pressure coefficients

Fig. 3.3 shows the largest positive peak net pressure coefficient ($\hat{C}_{p-net}(i,\Phi_B)$) distributions for different geometries for building opening ratios of 0%. For each measurement point, the largest positive value was chosen from all wind directions. For geometries IL, IS, IIL, IIS and LL, the largest values among all measurement points were significantly larger than for the other geometries. The positions of the largest

values are different as well. For geometries IL, IS, IIL, IIS, LL and LS, the largest values occur at the top corner of the scaffolding. For those geometries, scaffolding was placed on only one or two sides of the principal building, for which the wind directions result in the largest $\hat{C}_{p-net}(i,\Phi_B)$ generally from the side of the outer surface of the scaffolding and tilt toward the outer surface of scaffolding. Therefore, the largest $\hat{C}_{p-net}(i,\Phi_B)$ are found at the top corner of the scaffolding.

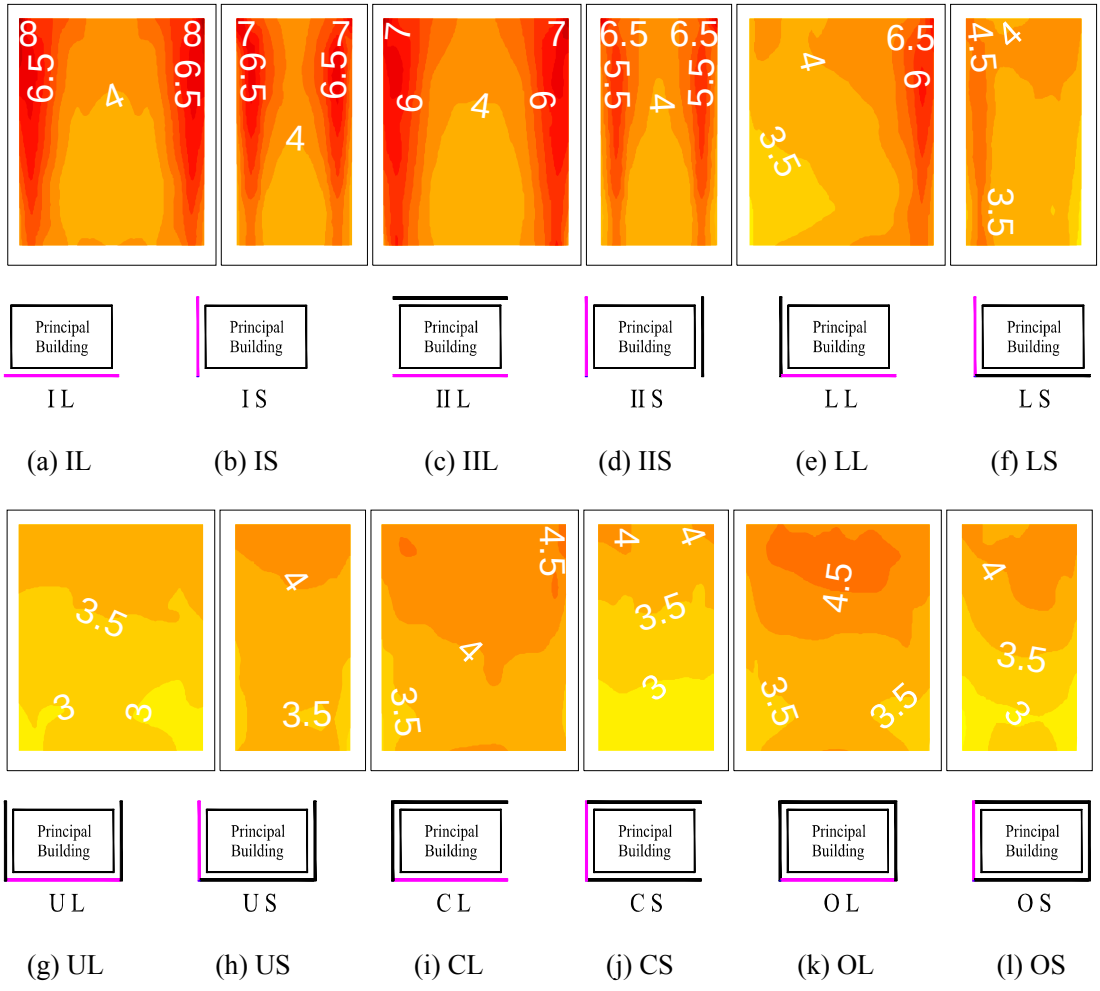

(a) IL (b) IS (c) IIL (d) IIS (e) LL (f) LS

(g) UL (h) US (i) CL (j) CS (k) OL (l) OS

Fig. 3.3 Largest positive local peak net pressure coefficient ($\hat{C}_{p-net}(i,\Phi_B)$) distributions for different scaffolding geometries, building opening ratio 0%.

But for geometries UL, US, CL, CS, OL and OS, the largest values were found at the top corner or the middle of the upper region. The wind directions resulting in the largest positive peak net pressures are mostly perpendicular to the outer surface of the

scaffolding.

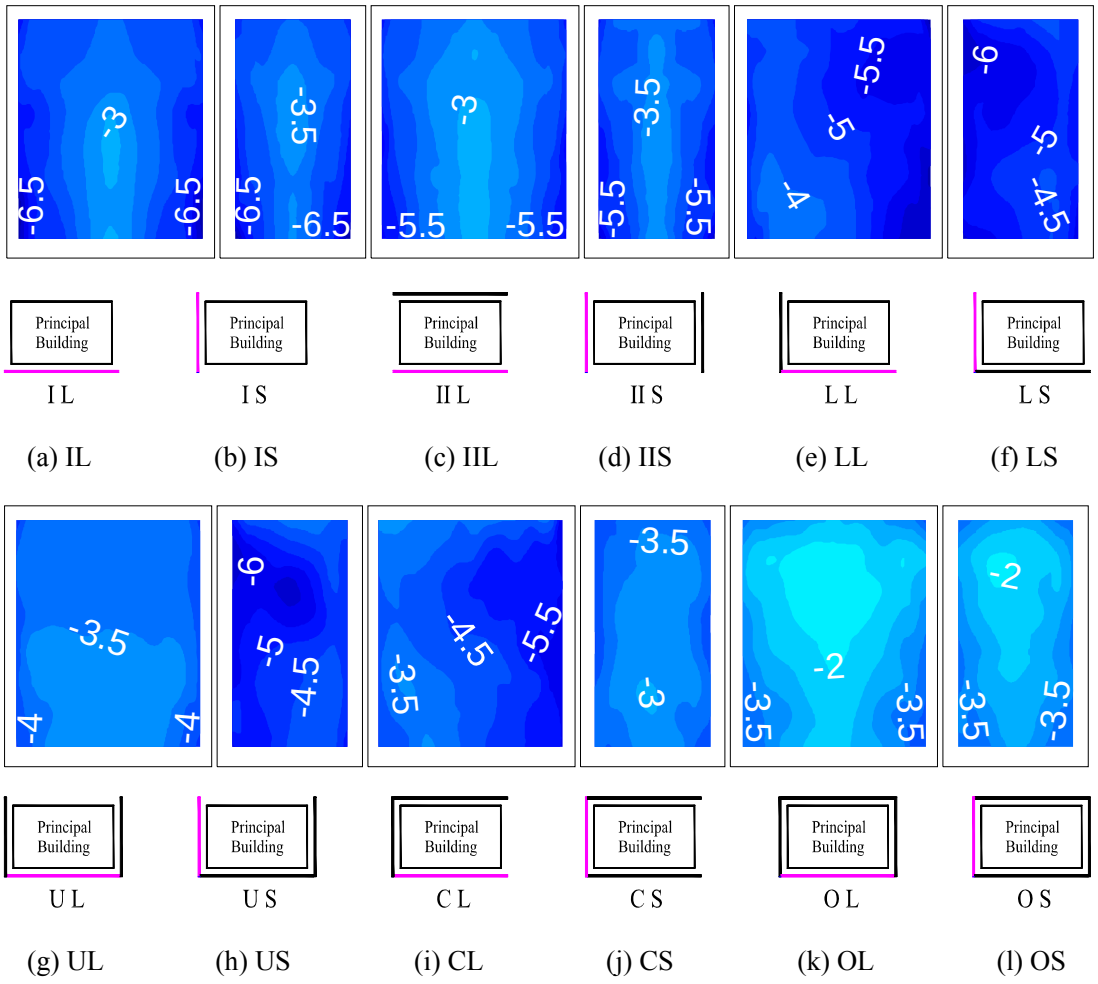

Fig. 3.4 Largest negative local peak net pressure coefficient ($\check{C}_{p-net}(i,\Phi_B)$) distributions for different scaffolding geometries, building opening ratio 80%.

Fig. 3.4 shows the largest negative peak net pressure coefficient ($\check{C}_{p-net}(i,\Phi_B)$) distributions for different geometries for building opening ratios of 80%. For each measurement point, the largest negative value was chosen from all wind directions. The largest $\check{C}_{p-net}(i,\Phi_B)$ among all measurement points is always found at the side edge of the scaffolding for each geometry. The wind directions resulting in the largest $\check{C}_{p-net}(i,\Phi_B)$ are generally parallel to the scaffolding or within small angles toward the inner surface of scaffolding, resulting in large negative net pressures at the side edge of

the scaffolding. The largest $\check{C}_{p-net}(i,\Phi_B)$ are greater for geometries IL and IS and smaller for geometries OL and OS. For geometries IL and IS, the scaffolding is placed on only one side of the principal building, and for geometries OL and OS, the scaffolding completely encloses the principal building.

Fig. 3.3 and Fig. 3.4 show how the largest peak net pressure coefficient distributions on scaffolding vary a lot for different geometries. For some geometries, even though the largest peak values are always found in similar positions, their magnitudes varied significantly. The magnitudes of both the largest positive and negative peak pressures tended to be smaller when scaffolding was placed on more building sides. This may have been because the scaffolding on different sides interfered with each other.

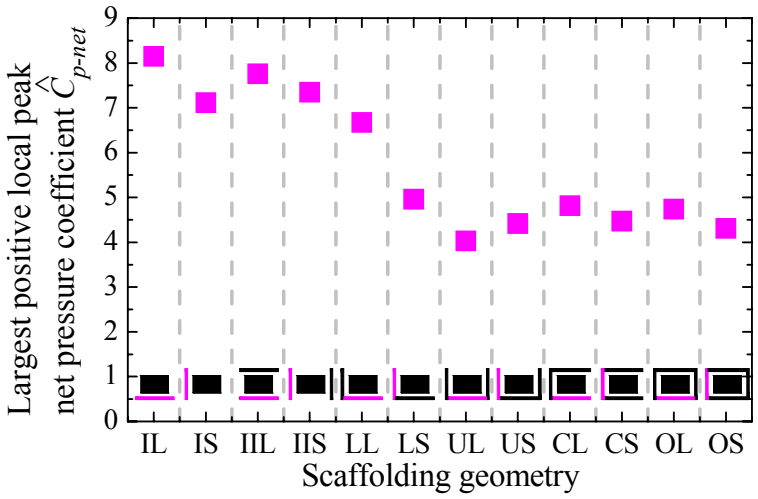

Fig.3.5 Largest positive local peak net pressure coefficient ($\hat{C}_{p-net}$) distributions for different scaffolding geometries.

Fig. 3.5 shows the largest positive local peak net pressure coefficient ($\hat{C}_{p-net}$) distributions for different scaffolding geometries. For scaffolding geometry, the largest positive value was chosen from all measurement points, all wind directions and all building opening ratios. For positive peak pressures, the values for geometry which only one or building sides placing scaffolding are larger than for other scaffolding

geometries. There is a change tendency is that $\hat{C}_{p-net}$ slows down when there are more building sides placing scaffolding. The scaffolding on the others building sides affects the wind flow between building face and scaffolding, what decreasing the negative pressures on the inner surface of scaffolding and resulting in smaller peak net pressures.

Fig. 3.6 shows the largest positive local peak net pressure coefficient ($\check{C}_{p-net}$) distributions for different scaffolding geometries. For scaffolding geometry, the largest negative value was chosen from all measurement points, all wind directions and all building opening ratios. For geometries UL, CS, OL and OS, both two adjacent building sides of the measured scaffolding are placing scaffolding. The positive pressures on the inner surface of the measured scaffolding are smaller comparing to other geometries, what resulting in smaller negative net pressures.

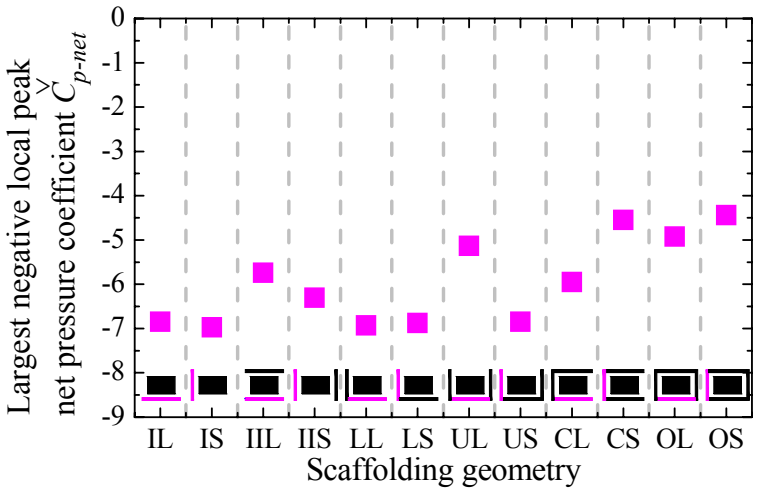

Fig.3.6 Largest negative local peak net pressure coefficient ($\check{C}_{p-net}$) distributions for different scaffolding geometries.

From Fig. 3.5 and Fig.3.6, the scaffolding geometry affects both $\hat{C}_{p-net}$ and $\check{C}_{p-net}$ dramatically. For given condition, the less building sides placing scaffolding, both $\hat{C}_{p-net}$ and $\check{C}_{p-net}$ are larger.

3.3.3 Unfavorable wind directions

The most unfavorable wind direction is the one resulting in the largest local positive or negative peak net pressure coefficient ($\hat{C}_{p-net}(\Phi_B)$ or $\check{C}_{p-net}(\Phi_B)$) of all measurement points. In Fig. 3.7, the red arrows indicate the wind directions causing the largest positive peak net pressures, and the blue arrows indicate those causing the largest negative peak net pressures. The numbers near the arrows represent the corresponding building opening ratios. At most, four red arrows and four blue arrows can be found for each geometry because four building opening ratios were tested for each geometry. For different building opening ratios, $\hat{C}_{p-net}(\Phi_B)$ may occur for the same wind direction.

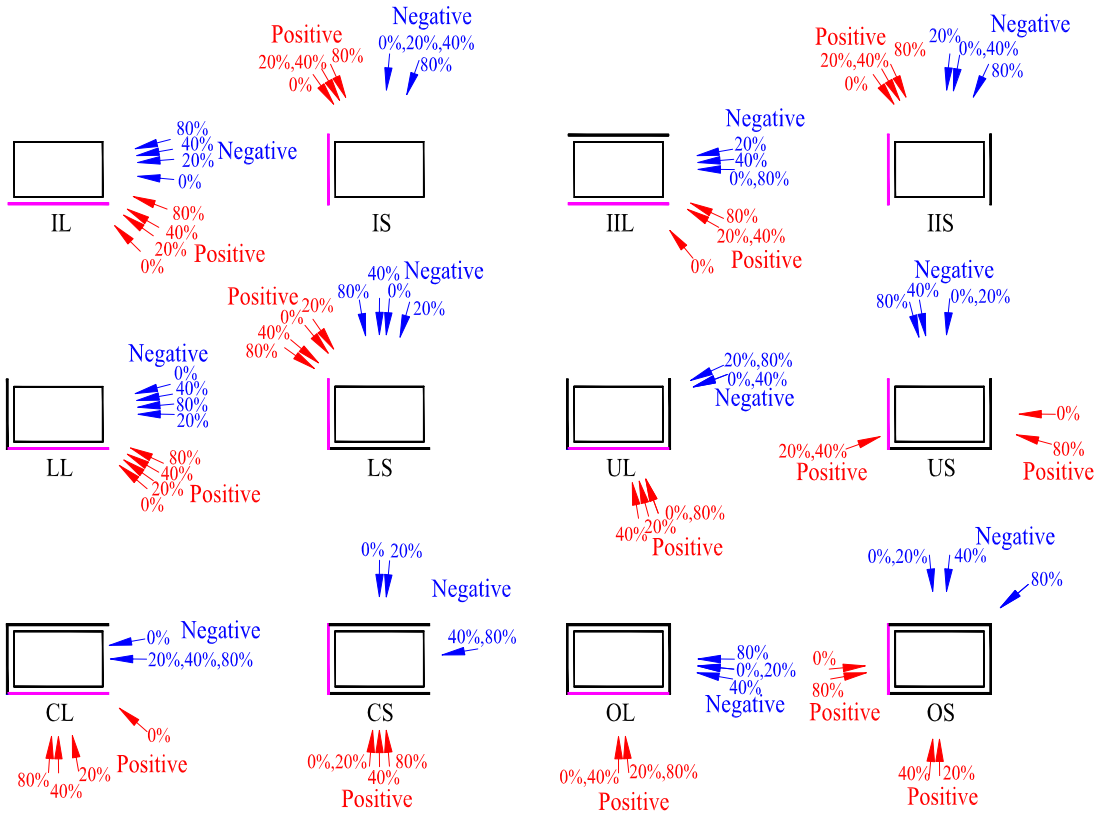

Fig. 3.7 Wind directions resulting in the largest local peak net pressures (unfavorable wind directions) for different scaffolding geometries.

For the largest positive peak net pressures, the unfavorable wind directions are oblique and toward the outer surface of the scaffolding for geometries IL, IS, IIL, IIS,

LL and LS. For these wind directions, $\hat{C}_{p-net}(\Phi_B)$ can be found at the top corner of the scaffolding. For geometries UL, US, CL, CS, OL and OS, the most unfavorable wind directions are perpendicular to the outer surface of the scaffolding. For geometries IL, IS, IIL, IIS, LL and LS, which represent cases where scaffolding is placed on only one or two building sides, $\hat{C}_{p-net}(\Phi_B)$ are always found in the same position on the scaffolding, and also the unfavorable wind directions are similar for each geometry. For geometries UL, US, CL, CS, OL and OS, scaffolding is placed on three sides of the building or completely encloses the building. The scaffolding on different building sides may interfere with each other dramatically. Also, the wind directions resulting in the largest peak net pressures may vary a lot. For example, for most measurement points (located below the top height of the principal building) on scaffolding model S, large positive peak net pressures occur for only wind directions around 270°, which is perpendicular to the outer surface of the scaffolding. However, for the measurement points at the top corner of scaffolding model S, large positive peak net pressures may occur for wind directions around 90° and 270° for geometry US, for wind directions around 180° and 270° for geometry CS and for wind directions around 90°, 180° and 270° for geometry OS. The largest positive peak net pressures may occur at the top corner or the middle of upper region of the scaffolding for these three geometries, and the corresponding unfavorable wind directions may be quite different for different building opening ratios.

For all geometries, the unfavorable wind directions caused $\check{C}_{p-net}(\Phi_B)$ are generally parallel to the scaffolding or toward to the inner surface within small angles. Therefore, it is remarkable that the building opening ratio has a major effect on unfavorable wind directions.

3.3.4 Current design force coefficients for scaffolding

In most wind load recommendations, wind loads on scaffolding are calculated by an equation including three main components: velocity pressure, reference area and mean panel force coefficient.

For clad scaffolding, BS EN 12811 (British Standards Institution, 2003) states that the aerodynamic force coefficient for the cladding shall be assumed as 1.3 and 0.1 for perpendicular direction and parallel direction, respectively. However, this method may not be applied to scaffolding that completely encloses a building.

JGJ 128 (The Ministry of Construction of People's Republic of China, 2000) uses the shape coefficient of wind load to represent aerodynamic force coefficient. For clad scaffolding, JGJ 128 provides a shape coefficient of wind load by considering a solidity ratio of cladding and principal building openings. If the principal building has wall openings, the shape coefficient of wind load shall be 1.3φ, where φ is the solidity ratio of the scaffolding. If the principal building does not have openings, the shape coefficient of wind load shall be 1.0φ.

SCEA recommendation (Scaffolding and Construction Equipment Association of Japan, 1999) suggests a shape compensation factor and a position compensation factor for wind force coefficient for clad scaffolding. The shape compensation factor is related to the aspect ratio of the cladding, and distinguishes between elevated scaffolding and

scaffolding on the ground. The position compensation factor supplies positive and negative factors for positive and negative wind loads. Scaffolding is divided into three main zones: top two-storey scaffolds, side two-bay scaffolds and middle part, each zone having a different position compensation factor. Furthermore, the position compensation factor for side zone is distinguished by whether or not it is connected to adjacent side scaffolding.

3.3.5 Mean panel force coefficient

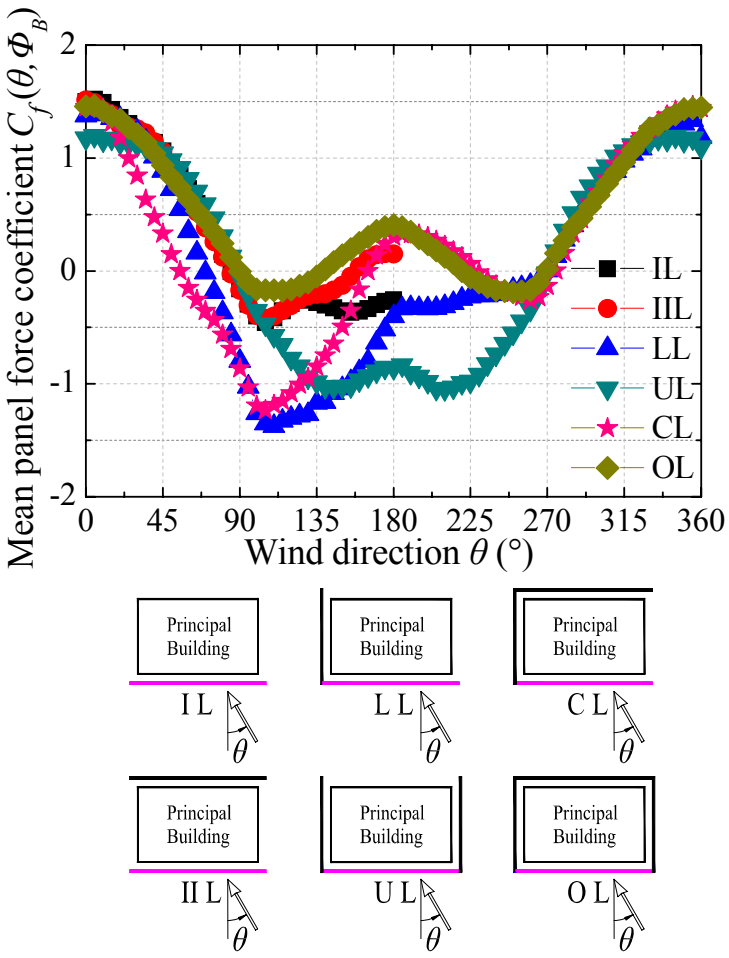

Fig. 3.8 Mean panel force coefficients for each wind direction, building opening ratio 0%.

Fig. 3.8 shows mean panel force coefficients for each wind direction for an building opening ratio of 0%. For each scaffolding geometry, the largest positive mean

panel force coefficient occurs for wind directions near 0º and the value varies from 1.2 to 1.5. The largest negative mean panel force coefficient occurs for wind directions 105º or 110º for most scaffolding geometries, except geometry UL for 210º and geometry OL for 250º. The largest negative mean panel force coefficient for geometry LL is largest around -1.4, and for geometry OL is smallest around -0.2. The differences between the values are mainly due to the scaffolding models placed on other sides of the principal building, which affects the pressures on the measured scaffolding model.

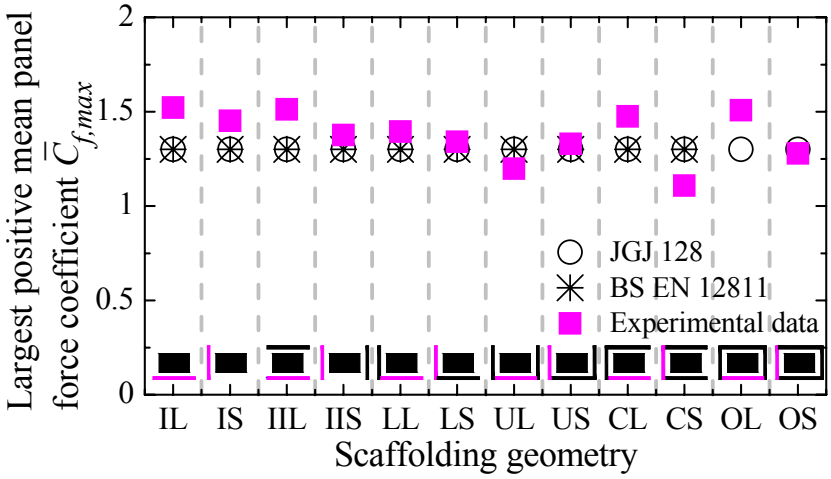

(a) Largest positive mean panel force coefficients.

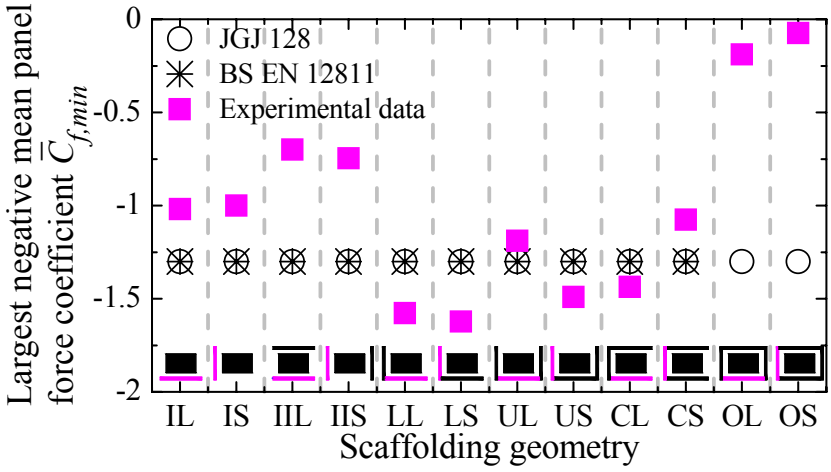

(b) Largest negative mean panel force coefficients.

Fig. 3.9 Comparison of the largest mean panel force coefficients with current design recommendations.

Fig. 3.9 shows the largest positive and negative mean panel force coefficients ($\overline{C}_{f,max}$ and $\overline{C}_{f,min}$) for different scaffolding geometries. For each scaffolding geometry, the largest positive and negative mean panel force coefficients were chosen from all wind directions and all building opening ratios. The largest mean panel force coefficients for the prototype scaffolding were calculated by the previously mentioned design recommendations. BS EN 12811 and JGJ 128 recommend that the largest force coefficients for the entire scaffolding in this study be the same value of 1.3. Based on the statement in BS EN 12811, this value is not applicable for geometries OL and OS. For most scaffolding geometries, the largest positive mean panel force coefficients are greater than 1.3. Furthermore, the recommendations also underestimate the largest negative mean panel force coefficients for geometries LL, LS, US and CL.

3.3.6 Area-averaged wind force coefficient

The pressure coefficient distributions for scaffolding show that the largest pressures usually occur in the top or side regions, and area-averaged wind force coefficients are important for scaffolding design as well. As SCEA recommendations suggest, scaffolding is divided into zones, as shown in Fig. 3.10. The top zone represents the top two-story scaffolds in full scale, which is also the part higher than the rooftop of the principal building. The side zone corresponds to approximate side two-bay scaffolds in full scale, and the middle zone is the rest. There are two area-averaged wind force coefficients corresponding to the two side zones. In this study, the larger one is chosen to represent the area-averaged wind force coefficient for the side zone.

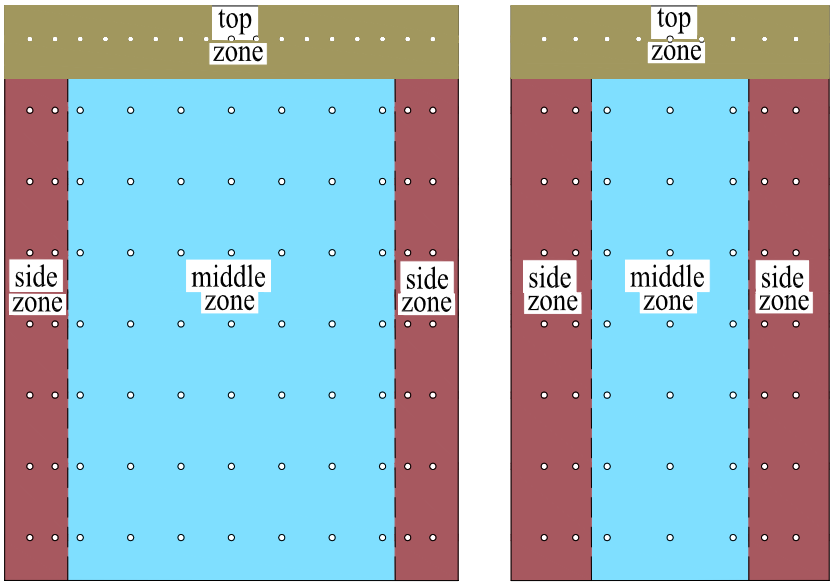

(a) model L (b) Model S

Fig. 3.10 Definitions for zones of models.

SCEA recommendations provide basic mean wind force coefficients, shape compensation factors and position compensation factors for clad scaffolding. There are two position compensation factors for positive wind loads: one for top zone and the other for both side zone and middle zone. There are three position compensation factors for negative wind load: one for top zone, one for side zone and one for middle zone. According to SCEA recommendations, the aspect ratio of model S is a little larger than that of model L, so the shape compensation factor of model S is also a little larger. The positive and negative area-averaged wind force coefficients for each zone were calculated using the method from SCEA recommendation (Section 3.3.4).

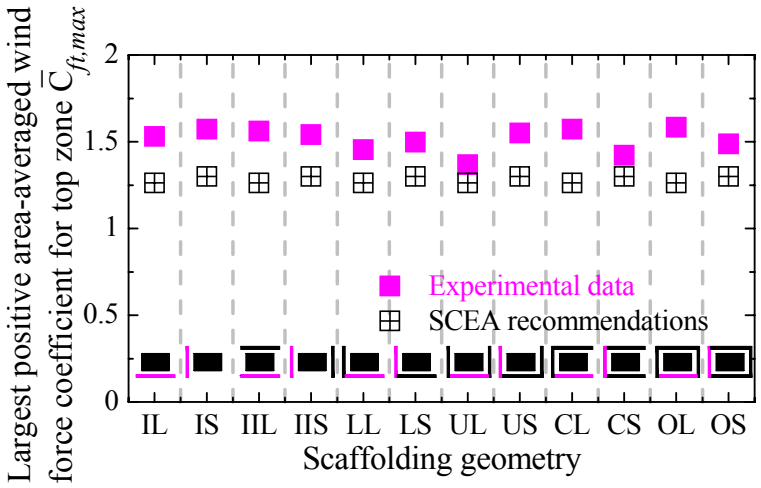

(a) Largest positive area-averaged wind force coefficients for top zone

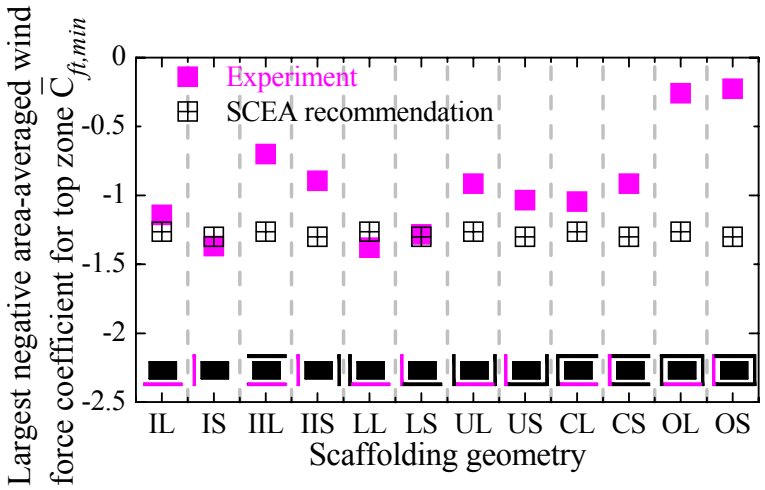

(b) Largest negative area-averaged wind force coefficients for top zone

Fig. 3.11 Comparison of the largest area-averaged wind force coefficients for top zone with SCEA recommendations.

The largest area-averaged wind force coefficients for top zone, side zone and middle zone are shown in Fig. 3.11, Fig. 3.12 and Fig. 3.13, respectively. For each scaffolding geometry for each zone, the largest positive and negative area-averaged wind force coefficients were chosen from all wind directions and all building opening ratios. $\overline{C}_{ft,max}$, $\overline{C}_{fs,max}$ and $\overline{C}_{fm,max}$ represent the largest positive area-averaged wind force coefficients for top zone, side zone and middle zone, respectively. $\overline{C}_{ft,min}$, $\overline{C}_{fs,min}$ and $\overline{C}_{fm,min}$ represent the negative ones.

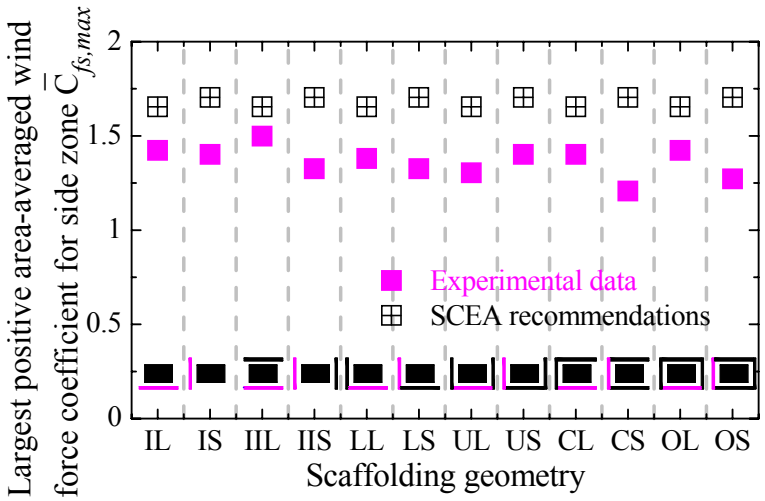

(a) Largest positive area-averaged wind force coefficients for side zone

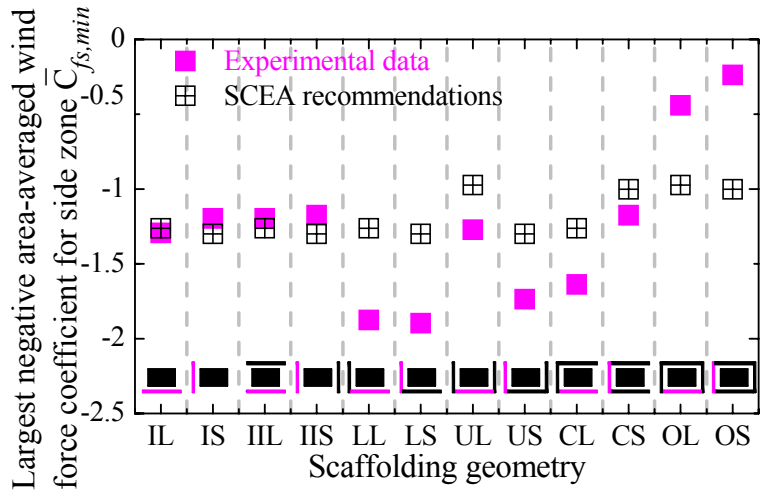

(b) Largest negative area-averaged wind force coefficients for side zone

Fig. 3.12 Comparison of the largest area-averaged wind force coefficients for side zone with SCEA recommendations.

In Fig. 3.11, the largest positive area-averaged wind force coefficient for top zone from experimental data is greater than the value recommended by SCEA for each geometry SCEA underestimates the positive area-averaged wind force coefficient for top zone. The largest negative area-averaged wind force coefficients for top zone from experimental data are greater than the recommended values for geometry IS and LL. As shown in Fig. 3.11(b), the negative values for IL, IS, LL and LS are larger than for the other geometries. The measured scaffolding model usually experiences negative force coefficients when it is located on the leeward side. For each other geometry, the

scaffolding model is located on the opposite side to the measured model, which affects the pressures on the top zone of the measured model.

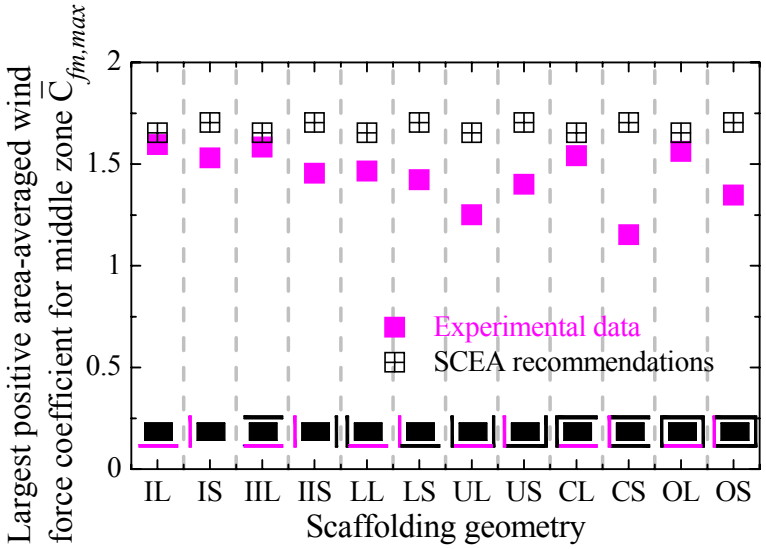

(a) Largest positive area-averaged wind force coefficients for middle zone

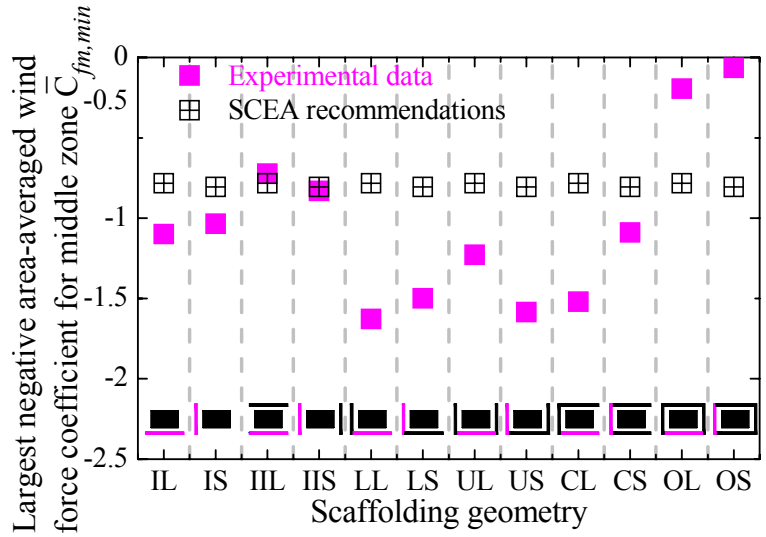

(b) Largest negative area-averaged wind force coefficients for middle zone

Fig. 3.13 Comparison of the largest area-averaged wind force coefficients for middle zone with SCEA recommendations.

Fig. 3.12 and Fig. 3.13 show that the largest positive area-averaged wind force coefficients for the side zone and middle zone are always smaller than the recommended values from SCEA. The SCEA recommendations suggest appropriate values for the positive area-averaged wind force coefficients for the side zone and

middle zone. However, it underestimates the negative area-averaged wind force coefficients for some scaffolding geometries. For geometries LL, LS, US and CL, the largest negative area-averaged wind force coefficients for the side zone and middle zone are obviously larger than the values for the other geometries and greater than the recommended values from SCEA. For these geometries, the wind directions causing the largest negative area-averaged wind force coefficients come from the free side of the measured scaffolding and are generally parallel to it. As discussed, larger positive pressures occur on the inner surface of scaffolding due to the adjacent scaffolding and result in larger negative force coefficients.

The wind directions resulting in the largest negative mean panel force coefficient and the area-averaged wind force coefficient are almost the same for each geometry, but the magnitudes of those force coefficients are different. The negative area-averaged wind force coefficients for the side zone and middle zone experience a similar change for different geometries. However, the area-averaged wind force coefficients for the top zone are affected significantly by the scaffolding model located on the opposite side of the principal building. Furthermore, based on Fig.3.11 to Fig. 3.13, for most scaffolding geometries, the positive area-averaged wind force coefficient for the side zone is the smallest and the negative value is the largest of the three zones.

3.5 Summary

The largest local peak net pressure coefficient usually occurs in the upper region or side edge of scaffolding. The magnitude of both positive and negative peak pressures tend to be smaller when scaffolding is placed on more building sides, because they may interfere with each other. Building openings have significant effects on unfavorable wind directions for the largest local peak net pressures.

When scaffolding completely encloses the building, the negative mean and

area-averaged wind force coefficients are quite small.

BS EN 12811 and JGJ 128 underestimate the mean panel force coefficients of scaffolding for some scaffolding geometries. SCEA recommends appropriate positive area-averaged wind force coefficients for the side zone and middle zone, but still underestimates the negative area-averaged wind force coefficients for some geometries.

CHAPTER IV : INTERFERENCE EFFECTS OF NEIGHBORING BUILDING ON WIND LOADS ON SCAFFOLDING

4.1 Introduction

Past research on wind loads acting on scaffolding have mainly focused on the isolated building condition. However, wind loads on structures in real environments can be quite different from those measured on isolated structures. Surroundings can significantly increase or decrease wind forces on interfered structures. Orlando (2001) carried out wind tunnel experiments on a rigid model of two adjacent cooling towers. Lam et al (2008) investigated interference effects on a row of square-plan tall buildings arranged in close proximity. Kim et al (2011) and Hui et al (2012) discussed interference effects on local peak pressures on a principal building with various configurations and different height ratios of a neighboring building. Many studies have been done on interference effects on wind loads on buildings and other structures, which showed that a neighboring building may cause significant interference effects under some conditions.

Scaffolding and Construction Equipment Association of Japan (SCEA) introduced influence coefficient in their recommendation for wind loads on scaffolding. It stated that the building taller than 50m would affect wind loads on scaffolding. This chapter is

to discuss the interference effects of neighboring building on wind loads on scaffolding.

Wind tunnel experiments were carried out based on a prototype of nonporous sheet-clad scaffolding. A medium height building with rectangular cross-section was selected as the principal building. The buildings with same cross-section dimensions of principal building and different height ratios were selected as the neighboring buildings. Effects of neighboring building locations, neighboring building height ratios, principal building opening ratios and wind directions are investigated. Mean pressure coefficients and mean panel force coefficients are determined.

4.2 Experimental setup and data processing method

4.2.1 Wind speed and turbulent intensity profiles

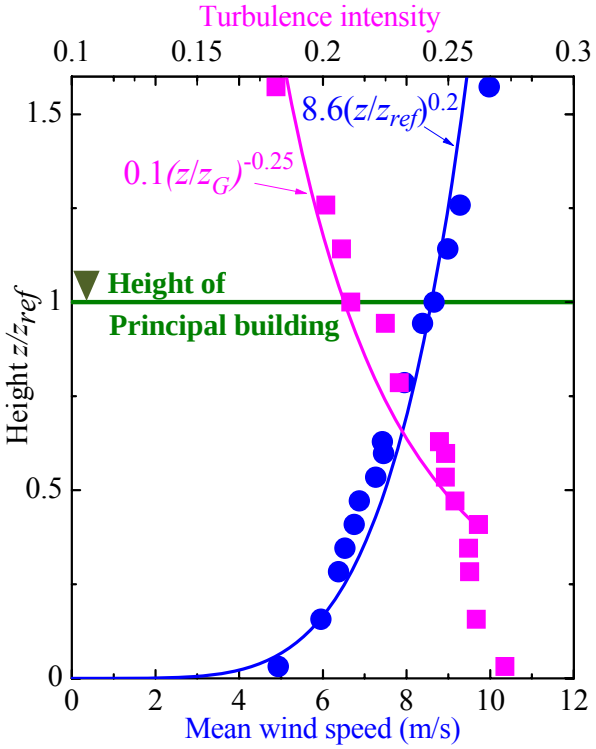

Fig. 4.1 Mean wind speed and turbulence intensity profile.

Wind tunnel experiments were carried out in a Boundary Layer Wind Tunnel in Tokyo Polytechnic University, Japan. The test section was 2.2m wide and 1.8m high. The atmospheric boundary layer was simulated as a geometrical scale of 1:75. Open

terrain characteristics were simulated and a velocity scale of 1:2.5 was adopted. The power law exponent α of mean wind speed was 0.2. The mean wind speed at the reference height z_{ref} (top of the principal building which is 318mm above the bottom of the tunnel) was around 8.6m/s, the corresponding turbulence intensity was approximately 21%, as shown in Fig. 4.1.

4.2.2 Experimental models

The dimensions of the prototype principal building were 19.2m×12m in plan and 23.8m in height. The building comprised seven stories 3.4m high. The scaffolding was assembled by using typical door-type tubular-steel scaffold units 1.7m high, 0.9m wide and 1.8m in span (one-bay). The prototype scaffolding was 27.2m high, and comprised sixteen stories. The scaffolding was 3.4m (two-stories) higher than the principal building. The distance between the building surface and the cladding of the scaffolding was 1.2m in full scale. There were four scaffolding models for the four sides of the principal building. There was one pressure-measured model and three dummy models. Nonporous acryl models 5mm thick were made to simulate the nonporous clad scaffolding (scaffolding pipes were ignored). Pressure taps were fixed symmetrically on both the outer and inner surfaces of the scaffolding models. 188 pressure taps were fixed on the measured scaffolding model, as shown in Fig. 4.2.

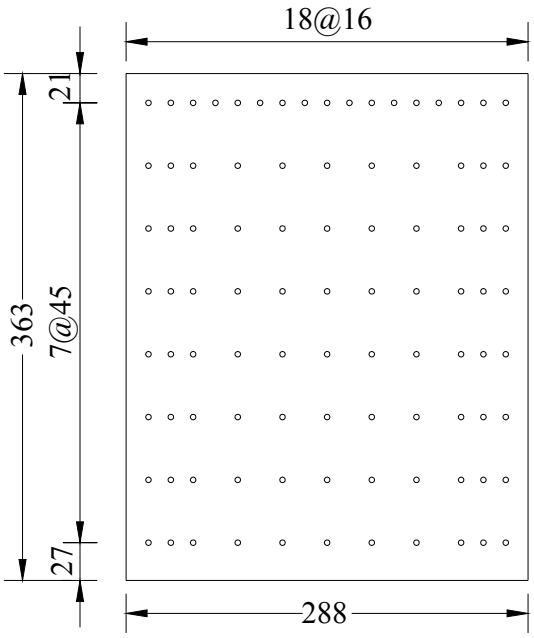

Fig. 4.2 Pressure tap positions on measured scaffolding model (unit: mm).

The experimental buildings were made from plexiglass. All the principal building models were 318mm in height (H), 256mm in breadth (B) and 160mm in depth (D). Four principal building models were tested. The building opening ratios (Φ_B) were 0%, 20%, 40%, 80%, as shown in Fig. 4.3.

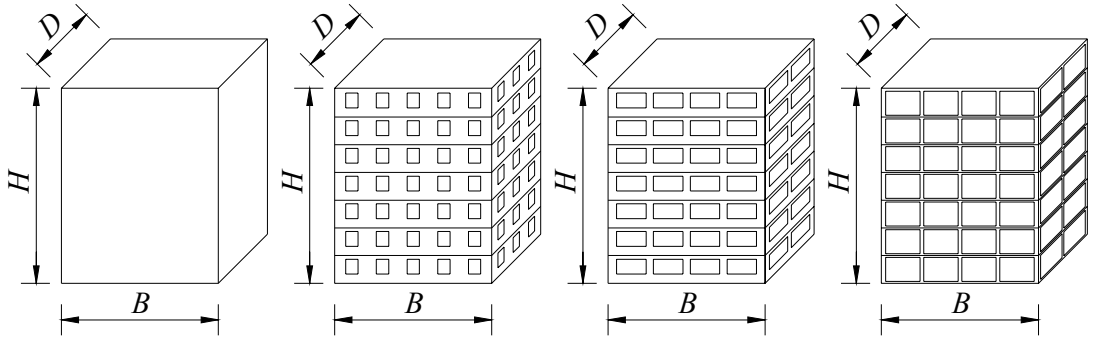

(a) Building opening ratio (Φ_B) 0% (b) Building opening ratio (Φ_B) 20% (c) Building opening ratio (Φ_B) 40% (d) Building opening ratio (Φ_B) 80%

Fig. 4.3 Principal building models.

Three neighboring building models were tested. The neighboring building models had the same cross-sectional dimensions as the principal building. The neighboring building height ratio (Hr) was defined as the neighboring building height dividing by the principal building height (H). The neighboring building height ratios were 0.5, 1

and 1.5, as shown in Fig. 4.4. In this study, the neighboring building opening ratios were always 0%.

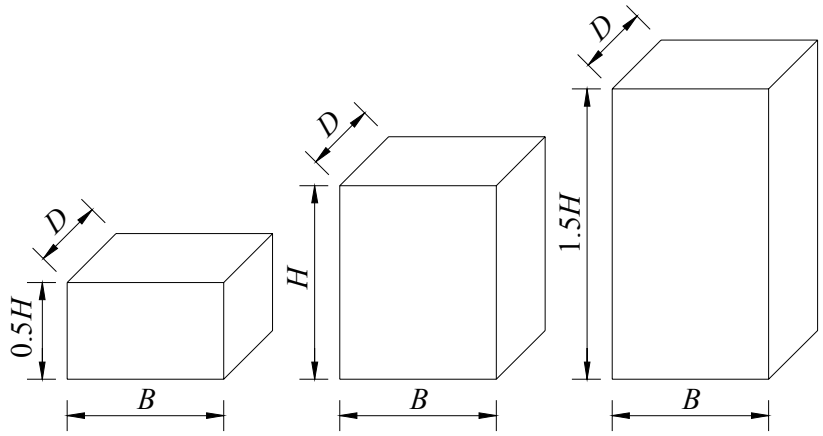

(a) Neighboring building height ratio (*Hr*) 0.5 (b) Neighboring building height ratio (*Hr*) 1 (c) Neighboring building height ratio (*Hr*) 1.5

Fig. 4.4 Neighboring building models.

Three scaffolding geometries were tested. There was only one measured scaffolding model for each geometry. The scaffolding geometries were named I, L and O, as shown in Fig. 4.5. Geometries I, L and O are corresponding to geometries IL, LL and OL.

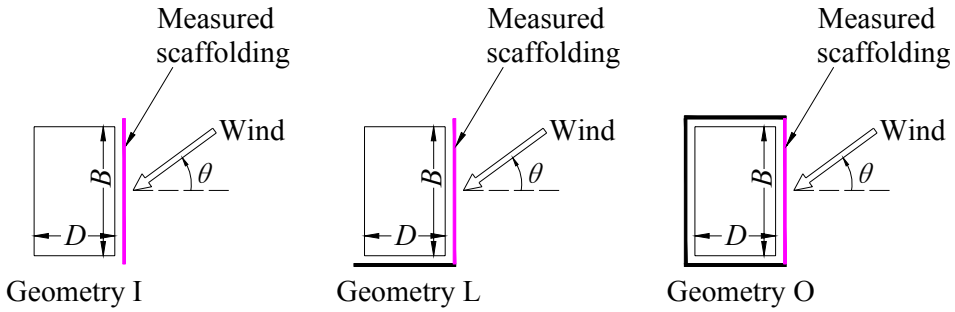

Fig. 4.5 Scaffolding models and geometries.

The experimental arrangements were as shown in Fig. 4.6. The red solid dots represent the locations of the neighboring building. When the neighboring building was located on the X-axis, the building distances were 1, 1.2, 1.5, 2, 3 and 4 times the building depth (*D*). When the neighboring building was located on the Y-axis, the building distances were 1.6, 1.92, 2.4, 3.2 and 4 times the building depth (*D*), which were also 1, 1.2, 1.5, 2 and 2.5 times the building breadth (*B*), respectively.

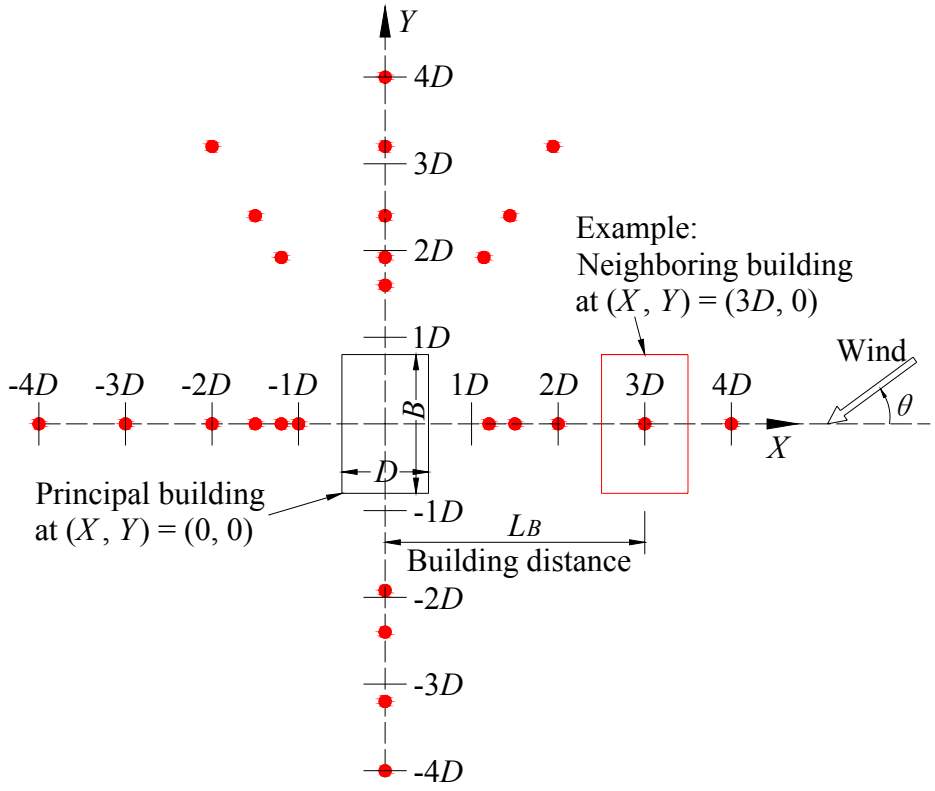

Fig. 4.6 Experimental arrangements.

The wind tunnel setup and experimental models are shown in Fig.4.7.

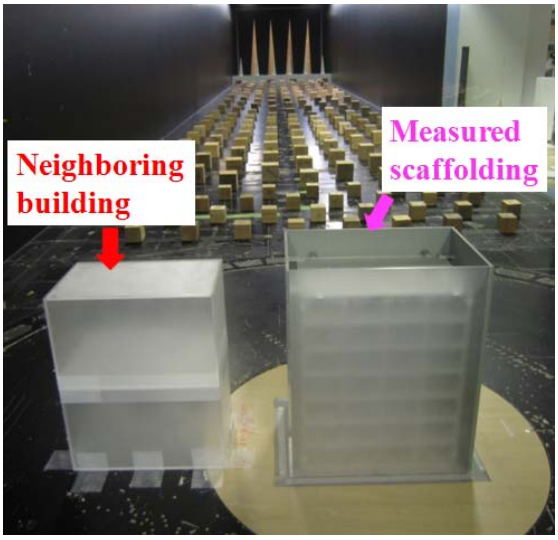

Fig. 4.7 Wind tunnel setup and models in experiment. (Neighboring building at (X,Y)= (0, 2.4D), geometry O, Φ_B= 0%, Hr=1.)

4.2.3 Experimental procedure

Pressure coefficients were obtained at a sampling frequency of 781Hz using a

multi-channel simultaneous-scanning pressure measurement system. For each case, ten 20s-long samples were collected, which corresponded to 26Hz and ten 10min-long samples in full scale. Wind direction (θ) was changed at intervals of 15° for each case. The tubing effects were compensated by the gain and phase-shift characteristics of the pressure measuring system (Irwin et al., 1979). Table 4.1 shows the experimental cases. Basic isolated cases are the condition that without neighboring building and the principal building opening ratios are all 0%.

Table 4.1 Experimental cases of interference effects

	Scaffolding geometries	Number of neighboring building locations	Wind directions θ (interval 15º)	Principal building opening ratios Φ_B	Neighboring building height ratios Hr
Isolated cases	I, L, O		0°~360°	0%	
Effects of neighboring building locations	I	21	0°~360°	0%	1
	L	19			
	O	14			
Effects of principal building opening ratios	I, O	3		0%, 20%, 40%, 80%	1
Effects of neighboring building height ratios	I, O	3		0%	0.5, 1, 1.5
Two neighboring buildings	I, L, O	2	0°~360°	0%	1

4.2.4 Data processing method

Wind pressures on the models are expressed in the form of a non-dimensional pressure coefficient, defined as:

$$C_{p\text{-}outer}(i,t)=\frac{P_{outer}(i,t)-P_0}{0.5\rho U_H^2} \qquad C_{p\text{-}inner}=\frac{P_{inner}(i,t)-P_0}{0.5\rho U_H^2} \tag{4.1}$$

where $C_{p\text{-}outer}(i,t)$ and $C_{p\text{-}inner}(i,t)$ are the wind pressure coefficients at tap i and time t on the outer and inner surfaces of the models, respectively, P_0 is the static reference pressure, U_H is the mean longitudinal wind speed at the reference height (building top) and ρ is air density. Wind net pressure coefficient:

$$C_{p\text{-}net}(i,t) = C_{p\text{-}outer}(i,t) - C_{p\text{-}inner}(i,t) \tag{4.2}$$

The positive wind net pressure coefficient direction is from the outer surface to the inner surface, namely, from the scaffolding toward the principal building.

Pressure data obtained from wind tunnel experiments can be used to analyze not only local pressures but also overall wind loads. For most scaffolding design standards and recommendations, mean panel force coefficient (mean wind force coefficient for the entire scaffolding) $\overline{C}_f$ was proposed for calculating wind loads on scaffolding. Thus, mean panel force coefficient was studied as well.

4.3 Results and discussions

4.3.1 Mean pressure coefficient distribution

4.3.1.1 Effects of neighboring building location

Fig. 4.8 compares mean pressure coefficient distributions on scaffolding for the isolated condition and a neighboring building at (X,Y)= (1.5D,0) for wind direction θ=30º and geometry O. When a neighboring building is located in front of the measured scaffolding for wind direction θ=30º, the positive mean net pressures on the scaffolding decrease dramatically, as shown in Fig. 4.8 (a) and (d). The measured scaffolding is in the wake of the neighboring building. Mean wind pressures on the outer and inner surfaces of the scaffolding are both affected by the neighboring building. In particular, the wind pressures on the outer surface change from positive to negative due to the shielding effect of the neighboring building.

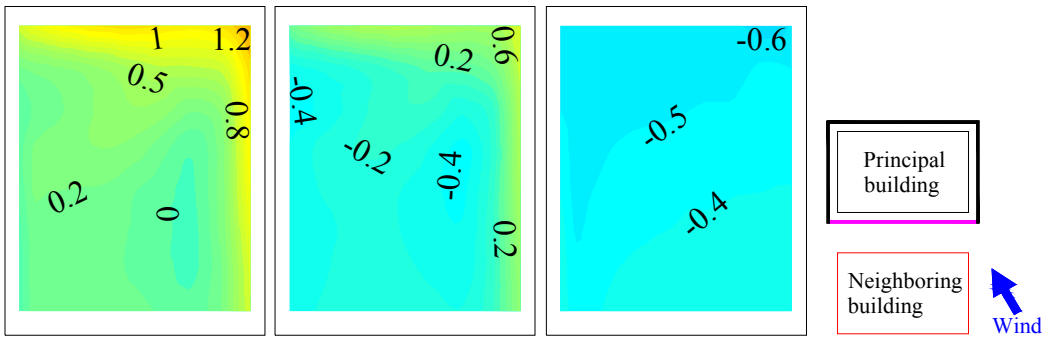

(a) Net pressure, neighboring building at $(X,Y)=(1.5D,0)$

(b) Outer surface, neighboring building at $(X,Y)=(1.5D,0)$

(c) Inner surface, neighboring building at $(X,Y)=(1.5D,0)$

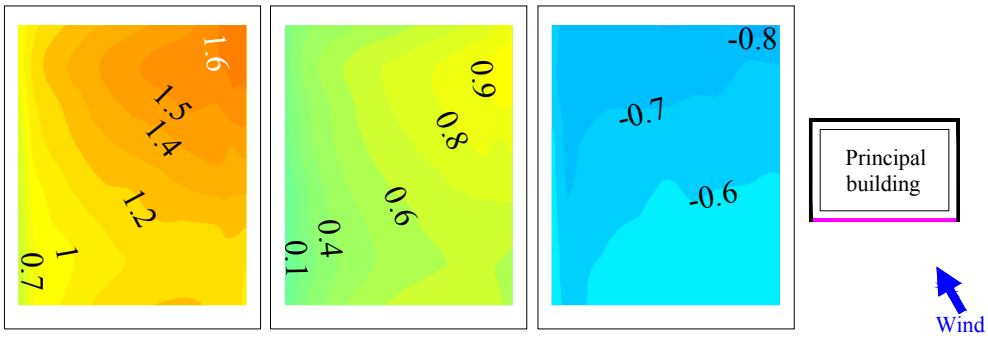

(d) Net pressure, isolated building

(e) Outer surface, isolated building

(f) Inner surface, isolated building

Fig. 4.8 Mean pressure coefficient distributions for isolated condition and neighboring building at $(X,Y)= (1.5D,0)$, θ=30º, geometry O, Φ_B= 0%, Hr=1.

Fig. 4.9 compares the mean pressure coefficient distributions for the isolated condition and a neighboring building at $(X,Y)= (2.0D,0)$ for wind direction θ=135º and geometry L. For the isolated condition, the scaffolding experiences negative mean net pressures. The neighboring building has almost no effect on the wind pressures on the inner surface of the scaffolding. However, larger negative wind pressures are generated on the outer surface of scaffolding because of the existence of the neighboring building, as shown in Fig. 4.9 (b) and (e). Thus, the positive mean net pressures on the scaffolding become larger. Both the magnitudes and distributions of mean net pressure coefficients are affected by the neighboring building.

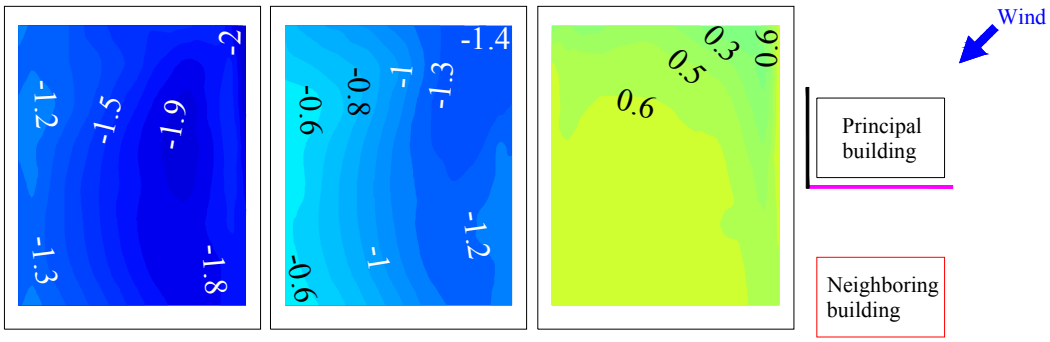

(a) Net pressure, neighboring building at $(X,Y)=(2D,0)$

(b) Outer surface, neighboring building at $(X,Y)=(2D,0)$

(c) Inner surface, neighboring building at $(X,Y)=(2D,0)$

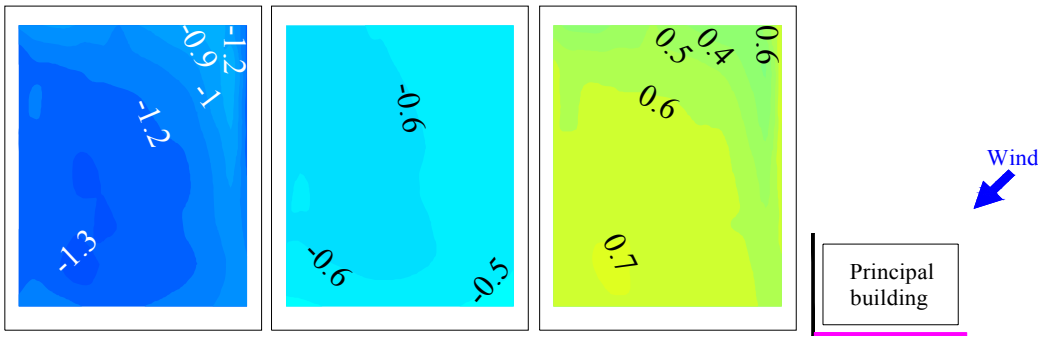

(d) Net pressure, isolated building

(e) Outer surface, isolated building

(f) Inner surface, isolated building

Fig. 4.9 Mean pressure coefficient distributions for isolated condition and neighboring building at $(X,Y)= (2D,0)$, θ=135º, geometry L, Φ_B= 0%, Hr=1.

Fig. 10 compares the mean net pressure coefficient distributions for the isolated building and neighboring building at $(X,Y)=(0, 1.6D)$ and $(X,Y)=(0, 1.92D)$ for wind direction θ=330º and geometry I. When the neighboring building is located at $(X,Y)=(0, 1.92D)$, the positive mean net pressures on the scaffolding increase significantly, especially at the side edge of the scaffolding. However, when the neighboring building is connected to the principal building ($(X,Y)=(0, 1.6D)$), which means that the principal building becomes a bigger building and the building is partially covered by the scaffolding, increments of positive mean net pressures are only found within a small region at the right side of the scaffolding.

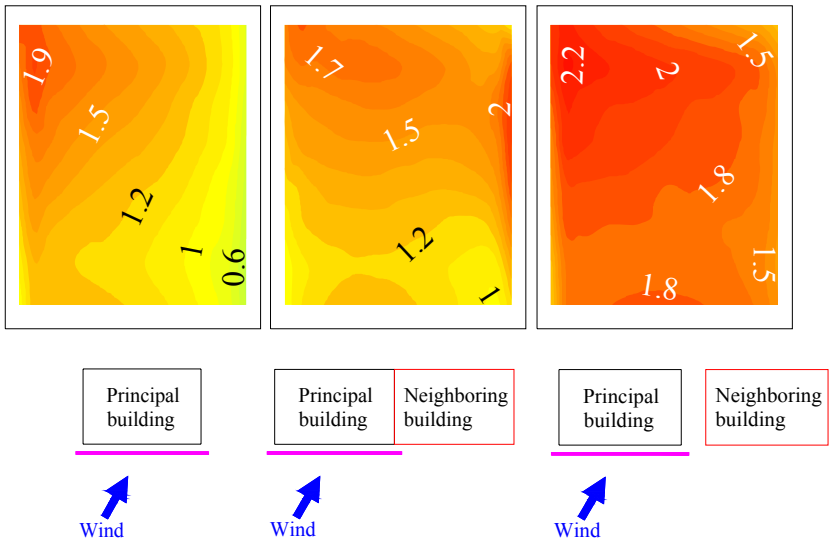

(a) Isolated building (b) (X,Y)= (0, 1.6D) (c) (X,Y)= (0, 1.92D)

Fig. 4.10 Mean net pressure coefficient distributions for isolated building and neighboring building at (X,Y)= (0,1.6D) and (X,Y)= (0, 1.92D), θ=330º, geometry I.

Fig. 4.11 shows the comparison of mean net pressure coefficient distributions for isolated building and neighboring building at (X,Y)= (0,1.6D) and (X,Y) =(0, 1.92D) for wind direction θ=210º for arrangement I. For wind direction θ=210º, neighboring building is in the leeward of scaffolding. In Fig. 4.11 (a) and (b), the net pressure coefficient distributions are almost the same. But in Fig. 4.11 (c), larger negative net pressure coefficients are found. Wind pressures on the inner surface of scaffolding are negative for isolated case and neighboring building at (X,Y)= (0,1.6D) because the scaffolding is in the wake of the principal building. There is a gap between principal building and neighboring building when neighboring building at (X,Y)= (0,1.92D). This induces the change of the flow pattern and leads to positive pressures appearing on the inner surface of scaffolding. Thus, larger negative net pressure coefficients are found in Fig. 4.11 (c).

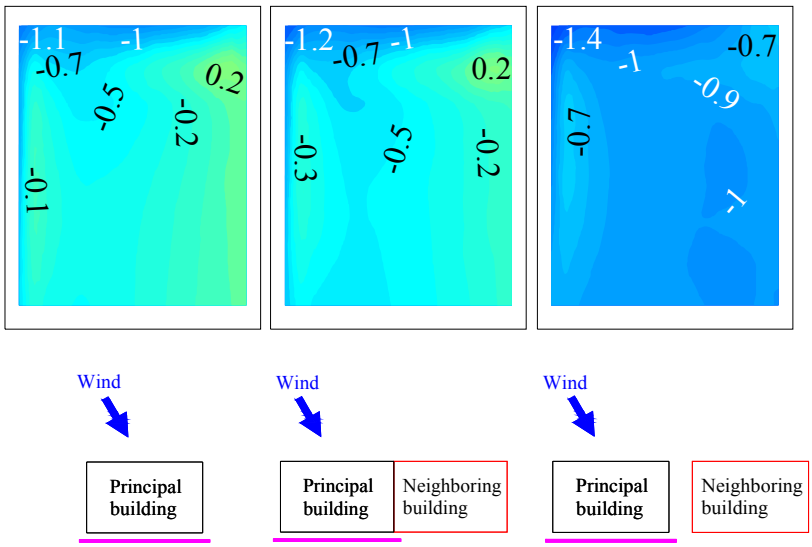

(a) Isolated building (b) (X,Y)= (0,1.0B) (c) (X,Y)= (0,1.2B)

Fig. 4.11 Mean net pressure coefficient distributions for isolated building and neighboring building at (X,Y)= (0,1.6D) and (X,Y)= (0, 1.92D), θ=210º, geometry I.

Figs. 4.8 to 4.11 indicate that a neighboring building can increase the positive or negative mean net pressures on scaffolding, which may cause more severe wind loads on it.

4.3.1.2 Effects of neighboring building height ratio

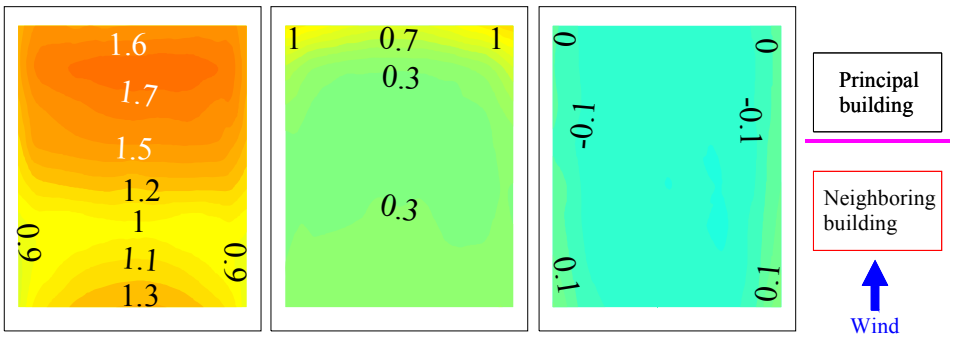

(a) Hr=0.5 (b) Hr=1 (c) Hr=1.5

Fig. 4.12 Mean net pressure coefficient distributions for different neighboring building height ratios of neighboring building at (X,Y)=(1.5D, 0), θ=0º, geometry I, Φ_B= 0%.

Fig. 4.12 shows mean net pressure coefficient distributions for different neighboring building height ratios for a neighboring building at (X,Y)=(1.5D, 0) for wind direction θ=0º and geometry I. The principal building and scaffolding are

located on the leeward side when the neighboring building is in front of the scaffolding for wind direction θ=0º. It is easy to imagine the interference effect of the neighboring building on the scaffolding. When the neighboring building height ratio increases, the positive mean net pressures on the scaffolding decrease significantly.

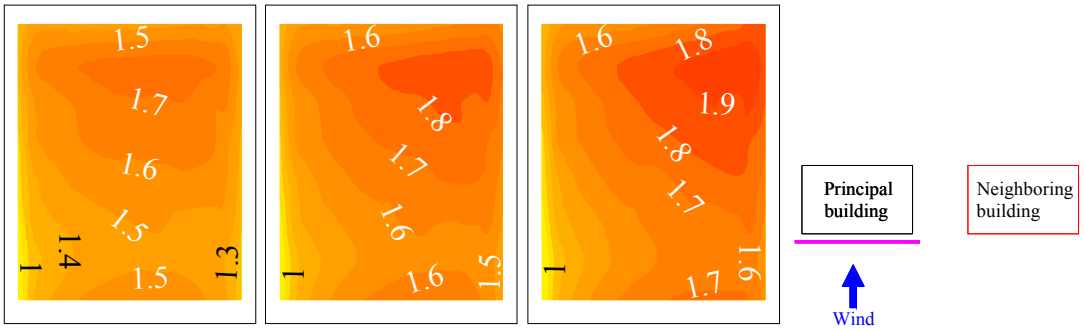

(a) *Hr*=0.5 (b) *Hr*=1 (c) *Hr*=1.5

Fig. 4.13 Mean net pressure coefficient distributions for different neighboring building height ratios of neighboring building at (X,Y)=(0, 2.4D), θ=0º, geometry I, Φ_B= 0%.

Fig. 4.13 shows the mean net pressure coefficient distributions for different neighboring building height ratios for a neighboring building at (X,Y)=(0, 2.4D) for wind direction θ=0º and geometry I. There is a clear change in which the positive mean net pressures tend to increase as the neighboring building height ratio increases. Based on Figs. 4.12 and 4.13, the increment of the neighboring building height ratio can intensify the interference effects, imposing continuous increasing or decreasing positive mean net pressures on the scaffolding.

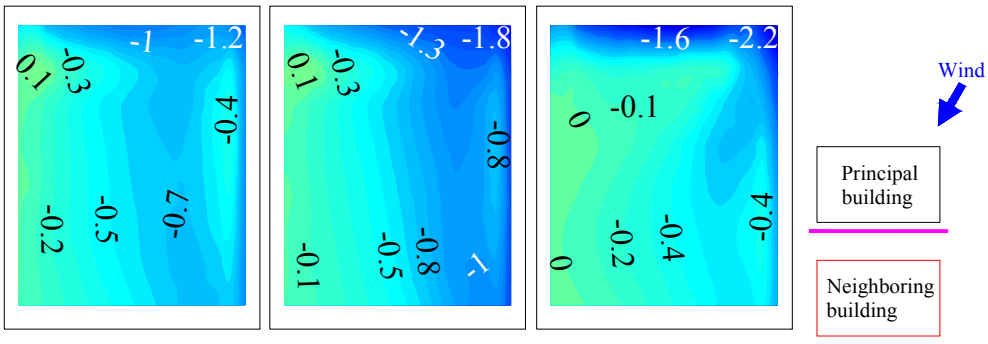

(a) *Hr*=0.5 (b) *Hr*=1 (c) *Hr*=1.5

Fig. 4.14 Mean net pressure coefficient distributions for different neighboring building height ratios of neighboring building at (X,Y)=(1.5D, 0), θ=150º, geometry I, Φ_B= 0%.

Fig. 4.14 shows mean net pressure coefficient distributions for different

neighboring building height ratios for a neighboring building at (X,Y)=(1.5D, 0) for wind direction θ=150º and geometry I. The largest negative mean net pressure coefficient is found at the top corner of the scaffolding and this value increases as the neighboring building height ratio increases. However, larger negative mean net pressure coefficients in the middle region are found when the neighboring building height ratio is 1. Therefore, the neighboring building height ratio also changes the distributions of mean net pressure coefficients.

4.3.1.3 Effects of principal building opening ratio

Fig. 4.15 shows mean pressure coefficient distributions for different principal building opening ratios for a neighboring building at (X,Y)=(1.5D, 0) for wind direction θ=45º and geometry I. Fig. 4.15 (a), (b), (c) and (d) show pressure distributions on the outer surface of the scaffolding for building opening ratios of 0%, 20%, 40% and 80%, respectively. When the building opening ratio varies from 0% to 80%, both the distributions and magnitudes of pressures on the outer surface are almost the same. Thus, building openings have almost no effect on mean pressures on the outer surface of scaffolding. Fig. 4.15 (e), (f), (g) and (h) show pressure distributions on the inner surface of scaffolding for building opening ratios of 0%, 20%, 40% and 80%, respectively. The pressure distributions show that all the largest negative pressure coefficients always occur at the top corner of the scaffolding. Moreover, negative pressures on the inner surface increase as the building opening ratio increases. When the opening ratio is 0%, wind speeds up as it flows into the gap between scaffolding cladding and building surface, leading to larger negative pressures. For other building opening ratios, wind flow inside the gap probably leaks out through the wall openings, resulting in smaller negative pressures.

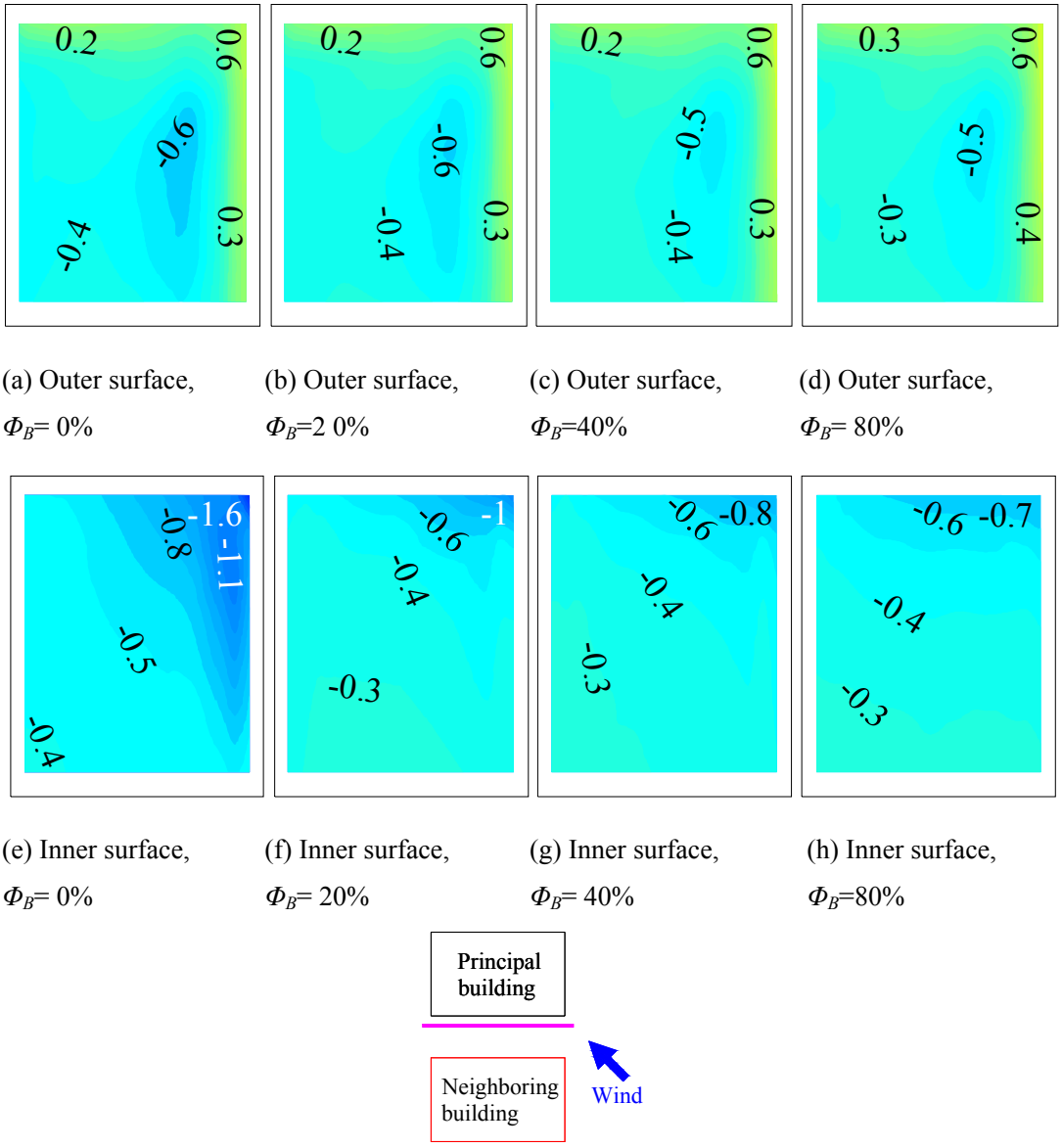

(a) Outer surface, Φ_B= 0%

(b) Outer surface, Φ_B=2 0%

(c) Outer surface, Φ_B=40%

(d) Outer surface, Φ_B= 80%

(e) Inner surface, Φ_B= 0%

(f) Inner surface, Φ_B= 20%

(g) Inner surface, Φ_B= 40%

(h) Inner surface, Φ_B=80%

Fig. 4.15 Mean pressure coefficient distributions for different building opening ratios of neighboring building at (X,Y)=(0, 1.5D), θ=45°, geometry I, Hr=1.

Fig. 4.16 shows mean pressure coefficient distributions for different building opening ratios for a neighboring building at (X,Y)=(0, 2.4D) for wind direction θ=135° and geometry I. Mean wind pressures on the outer surface of the scaffolding are the same for different building opening ratios. In Fig. 16, the principal building is located upstream. If the principal building has openings, wind can flow through the principal building. Thus, increment of building opening ratio leads to the negative pressures on the inner surface of scaffolding becoming smaller and finally turning positive.

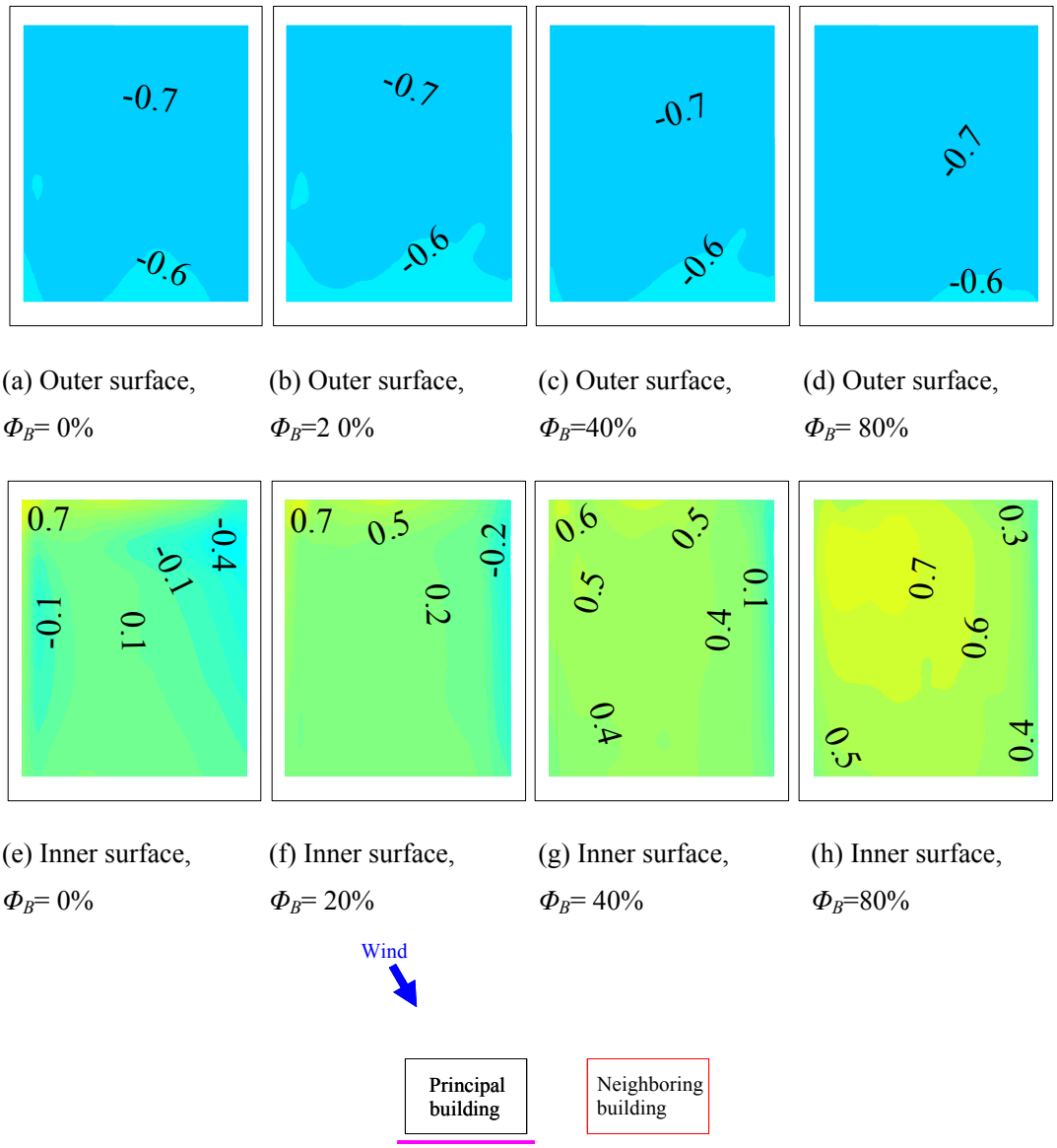

(a) Outer surface, Φ_B= 0%
(b) Outer surface, Φ_B=2 0%
(c) Outer surface, Φ_B=40%
(d) Outer surface, Φ_B= 80%

(e) Inner surface, Φ_B= 0%
(f) Inner surface, Φ_B= 20%
(g) Inner surface, Φ_B= 40%
(h) Inner surface, Φ_B=80%

Fig. 4.16 Mean pressure coefficient distributions for different building opening ratios of neighboring building at (X,Y)=(0, 2.4D), θ=135º, geometry I, Hr=1.

4.3.2 Mean panel force coefficient

Before discussion about interference effects of a neighboring building on mean panel force coefficient, the isolated condition is introduced. Fig. 4.17 shows the mean panel force coefficients ($\bar{C}_f(\theta)$) for the isolated condition for different wind directions for building opening ratio 0%. The largest positive mean panel force coefficient for all wind directions occurs for wind direction θ=0º for all scaffolding geometries, and the

magnitudes for geometries I, L and O are similar. The wind direction causing the largest negative mean panel force coefficient for all wind directions is around θ=105º for all scaffolding geometries, which is almost parallel to the scaffolding, tilting a little towards its inner surface. The largest negative value for geometry L is significantly larger than for geometries I and O. This is because of the dummy scaffolding model, which stops the wind flow and increases the positive wind pressures on the inner surface of the measured scaffolding model.

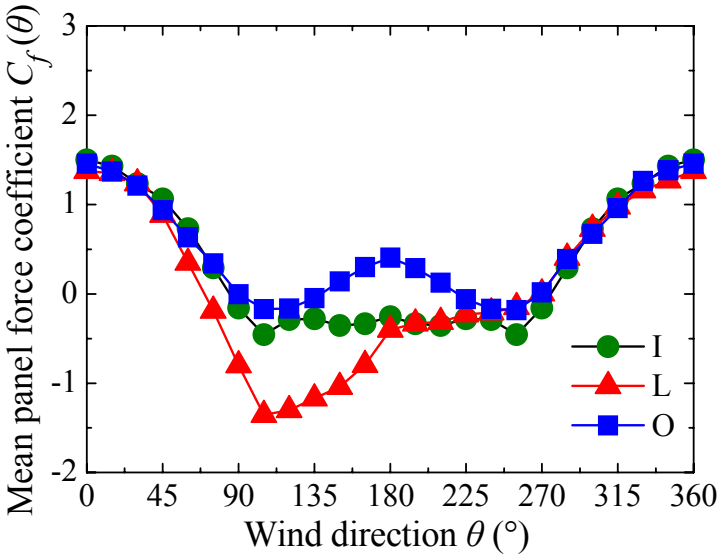

Fig 4.17 Mean panel force coefficients for entire scaffolding ($\overline{C}_f(\theta)$) of isolated condition for different wind directions, Φ_B= 0%.

4.3.2.1 Effects of neighboring building location

Fig. 4.18 shows the largest positive and largest negative mean panel force coefficients among all wind directions ($\overline{C}_{f,max}$ and $\overline{C}_{f,min}$) for different neighboring building locations (neighboring building located in front of the scaffolding or at the rear of the principal building). When the neighboring building is located in front of the measured scaffolding, the shielding effect on $\overline{C}_{f,max}$ is dramatic. $\overline{C}_{f,max}$ is obviously smaller than for the isolated case for all scaffolding geometries. When the neighboring

building is located further away, the shielding effect becomes lower and $\overline{C}_{f,max}$ becomes larger and closer to the isolated case, as shown in Fig. 4.18 (a).

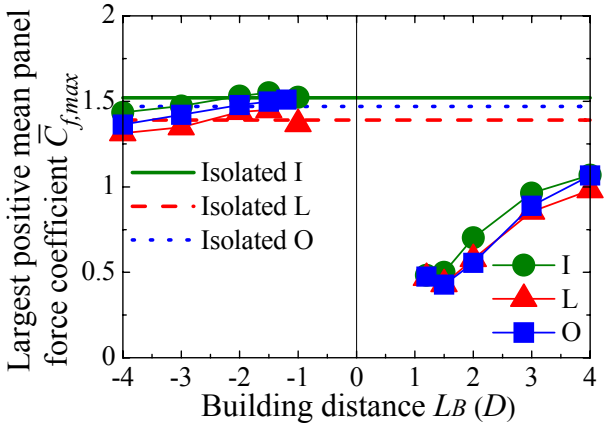

(a) Largest positive mean panel force coefficient $\overline{C}_{f,max}$

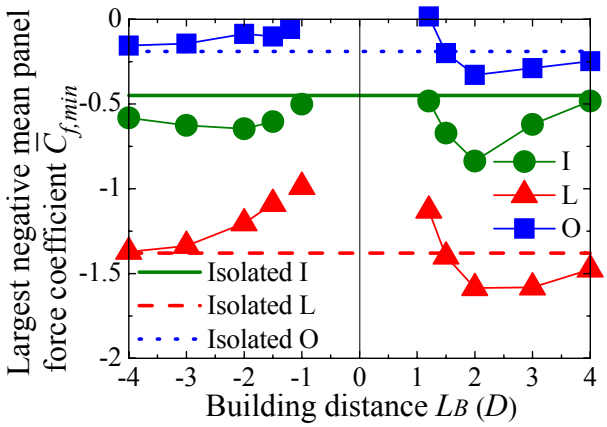

(b) Largest negative mean panel force coefficient $\overline{C}_{f,min}$

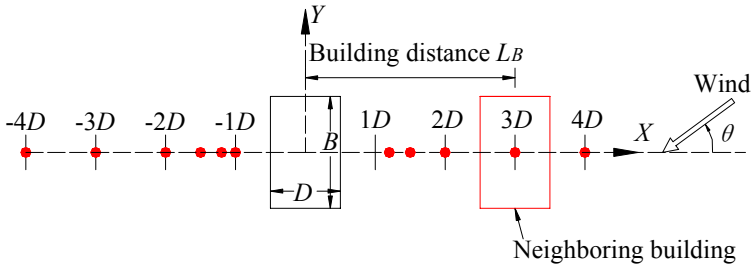

Fig. 4.18 Largest mean panel force coefficients for different neighboring building locations, (neighboring building located in front of scaffolding or at rear of principal building), Φ_B= 0%, Hr=1.

When the neighboring building is located to the rear of the principal building, interference effects on $\overline{C}_{f,max}$ are weak for all scaffolding geometries. Only when the neighboring building is located at (X,Y)=(-1.5D, 0) and (X,Y)=(-2D, 0), the $\overline{C}_{f,max}$

values are slightly larger than for the isolated conditions for geometries I and L. Fig. 4.18 (b) shows $\overline{C}_{f,min}$ for different neighboring building locations. When the neighboring building is located in front of the scaffolding, the $\overline{C}_{f,min}$ values are larger than for the isolated case as the building distance (L_B) varies from 1.5D to 4.0D. The largest negative value is found when the neighboring building is located at (X,Y)=(2D, 0) for all scaffolding geometries. When the neighboring building is located at the rear of the principal building, the $\overline{C}_{f,min}$ values are larger than for the isolated case only for geometry I. The largest negative value is found for the neighboring building at (X,Y)=(-2D, 0).

Fig. 4.19 shows the largest positive and negative mean panel force coefficients among all wind directions ($\overline{C}_{f,max}$ and $\overline{C}_{f,min}$) for different neighboring building locations (neighboring building located on left or right side of scaffolding). When the neighboring building is located on the left or right side of the measured scaffolding, the $\overline{C}_{f,max}$ values are larger than for the isolated cases, except for the neighboring building at (X,Y)=(0, 1.6D). The largest $\overline{C}_{f,max}$ is found for the neighboring building at (X,Y)=(0, 1.92D) for all scaffolding geometries. The interference effect weakens with increase of L_B, as shown in Fig. 4.19 (b). The $\overline{C}_{f,min}$ values are larger than for the isolated cases only for geometry I, also not including the case where the neighboring building is at (X,Y)=(0, 1.6D), and the interference effect weakens with increase of L_B.

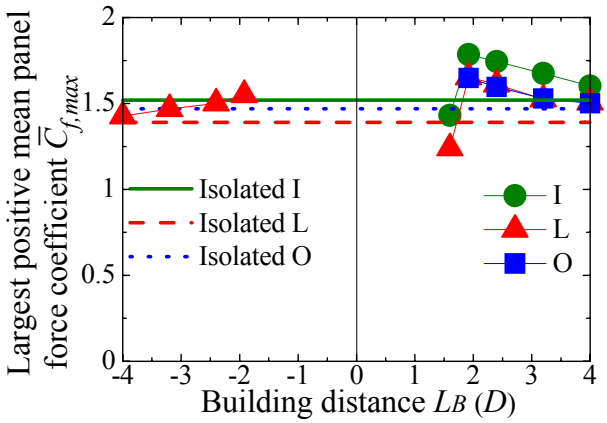

(a) Largest positive mean panel force coefficient $\overline{C}_{f,max}$

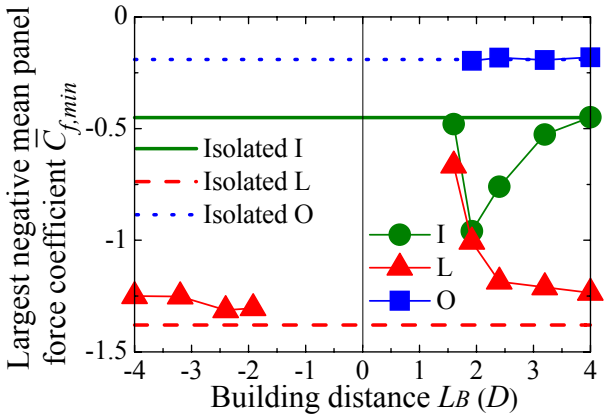

(b) Largest negative mean panel force coefficient $\overline{C}_{f,min}$

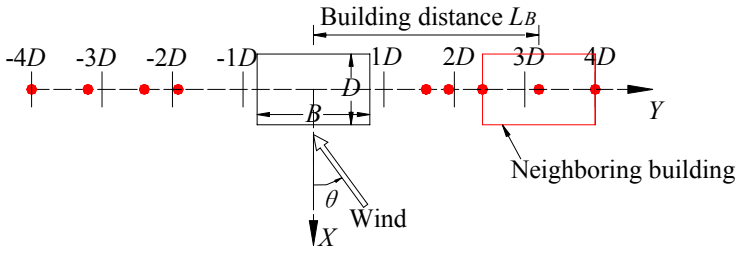

Fig. 4.19 Largest mean panel force coefficients for different neighboring building locations (neighboring building located on left or right side of scaffolding), Φ_B= 0%, Hr=1..

Fig. 4.20 shows the largest positive and negative mean panel force coefficients among all wind directions ($\overline{C}_{f,max}$ and $\overline{C}_{f,min}$) for oblique locations for geometry I. Six oblique locations were tested: locations A, B, C, D, E and F were at (X,Y)=(-2D, 3.2D), (-1.5D, 2.4D), (-1.2D, 1.92D), (1.2D, 1.92D), (1.5D, 2.4D) and (2D, 3.2D), respectively. The $\overline{C}_{f,max}$ values for the oblique locations were all smaller than for the

isolated case except for neighboring building location D, as shown in Fig. 4.20 (a). The absolute $\overline{C}_{f,min}$ values for the oblique locations were also no larger than $\overline{C}_{f,min}$ for the isolated case, except for neighboring building locations D and E. Thus, it seems that severe interference effects on $\overline{C}_{f,max}$ and $\overline{C}_{f,min}$ occur more often when the neighboring building is located in front of or beside the scaffolding.

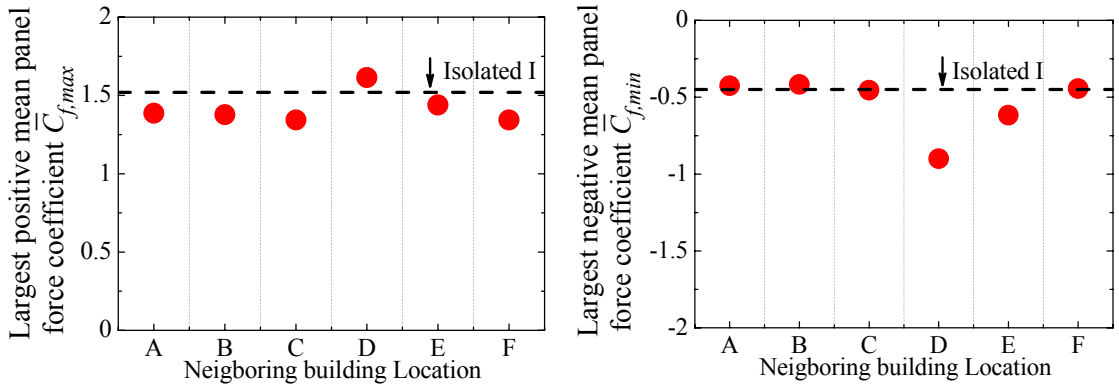

(a) Largest positive mean panel force coefficient $\overline{C}_{f,max}$.

(b) Largest negative mean panel force coefficient $\overline{C}_{f,min}$.

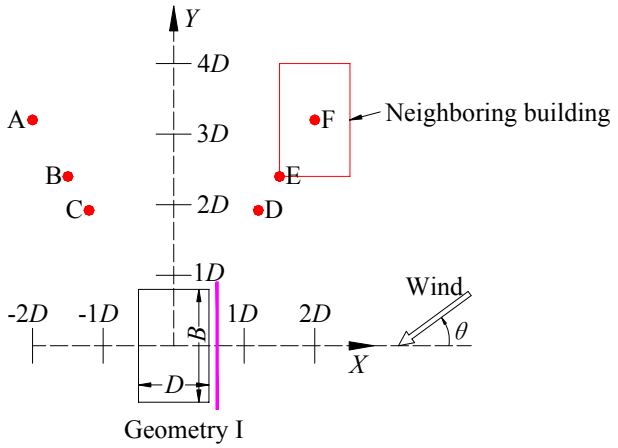

Fig. 4.20 Largest mean panel force coefficients for oblique locations，geometry I, Φ_B= 0%, Hr=1.

4.3.2.2 Effects of neighboring building height ratio

Effects of neighboring building height ratio on largest mean panel force coefficients were studied. Three neighboring building height ratios, three neighboring building locations and two scaffolding geometries were considered. As discussed in

Section 4.3.2.1, a neighboring building located in front of scaffolding can reduce the largest positive mean panel force coefficient ($\overline{C}_{f,max}$), and a neighboring building located on the left or right side of scaffolding can increase the $\overline{C}_{f,max}$ value. As shown in Fig. 4.21 (a), an increment of neighboring building height ratio intensifies interference effects such that $\overline{C}_{f,max}$ becomes larger at (X,Y)=(0, 2.4*D*) and smaller at (X,Y)=(1.5*D*, 0) for geometry I. For a neighboring building located at (X,Y)=(0,2.4*D*) for geometry I, the absolute value of $\overline{C}_{f,min}$ becomes larger as the height ratio increases, as shown in Fig. 4.21 (c). However, when a neighboring building is located at (X,Y)=(1.5*D*, 0) and (X,Y)=(-1.5*D*, 0), the largest negative $\overline{C}_{f,min}$ are found when the neighboring building height ratio is 1. Fig. 4.21 (b) and (d) shows $\overline{C}_{f,max}$ and $\overline{C}_{f,min}$ for different neighboring building height ratios for geometry O. As shown in Fig. 4.21 (b), an increment of height ratio also intensifies interference effects such that $\overline{C}_{f,max}$ becomes larger at (X,Y)=(0, 2.4*D*) and smaller at (X,Y)=(1.5*D*, 0). When the neighboring building is located at (X,Y)=(1.5*D*,0), the largest negative $\overline{C}_{f,min}$ is found when the neighboring building height ratio is 1.5, as shown in Fig. 4.21 (d). The neighboring building height ratio has almost no effect on $\overline{C}_{f,min}$ when the neighboring building is located at (X,Y)=(0, 2.4*D*). When the neighboring building is located at the rear of the principal building ((X,Y)=(-1.5*D*,0)), the absolute value of $\overline{C}_{f,min}$ decreases as the height ratio increases.

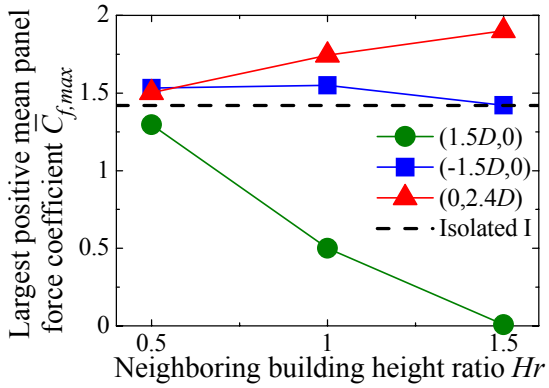

(a) Largest positive mean panel force coefficient $\overline{C}_{f,max}$, geometry I.

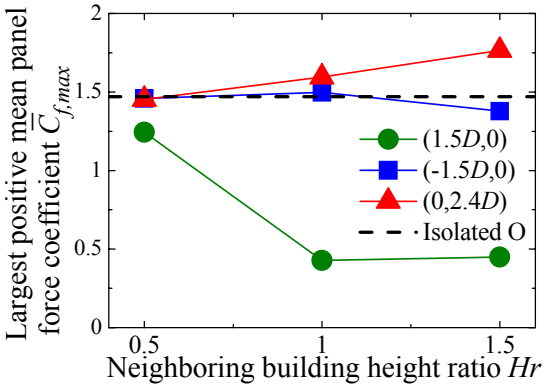

(b) Largest negative mean panel force coefficient $\overline{C}_{f,max}$, geometry O.

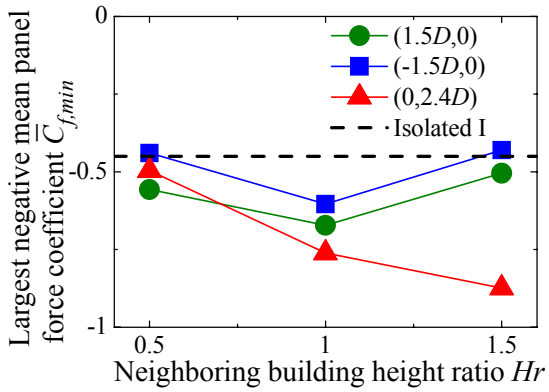

(c) Largest positive mean panel force coefficient $\overline{C}_{f,min}$, geometry I.

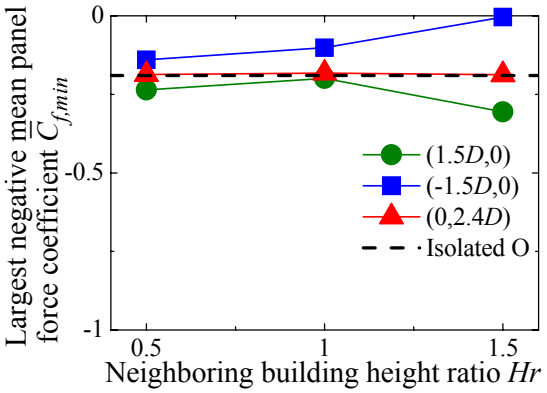

(d) Largest negative mean panel force coefficient $\overline{C}_{f,min}$, geometry O.

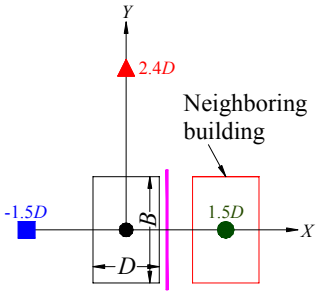

Geometry I

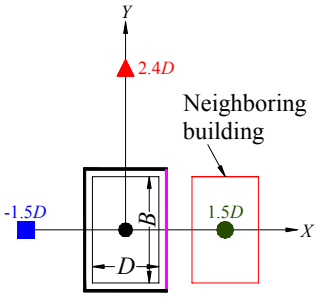

Geometry O

Fig. 4.21 Largest mean panel force coefficients for different neighboring building height ratios, Φ_B= 0%.

4.3.2.3 Effects of principal building opening ratio

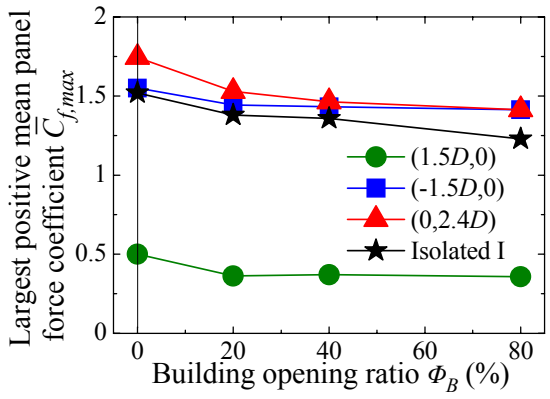

(a) Largest positive mean panel force coefficient $\overline{C}_{f,max}$, geometry I.

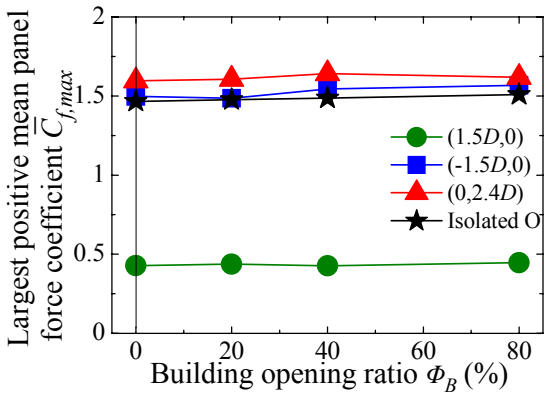

(b) Largest negative mean panel force coefficient $\overline{C}_{f,max}$, geometry O.

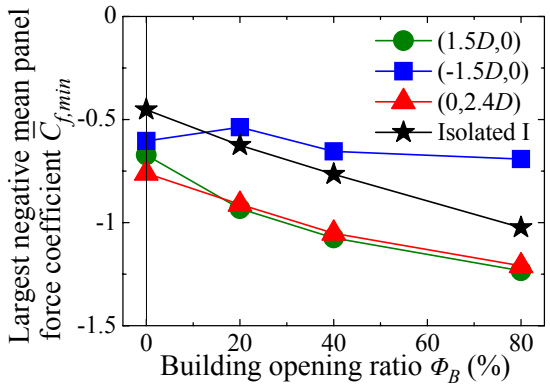

(c) Largest positive mean panel force coefficient $\overline{C}_{f,min}$, geometry I.

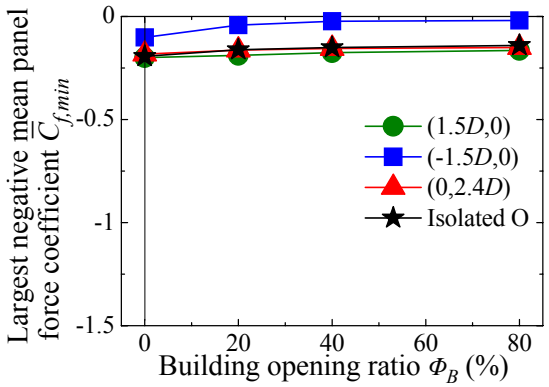

(d) Largest negative mean panel force coefficient $\overline{C}_{f,min}$, geometry O.

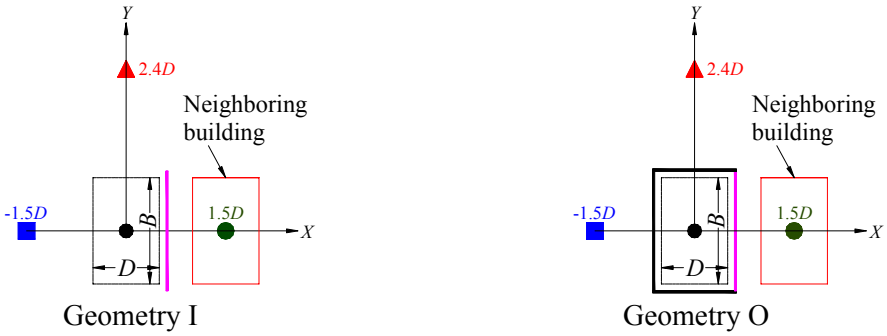

Fig. 4.22 Largest mean panel force coefficients for different building opening ratios, *Hr*=1.

As discussed, building openings can have significant effects on mean wind pressure distributions on the inner surface of scaffolding. Fig. 4.22 shows the largest positive and negative mean panel force coefficients among all wind directions ($\overline{C}_{f,max}$ and $\overline{C}_{f,min}$) for different building opening ratios for scaffolding geometries I and O,

respectively. For all three neighboring building locations and geometry I, $\overline{C}_{f,max}$ becomes smaller and the absolute value of $\overline{C}_{f,min}$ becomes larger when the building opening ratio increases. Building openings lead to larger positive pressures on the inner surface and smaller negative pressures on the inner surface. For geometry O, the largest mean panel force coefficient seems barely affected by the building openings. Both $\overline{C}_{f,max}$ and $\overline{C}_{f,min}$ remain almost the same for all opening ratios. This is because the scaffolding entirely encloses the principal building, so the building openings can not affect the wind pressures on the inner surface.

4.3.3 Two neighboring buildings

Interference effects of two neighboring building were also studied. For each scaffolding geometry, two neighboring building arrangements were considered. Neighboring buildings arrangement F&R is the two neighboring building are located at (X,Y)=(1.5D,0) and (X,Y)=(-1.5D,0), respectively. Neighboring buildings are located in front of measured scaffolding and at the rear of principal building. Neighboring buildings arrangement L&R is the two neighboring building are located at (X,Y)=(0, 1.92D) and (X,Y)=(0, -1.92D), respectively. Neighboring buildings are located on left and right side of measured scaffolding. Detailed arrangements are in Fig. 4.23.

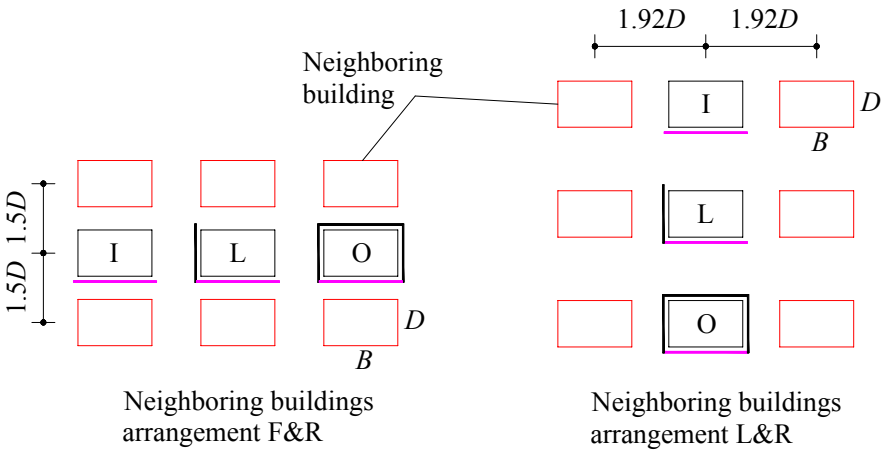

Fig. 4.23 Two neighboring building arrangements.

The largest positive mean panel force coefficient ($\overline{C}_{f,max}$) for neighboring buildings arrangement F&R is smaller than for isolated case for each scaffolding geometry. It is mainly because one the neighboring building is located in front of the measured scaffolding resulting in the shielding effect. For all scaffolding geometries, $\overline{C}_{f,max}$ are larger than for the isolated cases when the two neighboring buildings are located on left and right side of the scaffolding, which are similar to the results of with one neighboring building, as shown in Fig. 4.24(a).

The largest negative mean panel force coefficient ($\overline{C}_{f,\min}$) for geometry I is always larger than for isolated case and smaller than for isolated cases for geometries L and O due to the two neighboring buildings. In Fig. 4.24(b), $\overline{C}_{f,\min}$ for two neighboring buildings for each scaffolding geometry shows similar results of for only one neighboring building which discussed in Section 4.3.2.1. It is seems that the interference effects on $\overline{C}_{f,\min}$ of two neighboring building are no more severe than for only one neighboring building in these neighboring building arrangements.

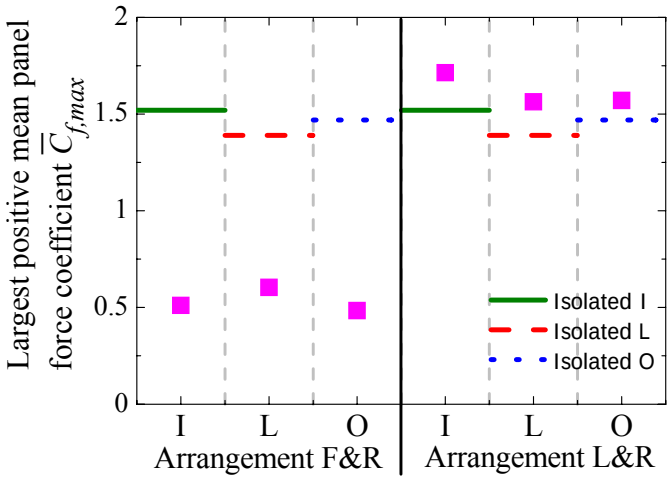

(a) Largest positive mean panel force coefficient $\overline{C}_{f,max}$

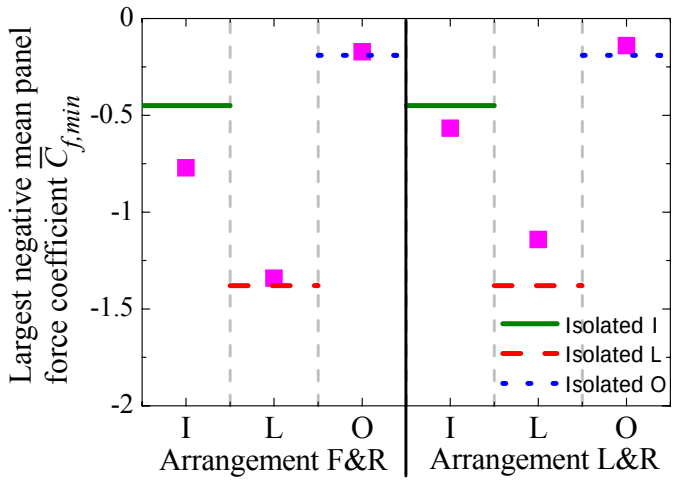

(b) Largest negative mean panel force coefficient $\overline{C}_{f,min}$

Fig. 4.24 Largest mean panel force coefficient for two neighboring buildings.

4.4 Summary

Interference effects of a neighboring building on wind loads on nonporous sheet-clad scaffolding were investigated by wind tunnel experiments. Three scaffolding geometries, four building opening ratios, three neighboring-building height ratios and different neighboring-building locations were studied.

(1) When the neighboring building is located in front of the measured scaffolding, the positive mean panel force coefficients decrease significantly, and the negative mean panel force coefficients increase. When the neighboring building is located on the left

or right side of the measured scaffolding, the positive mean panel force coefficients are greater than those for the isolated case.

(2) The increment of neighboring building height ratio dramatically intensifies the interference effects, continuously increasing or decreasing the largest mean panel force coefficients.

(3) For geometry I, the largest positive mean panel force coefficient tends to become smaller and the largest negative mean panel force coefficient tends to become larger when the building opening ratio increases. For geometry O, the building opening ratio barely affects the mean panel force coefficient of the scaffolding because the scaffolding completely encloses the principal building.

CHAPTER V : PEAK TENSILE FORCES IN TIE MEMBERS

5.1 Introduction

Tie member is the component of scaffolding which connecting scaffolding and the principal building. Tie members are mainly contributing to the horizontal stability of scaffolding and preventing scaffolding from collapse. The tensile force in tie members induced by wind loads imperil the horizontal stability of scaffolding strongly. The failure of tie member may cause severe casualties and losses. Different recommendations for scaffolding ties state different requirements of tying pattern of tie members.

Safety and technical code and for frame scaffoldings with steel tubules in construction (JGJ-128, 2000) states that the horizontal distance between ties should be no larger than 4m for sheeted scaffolding. When scaffolding does not completely enclosed the principal building, more ties are needed at the side edge or corner of scaffolding and the vertical distance between ties should be smaller than 4m. Furthermore, technical code for safety of steel tubular scaffold with couplers in construction (JGJ-130, 2011) states that the vertical spacing of ties should also smaller than floor height.

Façade scaffolds made of prefabricated components (BS EN 12810, 2003) gives

the examples for typical tying patterns for tie members, as shown in Fig. 5.1. They state that it is preferable for the tie free zone to be twice the normal distance between working levels. The requirement for a tie free zone is to ensure that scaffold has sufficient strength integral in the design.

Ordinance on Industrial Safety and Health (by Japan International Center for Occupational Safety and Health) suggests for prefabricated scaffolding that the distances between two ties should less than 8m in horizontal and 9m in vertical. For tube and coupler scaffolding, the distances between two ties should less than 5.5m in horizontal and 5m in vertical which tie free zone almost equal to six typical scaffold units.

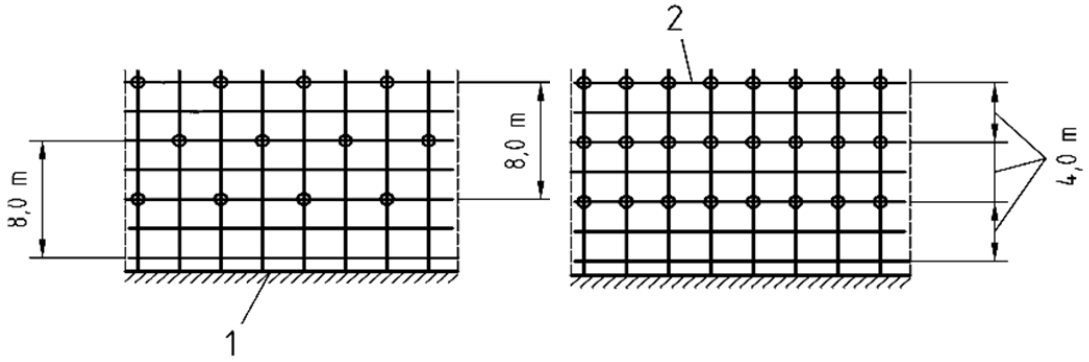

(a) Typical taggered tying pattern. (b)Typical continus horizontal tying pattern.

Fig. 5.1 Examples for typical tying patterns given by BS EN 12810.

Three kinds of tying pattern of scaffolding ties are discussed in this chapter. Each tie member corresponding to two scaffold units, four scaffold units and six scaffold units, as Fig. 5.2 shown. Two scaffold units represent one tie for one-bay-two-stories scaffolds. Four and six scaffold units represent one tie for two-bays-two-stories scaffolds and three-bays-two-stories scaffolds, respectively.

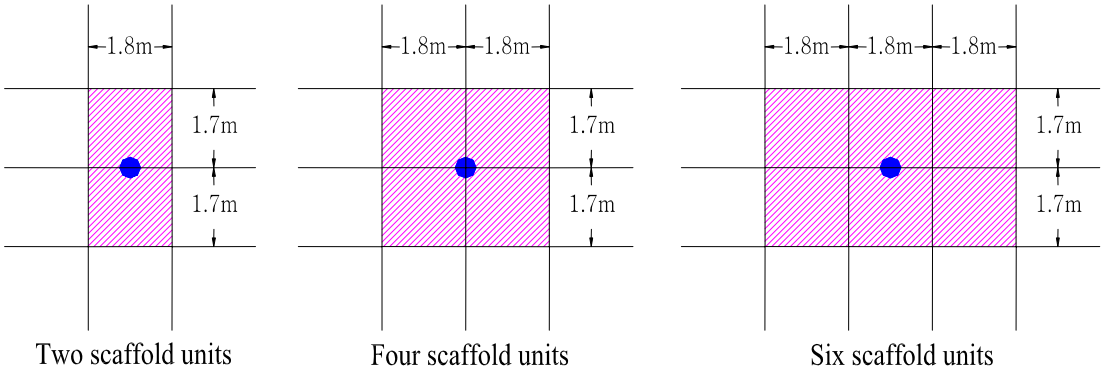

Fig. 5.2 Configurations of different tying patterns.

5.2 Analytical methods

5.2.1 Estimation of wind forces in tie members

Based on wind tunnel experimental data, external force acting on each tie member can be estimated by a pressure integration method. As mentioned, net wind pressure coefficient at time *t* at pressure tap *i* is calculated by equation (5.1).

$$C_{p\text{-}net}(i,t) = C_{p\text{-}outer}(i,t) - C_{p\text{-}inner}(i,t) \tag{5.1}$$

$C_{p-net}(j,t)$ is the wind net pressure coefficient at time *t* at scaffold unit *j* which can be interpolated and extrapolated using the "Biharmonic spline interpolation" method (David T. Sandwell,1987). The scaffolding elevation is shown in Fig. 5.3, the blue solid dots indicate the centers of scaffold units, and the black circles represent the pressure taps. Tie free zone in Fig.5.3 is two scaffold units

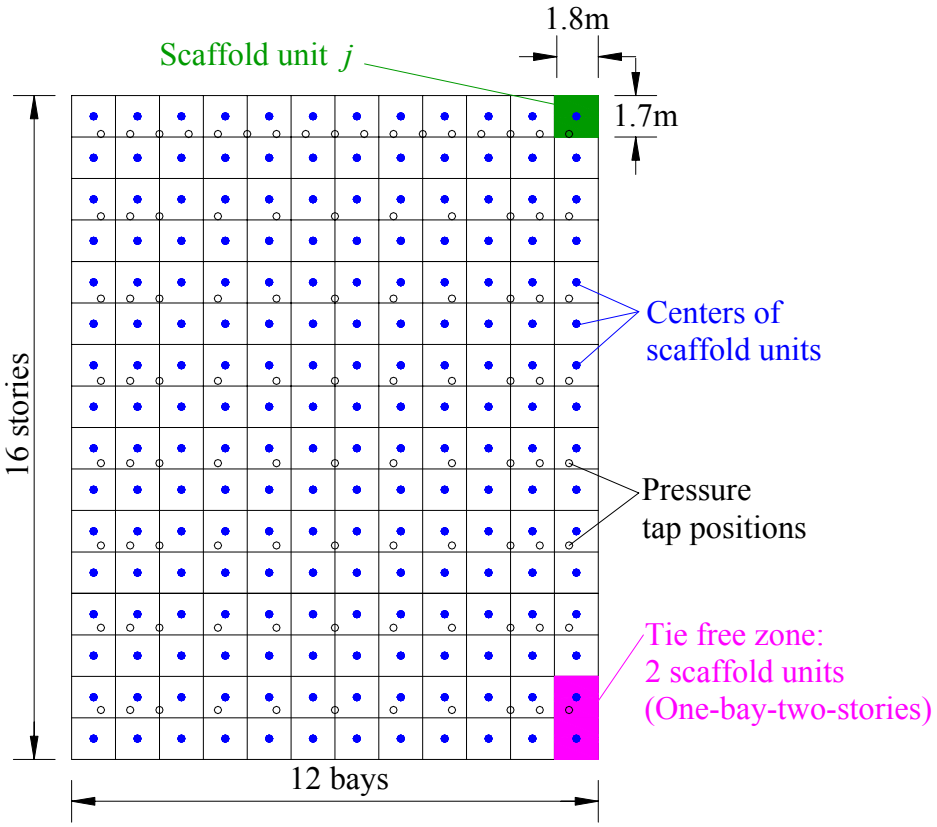

Fig. 5.3 Elevation of scaffolding and definition for tie free zone.

The wind force (external force) at time *t* acting on scaffold unit *j* can be calculated by equation (5.2):

$$F(j,t)=\frac{1}{2}\rho U_H^2 C_{p-net}(j,t)\times A(j) \tag{5.2}$$

where *A(j)* is the projected area of scaffold unit *j*. Design mean wind speed at building top is 30m/s for 50-year recurrence. Based on the design standards (BS EN 12811, 2003 and JGJ 128, 2000), a factor of 0.7 should be applied for the 50-year recurrence wind speed, finally, U_H=0.7×30m/s=21m/s was used.

An "Equivalent time averaging" method was used and a moving average time τ (Holmes, 1997) was calculated as:

$$\tau=1.0\times L/U_H \tag{5.3}$$

where *L* is the length of the diagonal for a scaffold unit of principal scaffolding in full scale. The dimensions of a scaffold unit were 1.7m×1.8m in the windward direction,

making L = 2.5m. In this study, 0.0039s corresponding to 0.12s in full scale was used for time averaging.

For one tie member, the wind force time history is calculated as sum of wind force time histories at two, four and six scaffold units. In each tie free zone, the tie is assumed to be located in the center of the zone. The whole scaffolding structure is divided into same size zones. Besides, the top part of scaffolding (higher than the building) is usually fixed on building top by the slant shoring bars in real engineering construction. This study focuses on external forces acting on tie members. The top part of scaffolding is also assumed as using horizontal tie members.

5.2.2 Evaluation of peak tensile force

Negative wind net pressures can result in tensile forces on scaffolding tie members, which may lead to outward collapse. The peak tensile forces were calculated by the "Cook-Mayne method" (Cook and Mayne, 1979) using the equation:

$$\hat{F} = U_{\hat{F}} + 1.4 / a_{\hat{F}} \tag{5.4}$$

where $U_{\hat{F}}$ and $1/a_{\hat{F}}$ are the mode and dispersion of the extreme distribution of tensile forces, respectively, which can be calculated by the Best Linear Unbiased Estimators (BLUE) as:

$$U_{\hat{F}} = \sum_{k=1}^{10} a_k \hat{F}_k \qquad 1/a_{\hat{F}} = \sum_{k=1}^{10} b_k \hat{F}_k \tag{5.5}$$

where, $\hat{F}_k$ is the kth value of the ascending array of maximum values of 10 samples of peak tensile forces and a_k and b_k are the BLUE coefficients.

5.3 Results and discussions

5.3.1 Effects of building opening ratio

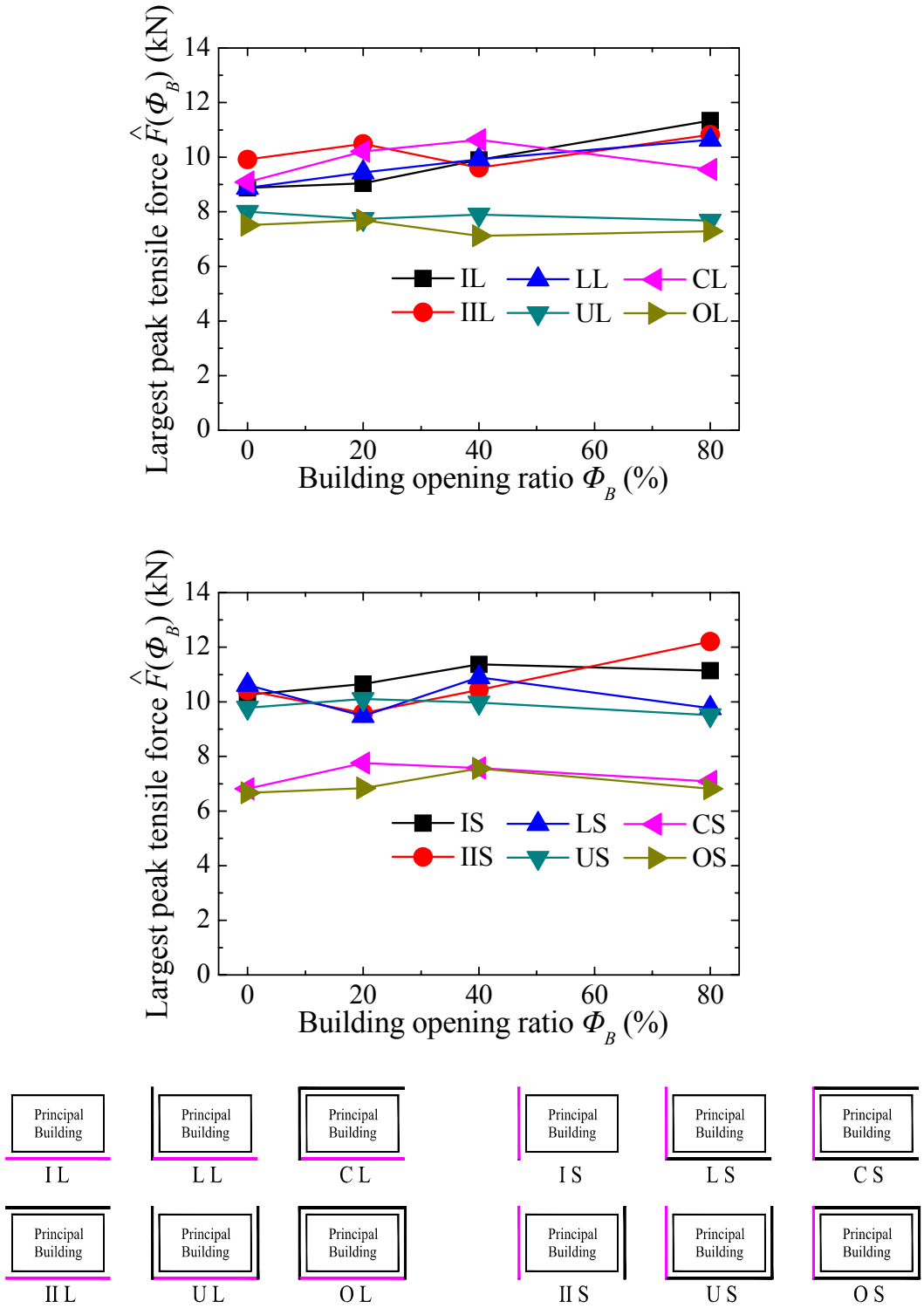

Fig. 5.4 Largest peak tensile force ($\hat{F}(\Phi_B)$) for different building opening ratios, 2 scaffold units, V_H=21m/s.

Fig. 5.4 shows the Largest peak tensile force ($\hat{F}(\Phi_B)$) for two scaffold units for different building opening ratios. For each case, the largest peak tensile force for all tie members and all wind directions for building opening ratio Φ_B was chosen. Geometries UL, OL, CS and OS are the situations that both two sides of scaffolding connecting to the scaffolding which located at adjacent building sides. $\hat{F}(\Phi_B)$ For this four geometries are obvious smaller than others. Besides, $\hat{F}(\Phi_B)$ has very little change with the increment of building opening ratio. For other geometries, $\hat{F}(\Phi_B)$ become larger when building opening ratio increasing from 0% to 80%.

A slight difference is that the change tendencies for geometries IL, IIL, IS and IIS are more significant. One side of scaffolding connecting to the scaffolding located at the adjacent building side for geometries LL, CL, LS and US, which decreases $\hat{F}(\Phi_B)$ in tie members.

5.3.2 Effects of scaffolding geometry

Fig. 5.5 shows the largest peak tensile force ($\hat{F}$) for different scaffolding geometries. For each case, the largest peak tensile force ($\hat{F}$) for all tie members, all wind directions and all building opening ratios was chosen. For the cases of tie free zone is two scaffold units, $\hat{F}$ for geometries UL, OL, CS and OS are obvious smaller due to the scaffolding located at the adjacent building sides. $\hat{F}$ for geometries IL, IIL, IS and IIS are a little bit larger than for geometries LL, CL, LS and US when $\hat{F}$ represents two scaffold units. But when $\hat{F}$ represents six scaffold units which means a larger region, $\hat{F}$ for geometries LL, CL, LS and US are significant larger than for

geometries IL, IIL, IS and IIS. Thus, when scaffolding geometry is that both two sides of scaffolding are free (no adjacent scaffolding), peak tensile force for a quite small area is the largest.

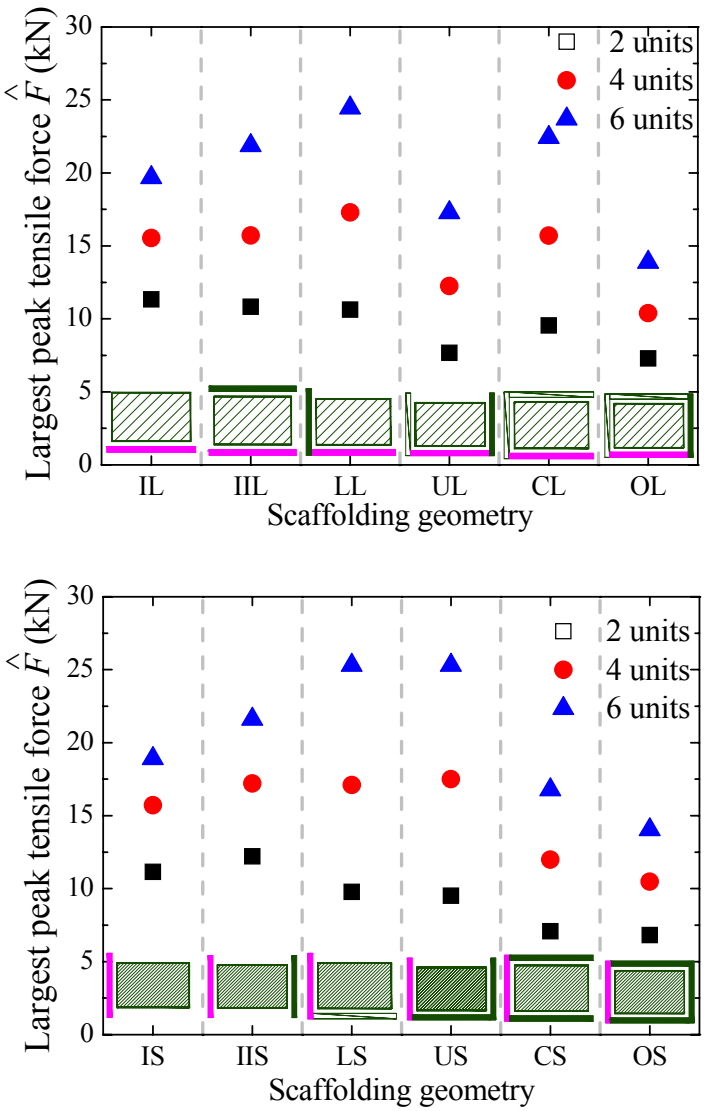

Fig. 5.5 Largest peak tensile force ($\hat{F}$) for different scaffolding geometries, V_H=21m/s.

When only one side of scaffolding is free, peak tensile force for a larger area is the greatest. When both two sides of scaffolding connecting to the scaffolding which located at adjacent building sides, peak tensile forces in ties are smaller. In other word, geometries IL, IIL, IS and IIS generate the greatest $\hat{F}$ but only for quite limited area. Geometries LL, CL, LS and US can influence larger area on scaffolding for suffering

tensile force.

5.3.3 Effects of turbulence intensity

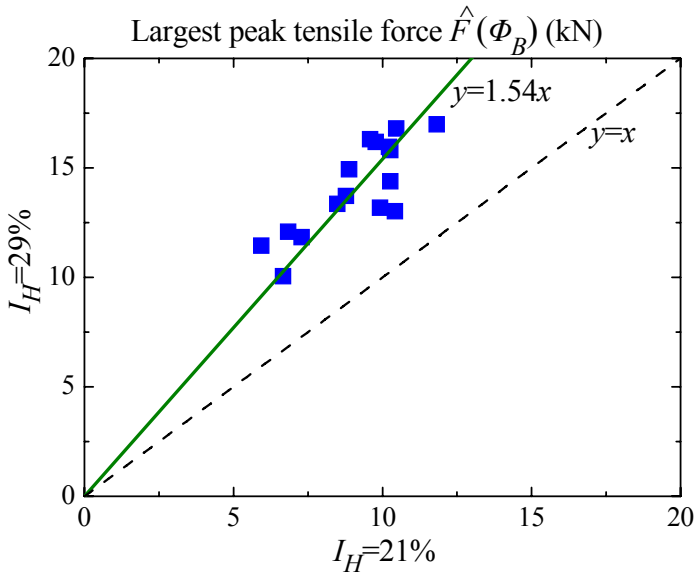

Fig. 5.6 Comparison of largest peak tensile force ($\hat{F}(\Phi_B)$) between different terrain categories, V_H=21m/s.

Fig. 5.6 shows the comparison of largest peak tensile force ($\hat{F}(\Phi_B)$) between different terrain categories. As discussed in chapter two, the increase of turbulence intensity leads to larger peak wind loads on scaffolding. From I_H=21% to I_H =29%, $\hat{F}(\Phi_B)$ for all cases are increase and the increments are around 54%. The increments of $\hat{F}(\Phi_B)$ are caused by the effects of turbulence intensity which increases from 21% to 29%.

5.3.4 Comparison to related design recommendations

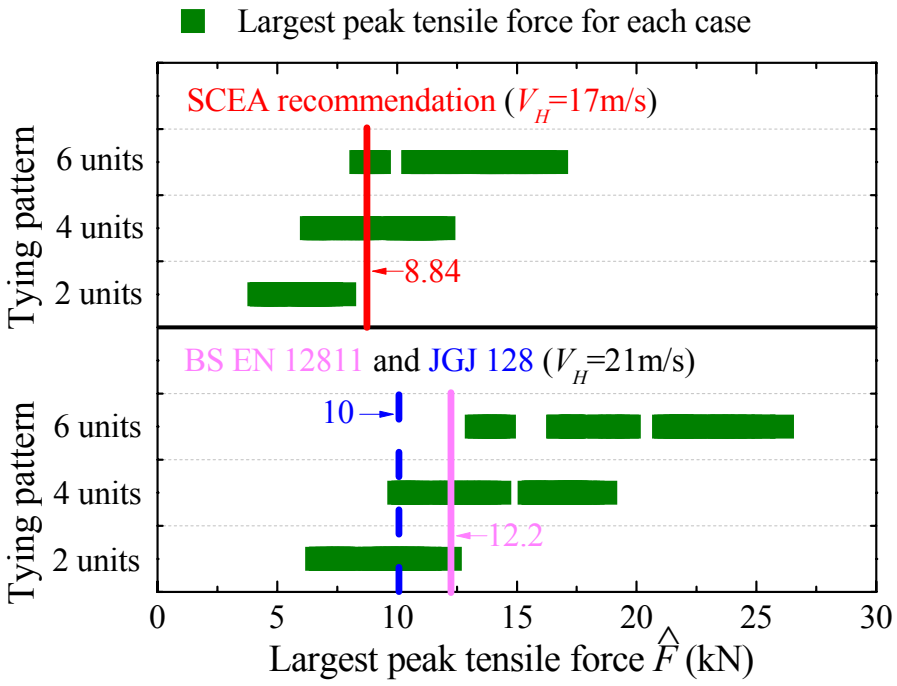

Fig. 5.7 Comparison of largest peak tensile forces ($\hat{F}(\Phi_B)$) and strength requirement of tie members.

BS EN 12811 and JGJ 128 provide requirements about the strength of tie members, the strength should be larger than 12.2kN and 10kN, respectively. Safety technical guideline for scaffolding to wind loads (by Scaffolding and Construction Equipment Association of Japan) suggests that the strength of tie should consider a safety factor of 2.0. Allowable tensile force for tie member is 4.41kN, so the requirement of tie strength is 8.82kN. BS EN 12811 and JGJ 128 recommend the design wind speed of 50-year recurrence by multiplying a reduced factor 0.7 which is 21m/s in this study. However, SCEA recommendations suggest the design wind speed of scaffolding is 1-year recurrence which is 17m/s in this study.

Fig. 5.7 shows the comparison of $\hat{F}(\Phi_B)$ and strength requirements of tie members. When tie free zone is four or six scaffold units, the largest peak tensile forces exceed the strength requirements. Almost all the design recommendations do not

specify the condition of scaffolding with nonporous cladding which increasing wind loads on scaffolding dramatically. Even if the free zone of tie is only for two scaffold units, failures still can be found in some cases.

5.3.5 Effects of tying pattern

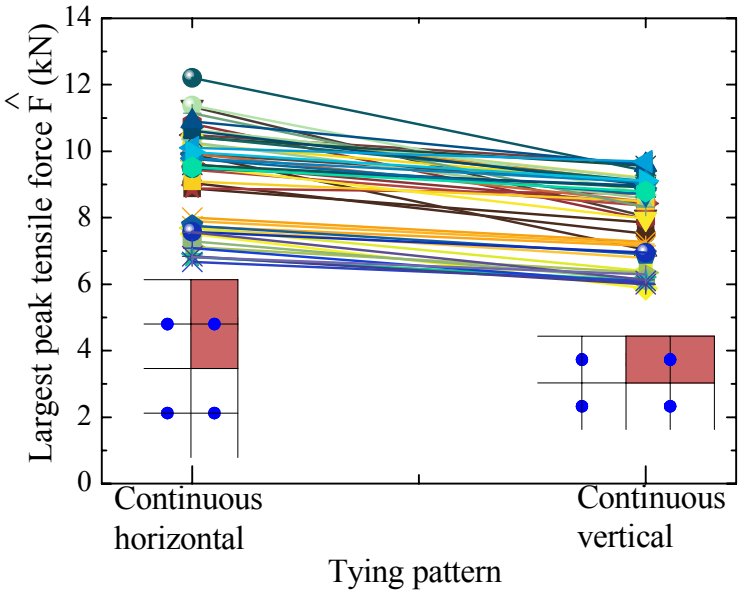

Fig. 5.8 Comparison of largest peak tensile forces ($\hat{F}(\Phi_B)$) between different tying patterns, V_H=21m/s.

Even if the area of tie free zone is the same, different tying patterns may also have effect on $\hat{F}(\Phi_B)$. For example, when free zone of tie is two scaffold units, the tying pattern can be continuous horizontal tying pattern (one tie for one-bay-two-stories) or continuous vertical tying pattern (one tie for two-bays-one-storey). Fig. 5.8 shows the comparison of largest peak tensile forces ($\hat{F}(\Phi_B)$) between different tying patterns. $\hat{F}(\Phi_B)$ for continuous vertical tying pattern is always smaller than for continuous horizontal tying pattern. The largest local peak net pressure coefficient distribution for each scaffolding geometry is studied in chapter three. The largest local peak pressures are usually found at the side edge of scaffolding. When continuous vertical tying

pattern is taken, more tie members are fixed at the side edge of scaffolding. Thus, vertical tying pattern diminish the largest peak tensile force among all tie members.

5.4 Finite element model analysis

Wind forces acting on scaffolding tie members were estimated by pressure integration method, which are the external forces. In real engineering construction, the boundary conditions could have significant effects on the internal forces in structural components. In this study, finite element model analysis was conducted to study the effects of boundary conditions on wind forces in tie members.

5.4.1 Finite element models

In this study, ANSYS software was used for the finite element modeling and analysis. The analytical scaffolding was assembled by using typical door-type tubular-steel scaffold units 1.7m high, 0.9m wide and 1.8m in span (one-bay). The prototype scaffolding was 27.2m high, and comprised sixteen stories. The scaffolding was 3.4m (two-stories) higher than the principal building. The prototype scaffolding was 19.2m wide, and comprised twelve spans. The lengths of tie members were 0.3m in full scale. Based on the equivalent stiffness theory, which means the scaffold has same displacement under same loads, the scaffolding frames were simplified, as shown in Fig. 5.9. This study is mainly focusing on wind loads which are horizontal, so only equivalent horizontal stiffness was considered. The original vertical and horizontal pipe of scaffold is steel tube which diameter is 42.7mm and thickness is 2.5mm. After simplification, the reinforced pips were removed and only the vertical pipe changed into steel bar of 45.3mm in thick. The tie members are steel bar which is solid and the diameter is 27mm. The X-bracings were ignored in this study.

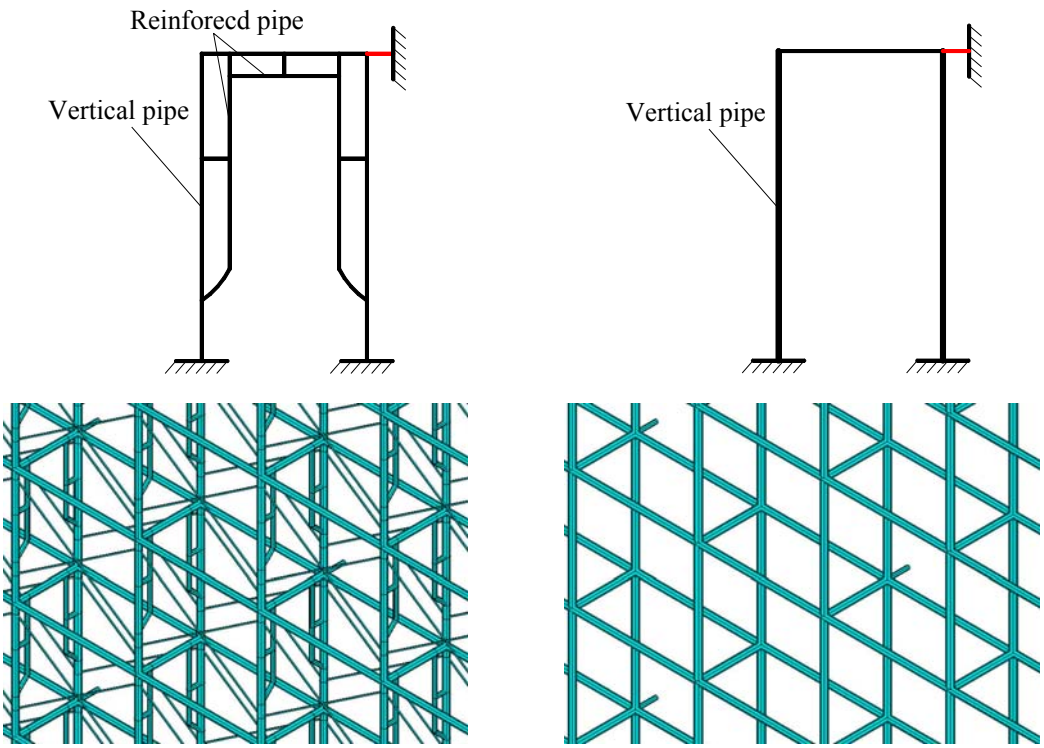

(a) Before simplification (b) After simplification

Fig. 5.9 Analytical model simplification.

A 3-D beam element, BEAM188, was chosen to model the scaffolding frames. This beam element also had 6 degrees of freedom per node. The vertical connection of different scaffolding layers was considered as a kind of half-rigid connection, which released the vertical torsion degree of freedom (ROT Z).

The tie members were rigid fixed into the building wall except the tie members for the top two scaffold stories (higher than the building top). Three models were created for different boundary conditions. In Model 1, the top two scaffold stories were fixed on the building top by a slant shoring bar (solid and the diameter is 27mm), as shown in Fig. 5.10. Base constraints were considered as pin constraint which only 3 degrees (UX, UY and UZ) were constrained, all the torsion degrees of freedom were released. Tie member positions on the scaffolding were every two spans and two stories.

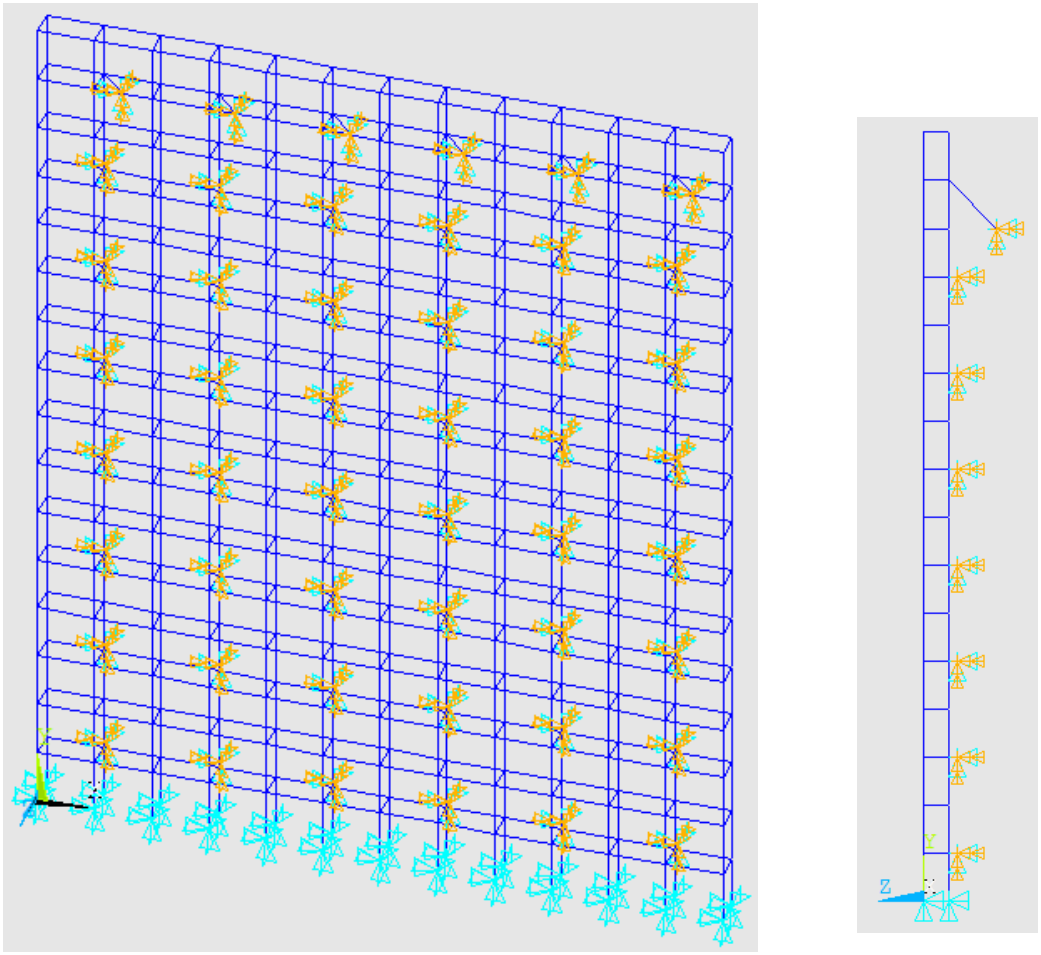

(a) 3-D view of Model 1 (b) Elevation

Fig. 5.10 Finite element Model 1.

Table 5.1 Top and base boundary conditions of finite element models.

	Model 1	Model 2	Model 3
Top condition	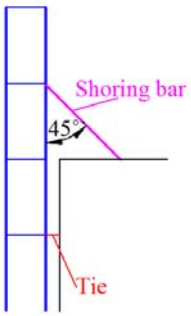 Shoring bar	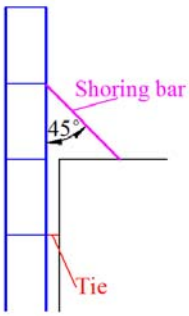 Shoring bar	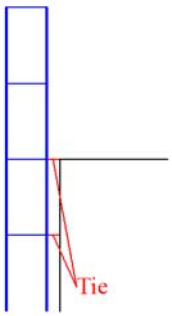 Tie member
Base constraint	Pin constraint	Rigid constraint	Pin constraint

Model 2 and 3 are only different to Model 1 for the top and base boundary conditions, as shown in Table 5.1. Model 1 and 2 are both using the slant shoring bar

for the top constraint, but the base constraint for Model 2 is rigid fixed. Model 3 has the same base constraint as Model 1, but the shoring bar at the top was changed into a tie member located at the same height of building top, and the top two scaffold stories are free.

5.4.2 Analysis results and discussions

The time-history analysis for the scaffolding was carried on by using the Transient Analysis Module in ANSYS. Loading time is ten 3-minutes in full scale. Damping ratio of the scaffolding is assuming as 5%. Wind net pressure coefficients were obtained from wind tunnel experiment. The wind velocity on the top of the model U_H is set to 21m/s. Wind loads on finite element model's nodes were interpolated and extrapolated by using "Biharmonic spline interpolation" method (David T. Sandwell,1987). The peak tensile forces were calculated by the "Cook-Mayne method" (Cook and Mayne, 1979).

One typical severe case of building opening ratio 80% for geometry LL and wind direction θ=95º was taken as the example for the study of finite element model analysis. Tie free zones are four scaffold units. Fig. 5.11 shows the peak tensile force distributions between Model 1 and the calculation result by pressure integration method. The black dots represent the position of tie members and shoring bars on scaffolding. The peak tensile forces of top part in Model 1 are larger, which is because of the shoring bars. Wind loads are horizontal and the shoring bars are 45 º down, which increase the internal forces in the shoring bars. The peak tensile forces of lower part in Model 1 are smaller because of the base boundary condition. The base constraint also resists the horizontal wind loads.

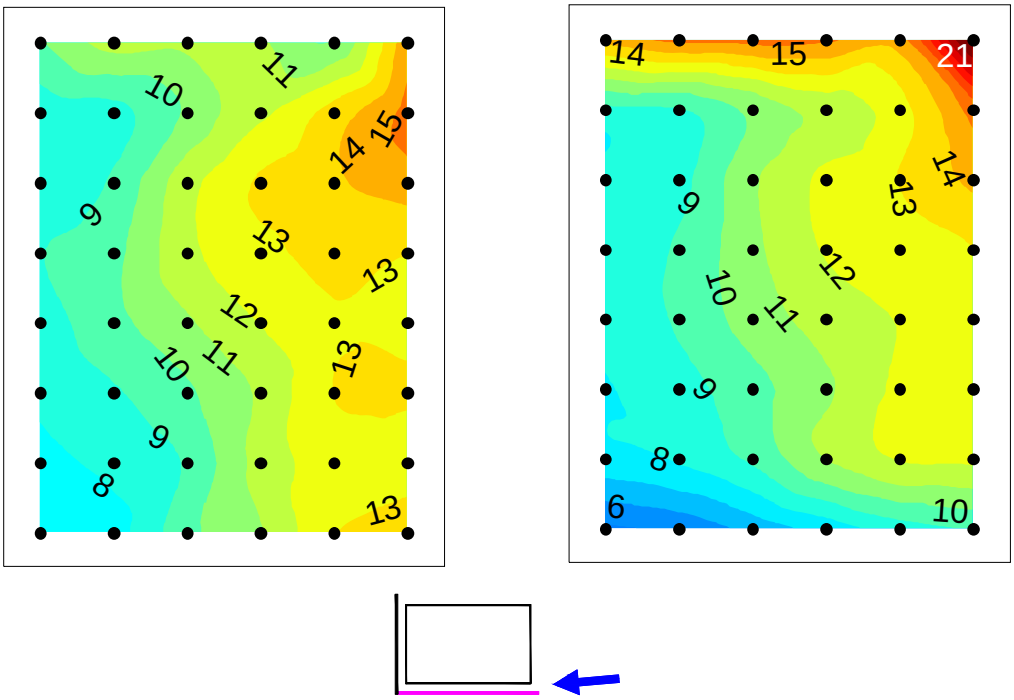

(a) Pressure integration method (b) Finite element model analysis (Model 1)

Fig. 5.11 Peak tensile force distributions between pressure integration method and finite element model analysis (unit: kN), geometry LL, θ=95°, U_H = 21m/s, tie free zone: four scaffold units.

Tie members were arranged into eight layers for different heights. The largest peak tensile force in each layer was picked out to compare. From the peak tensile force distributions (Fig. 5.11), the largest values are always found at the side edge of scaffolding because of wind direction wind direction θ=95° and scaffolding geometry LL. Fig. 5.12 shows the largest peak tensile force of each tie layer (different heights) for finite element Model 1 and Model 2. In each tie layer (tie members at same height), the largest peak tensile force was selected. As mentioned, the only difference between Model 1 and Model 2 is the base constraint. The results are almost same between the two models. The pin constraint and rigid constraint do not result in much difference for the peak tensile forces in tie members.

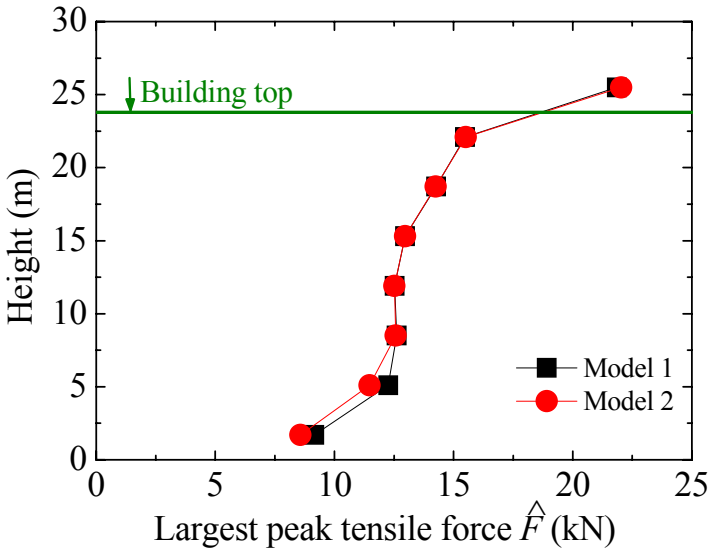

Fig. 5.12 Largest peak tensile force of each tie layer (different heights) for finite element Model 1 and Model 2.

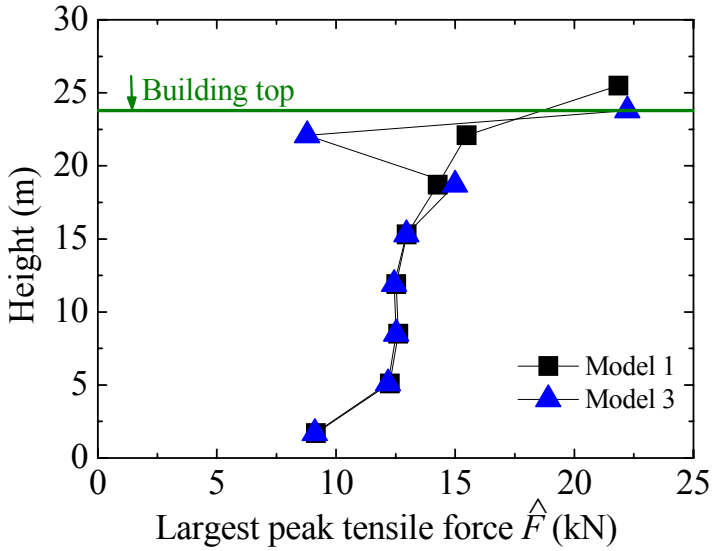

Fig. 5.13 Largest peak tensile force of each tie layer (different heights) for finite element Model 1 and Model 3.

Model 1 and Model 3 are different in the top condition. The top tie members are down to the building roof in model 3. The peak tensile forces in the second tie layer (counting from top) become smaller because the top tie members shared part of the wind loads, as shown in Fig. 5.13. Even suffered same wind loads, the internal force in the shoring bar should much larger than tie member. It is because the shoring bar is slant and long. However, The largest peak tensile force at the top layer in Model 3 which

using tie member still larger than in Model 1 which using slant shoring bar, which mainly due to the free top two scaffold stories.

5.5 Summary

IF both two sides of scaffolding are free (not connecting to other scaffolding which is placing at adjacent building sides), peak tensile force is the largest when the free zone of tie is quite small. When only one side of scaffolding is free, peak tensile force for a larger area is the greatest. When both two sides of scaffolding connecting to the scaffolding which located at adjacent building sides, peak tensile forces in ties are smaller than for other scaffolding geometries.

For most scaffolding geometries, the largest peak tensile force presents the increasing trend when building opening ratio of principal building increases. High turbulence intensity results in larger peak tensile forces.

For all scaffolding geometries, vertical tying pattern diminish the largest peak tensile force comparing to horizontal tying pattern.

CHAPTER VI : INTERFERENCE EFFECTS OF NEIGHBORING BUILDING ON PEAK TENSILE FORCES IN TIE MEMBERS

6.1 Introduction

Interference effects of neighboring building on peak tensile forces in tie members are going to be discussed in this chapter. Moreover, tie members mainly contribute to the horizontal stability of scaffolding and prevent scaffolding from collapse. Thus, wind induced external peak forces acting on tie members are estimated and interference factors are determined.

The largest peak tensile forces are estimated by the method introduced in Section 5.2. Experimental data for the calculation is from wind tunnel experiments which introduced in chapter four. For each case, the largest peak tensile force ($\hat{F}(\Phi_B)$) for building opening ratio Φ_B for all ties and all wind directions will be mainly discussed. In this chapter, $\hat{F}(\Phi_B)$ is the largest peak tensile force the tie which the free zone is an area of two scaffolds units, the design mean wind speed at building top , V_H=21m/s.

This section begins to discuss the interference effects of neighboring building on peak tensile forces in tie members. Interference factor (*IF*) was adopted to indicate the intensity of interference effect on the largest peak tensile force ($\hat{F}(\Phi_B)$) as follows:

$$IF = \frac{\hat{F}(\Phi_B)\text{with neighboring building}}{\hat{F}(\Phi_B)\text{without neighboring building}} \tag{6.1}$$

In this section, interference effects will be discussed based on Interference Factor (*IF*) defined in Eq. (6.1).

Before looking into the interference effect on the largest peak tensile force, some of their basic properties in the isolated situation need to be understood. Fig. 6.1 shows the largest peak tensile force distributions for the isolated condition for geometries I, L and O. Building opening ratios are 0%. For each tie member, the largest peak tensile force is chosen among all wind directions. In Fig. 6.1 (a), (b) and (c), large values are always found at the side edge of scaffolding, especially at the corners. The values for geometry O, which represents scaffolding completely enclosing the principal building, are smaller than those for geometries I and L.

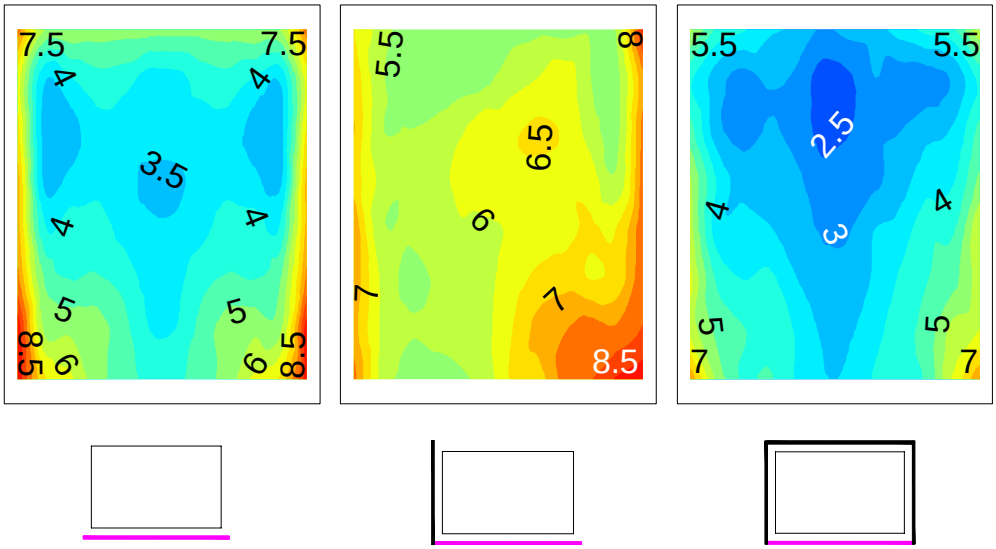

(a) Geometry I (b) Geometry L (c) Geometry O

Fig. 6.1 Largest peak tensile force distribution (among all wind directions) of isolated condition for each scaffolding geometry (unit: kN), Φ_B= 0%, U_H=21m/s.

6.2 Effects of neighboring building location

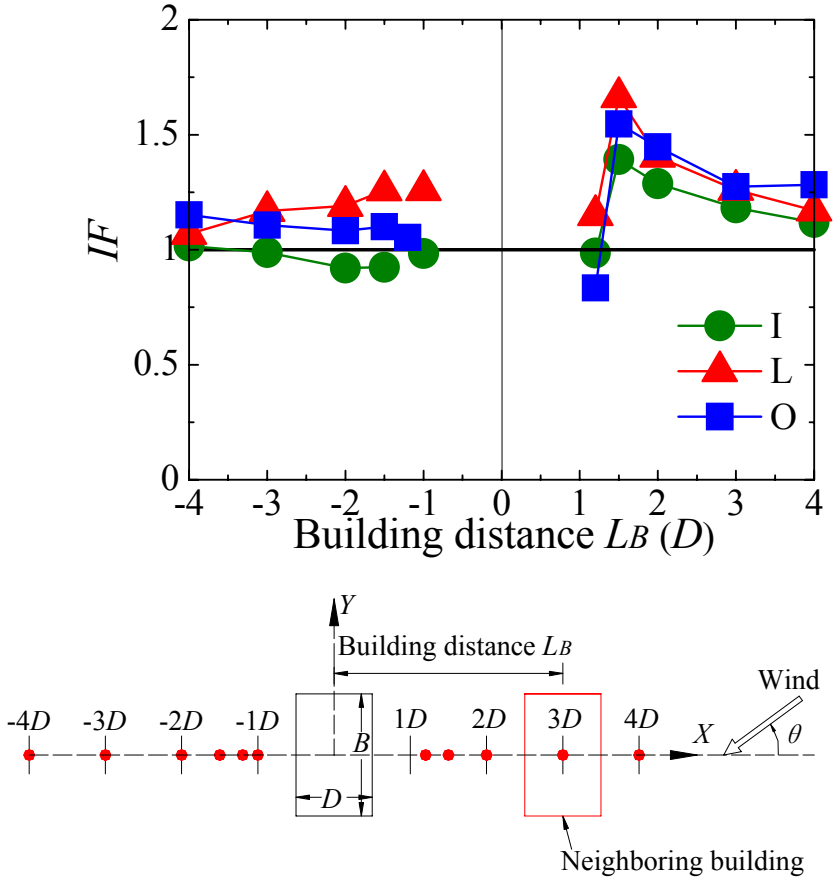

Fig. 6.2 Interference factor (*IF*) for different neighboring building locations (neighboring building is located front of scaffolding or at the rear of principal building), Φ_B= 0%, *Hr*=1.

The location of the neighboring building plays an important role in this study. As discussed, change of building distance (L_B) dramatically affects the magnitude of the largest mean panel force coefficient. Fig. 6.2 shows the interference factor (*IF*) for different neighboring building locations (neighboring building located in front of scaffolding or at the rear of the principal building). When the neighboring building is located in front of the scaffolding, the magnitudes of *IF* are larger than 1 as the building distance (L_B) varies from 1.5*D* to 4.0*D* for all scaffolding geometries. The largest *IF* is found for the neighboring building at (X,Y)=(1.5*D*, 0) for all geometries. The largest peak tensile forces ($\hat{F}$) are 39%, 55% and 66% larger than those for the isolated case for geometries I, L and O, respectively. When the neighboring building is located

further away, *IF* decreases and approaches that for the isolated case. When the neighboring building is located at the rear of the principal building, the *IF* values are larger than 1 for geometries L and O. For geometry L, the interference effect becomes weaker and *IF* becomes smaller when the building distance (L_B) increases. Conversely, *IF* becomes a little larger for geometry O.

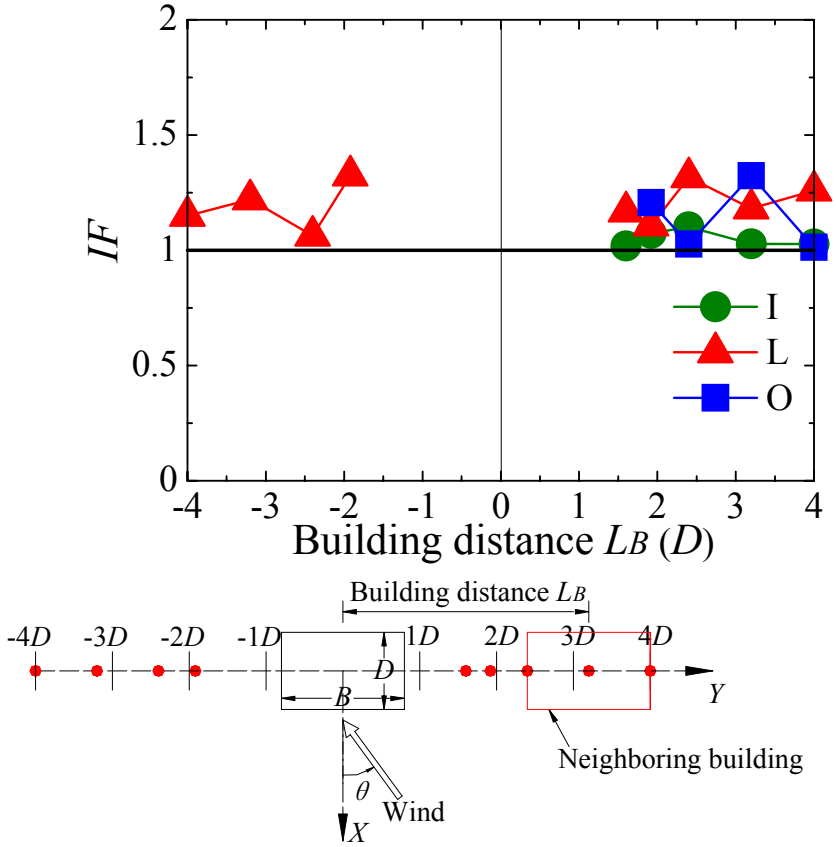

Fig. 6.3 Interference factor (*IF*) for different neighboring building locations (neighboring building located on left or right side of scaffolding), Φ_B= 0%, *Hr*=1.

Fig. 6.3 shows the interference factor (*IF*) for the neighboring building located on the left or right side of the measured scaffolding. The *IF* values are larger than 1 for all scaffolding geometries and all neighboring building locations. The largest *IF* is found to approach 1.4, which means the neighboring building causes about a 40% increment in the largest peak tensile force ($\hat{F}$). For geometry I, with an increase of building distance (L_B), *IF* changes from small to large and then back to small within a small

range around 1 to 1.1. This is different to the interference effects on the largest mean panel force coefficient (Section 4.3.2.1), where *IF* shows an alternate increasing and decreasing change tendency instead of the uniform change tendency for geometries L and O. When the neighboring building is located at the right side of the scaffolding, the wind directions causing the largest $\hat{F}$ are always around θ=90º for geometries L and O. Thus, the largest $\hat{F}$ occurs when the scaffolding is in the wake of the neighboring building. The largest $\hat{F}$ is always found at a similar position at the side edge of scaffolding for all scaffolding geometries. When the building distance (L_B) changes, $\hat{F}$ is affected by the vortex generated by the neighboring building, which is upstream.

6.3 Effects of neighboring building height ratio

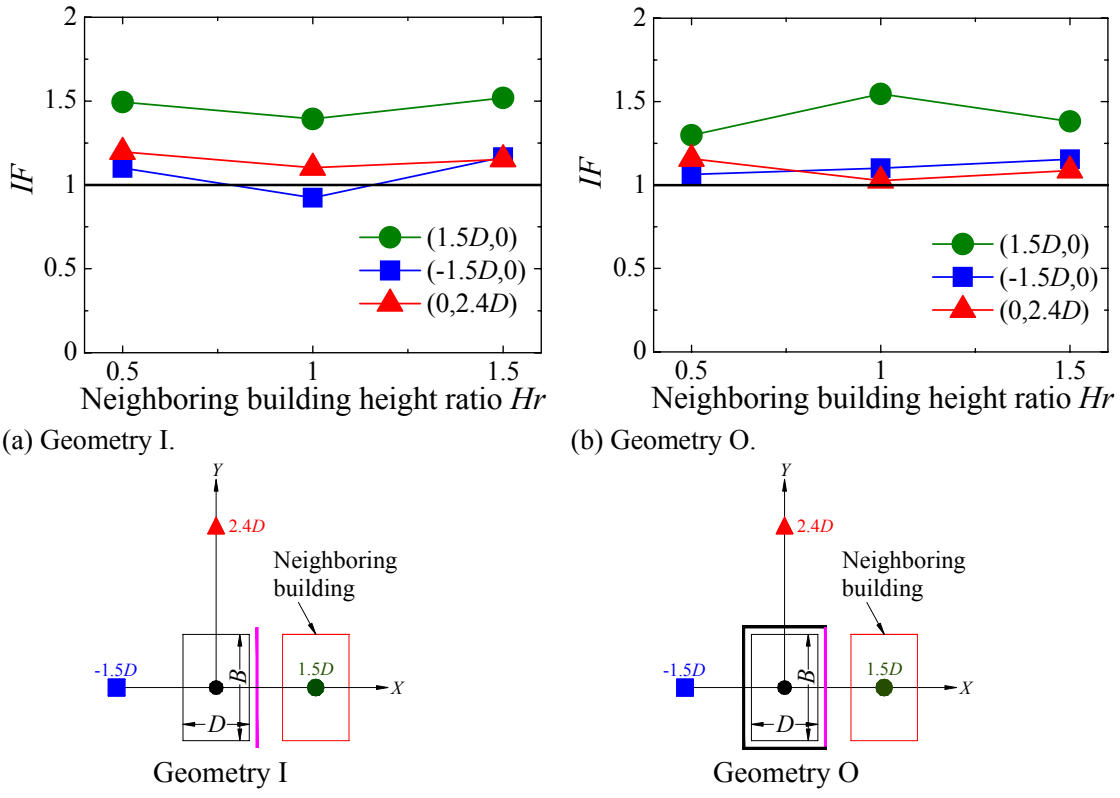

Fig. 6.4 Interference factor for different neighboring building height ratios, Φ_B= 0%.

The neighboring building can intensify the interference effects on the largest mean panel force coefficients for some experimental cases. Fig. 6.4 shows the interference factor (*IF*) for different neighboring building height ratios for geometries I and O. For geometry I, the smallest *IF* is always found when the neighboring building height ratio is 1 for all three neighboring building locations. For geometry O, the largest *IF* is found when the neighboring building height ratio is 1 for the neighboring building at (*X,Y*)=(1.5*D*, 0). Effects of neighboring building height ratio on mean panel force coefficient have been discussed in Section 4.3.2.2. The mean panel force coefficient changes a lot as the neighboring building height ratio increases. However, as shown in Fig. 6.4, the effect of the neighboring building height ratio on *IF* is not as significant as expected. Thus, the change of neighboring building height ratio does not affect the largest peak tensile force much.

6.4 Effects of principal building opening ratio

As mentioned, the building opening ratios for all isolated cases are 0%. The largest peak tensile forces for the isolated cases are the basic values for the calculation of interference factors. Fig. 6.5 shows the interference factors (*IF*) for different building opening ratios for scaffolding geometries I and O, respectively. For geometry I, *IF* increases when the building opening ratio increases from 0% to 80%, but shows little change with the increase of building opening ratio for geometry O. As discussed in Section 4.3.2.3, the effects of building opening ratio on *IF* are weak for geometry O because the scaffolding completely encloses the building. *IF* is sensitive to the building openings for geometry I because wind can flow into the gap between scaffolding and building.

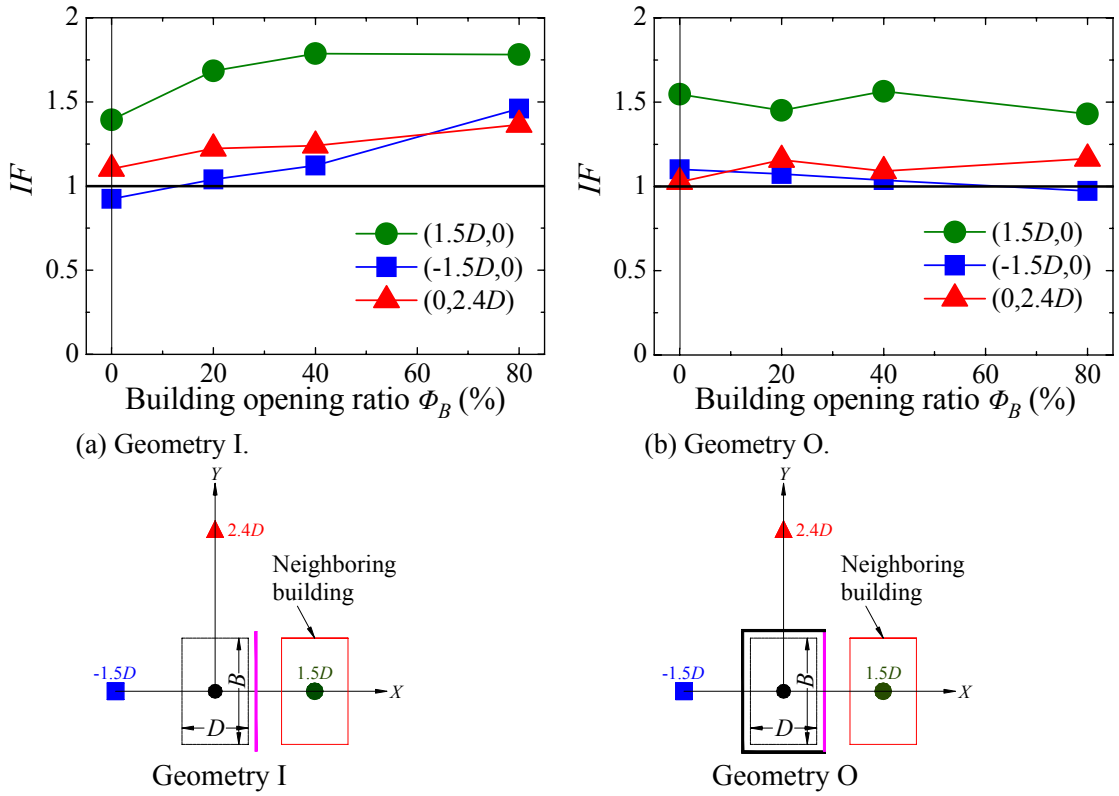

Fig. 6.5 Interference factor for different building opening ratios, *Hr*=1.

6.5 Wind direction caused the largest peak tensile force

Wind direction is also an important parameter for wind-resistant design. Wind directions causing the largest peak tensile forces are presented in Figs. 6.8 to 6.8. For isolated building cases, the wind directions causing the largest peak tensile forces are around θ=90º for geometries I and O and θ=105º for geometry L. When a neighboring building is located nearby, the wind directions causing the largest peak tensile forces are still almost parallel to the scaffolding. For most cases, the neighboring building barely affects the wind direction causing the largest peak tensile force. When the neighboring building is located in front of and close to the measured scaffolding, the wind directions cause similar change while tilting a little.

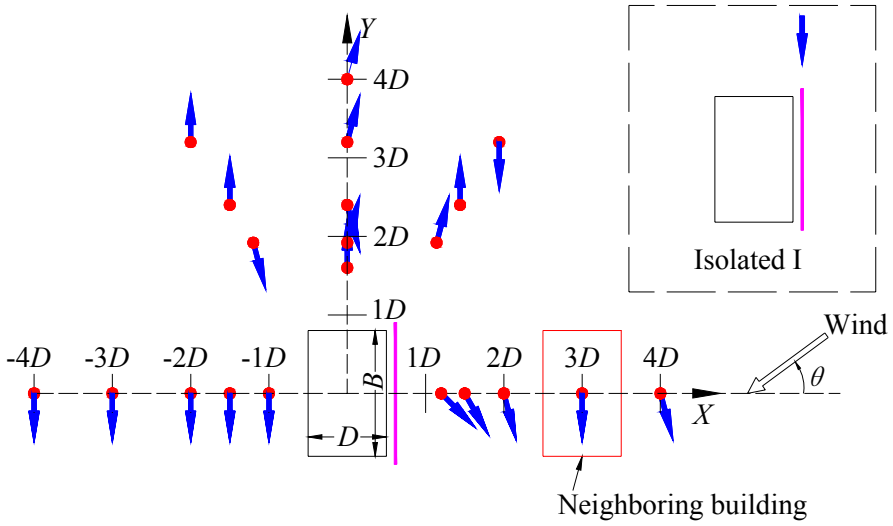

Fig. 6.6 Wind direction causing largest peak tensile force, geometry I, Φ_B= 0%, Hr=1.

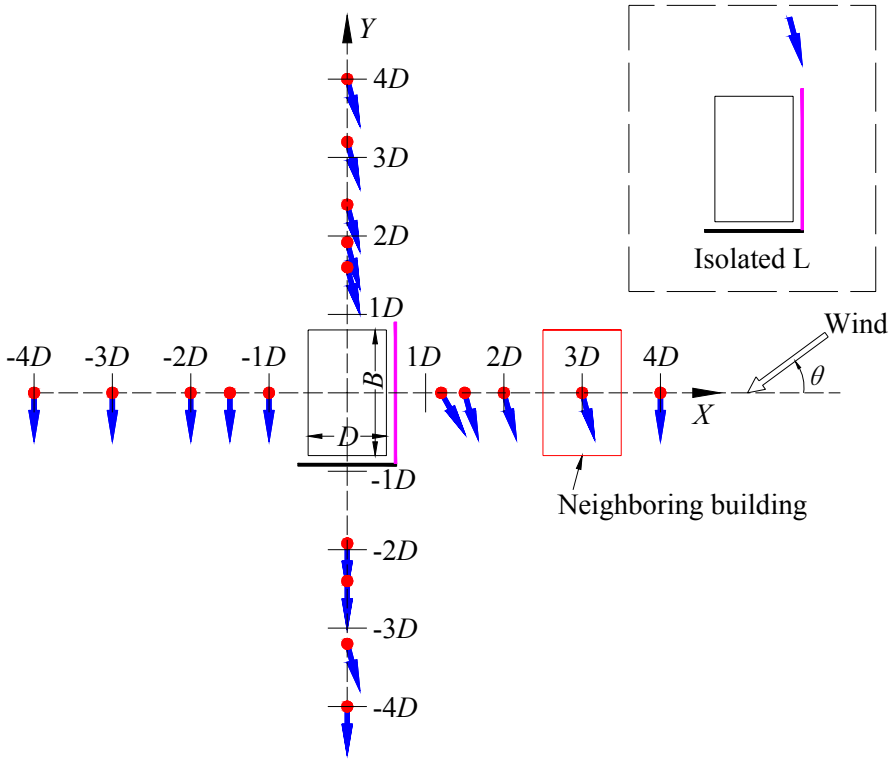

Fig. 6.7 Wind direction causing largest peak tensile force, geometry L, Φ_B= 0%, Hr=1.

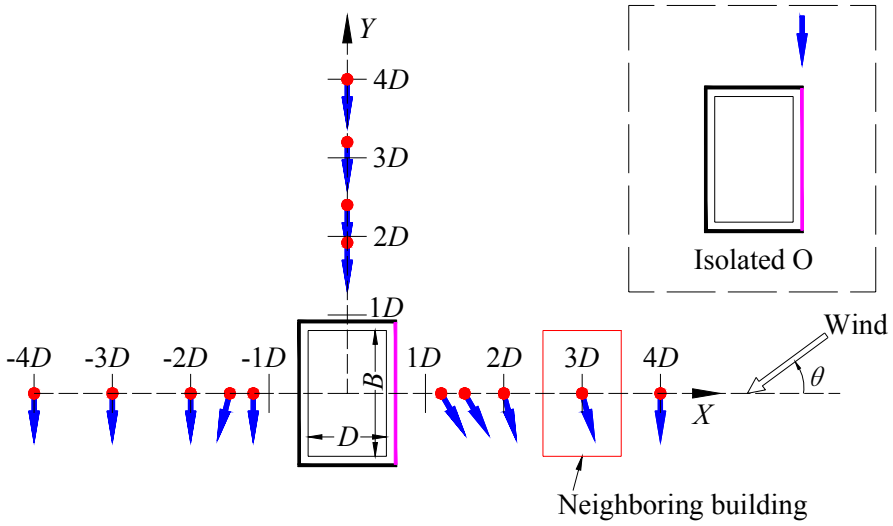

Fig. 6.8 Wind direction causing largest peak tensile force, geometry O, Φ_B= 0%, Hr=1.

6.6 Summary

For different scaffolding geometries, the largest interference factors are found when the neighboring building is located in front of the scaffolding for a building distance 1.5 times the building depth. When the neighboring building is located on the left or right side of the measured scaffolding, the interference factors are always larger than 1.

The Neighboring building has less effect on the wind direction which causing the largest peak tensile force. The height ratio of neighboring building affects the interference factor slightly. The largest peak tensile force among all tie members is usually occurs at the side edge of scaffolding.

CHAPTER VII : WIND RESISTANT DESIGN CONSIDERATIONS

In this study, Mean and area-averaged wind force coefficients for scaffolding were studied, largest peak tensile forces in tie members were estimated and interference factors were determined. Based on the wind tunnel experimental data and analyzing results, equivalent static wind load acting on scaffolding will be proposed by using the equation:

$$W = q_H \times A \times C \times G \times IF \tag{7.1}$$

where q_H is the velocity pressure at a reference height H, A is the reference area, C is aerodynamic force coefficient, G is gust loading factor and IF is the interference factor. In this chapter, the aerodynamic force coefficient, gust loading factor and interference factor will be discussed, respectively.

7.1 Aerodynamic force coefficient

Most design recommendations provide an aerodynamic force coefficient or wind force coefficient for scaffolding for wind loads calculation. Usually uniform coefficient will be given for entire scaffolding. BS EN 12811 (2003) states that the aerodynamic force coefficient for the cladding shall be assumed as 1.3 for perpendicular direction. JGJ 128 (2000) provides a shape coefficient of wind loads by considering a solidity

ratio of cladding and principal building openings. If the principal building has wall openings, the shape coefficient of wind load shall be 1.3φ, where φ is the solidity ratio of the scaffolding. For nonporous cladding, it will be 1.3.

Table 7.1 shows the largest positive and negative mean panel force coefficient for different geometries.

Table 7.1 Largest positive and negative mean panel force coefficient

Scaffolding geometry	IL	IIL	LL	UL	CL	OL	IS	IIS	LS	US	CS	OS
$C_{f,max}$	1.52	1.51	1.39	1.20	1.51	1.48	1.45	1.38	1.34	1.33	1.11	1.19
$C_{f,min}$	-1.02	-0.70	-1.57	-1.19	-1.43	-0.19	-1.00	-0.74	-1.65	-1.49	-1.08	-0.08

Mean panel force coefficients for many scaffolding geometries exceed the value of 1.3 which provided by BS EN 12811 and JGJ 128.

SCEA recommendation (Japanese Guideline) suggests shape compensation factor and position compensation factor for mean wind force coefficient for clad scaffolding. Without regard to the position compensation factor, mean panel force coefficient for the scaffolding models in this study are calculated by using the method from SCEA recommendation, which are around 1.26 and 1.3 for scaffolding model L and scaffolding model S, respectively. The position compensation factor is a kind of consideration of scaffolding geometry. SCEA recommendations provide the position compensation factor for positive and negative mean wind force coefficient separately. The position compensation factors for the positive wind force coefficients are larger than 1 and can be up to 1.31, so that the mean panel force coefficient suggested by SCEA recommendation for the scaffolding models in this study can be up to 1.7 for some area on scaffolding. However, the position compensation factors for the negative mean wind force coefficients are not larger than 1. Therefore, the negative mean panel force coefficient for the scaffolding models in this study are mostly smaller than 1.3,

also smaller than the results from wind tunnel experiment.

The aerodynamic force coefficient for scaffolding suggested by those design recommendations seems inadequate and rational increment will be needed for calculating design wind loads. Clad scaffolding is widely used in engineering constructions, a proper recommendation of aerodynamic force coefficient is needed and more safety consideration should be taken into account. Based on the data of all experimental cases, the largest positive and negative mean panel force coefficient are better to be larger than 1.6 and -1.7.

SCEA recommends area-averaged force coefficients for different scaffolding zones. Comparisons between the recommended values and experimental data were also made. Based on the experimental data, the largest positive area-averaged wind force coefficient for the top zone is 1.6 larger than the value 1.3 recommended by SCEA recommendations. The largest negative area-averaged wind force coefficients for the top zone, side zone and middle zone are -1.4, -1.9 and -1.7 larger than the values -1.3, -1.3 and -0.8 recommended by SCEA recommendations, respectively. Comparison of largest area-averaged force coefficient between experimental data and SCEA recommendations is shown in Table 7.2

Table 7.2 Comparison of largest area-averaged force coefficient between experimental data and SCEA recommendations

	Zone of scaffolding	Experimental data	SCEA recommendations
Largest positive area-averaged force coefficient	Top	1.6	1.3
	Middle	1.6	1.7
	Side	1.5	1.7
Largest negative area-averaged force coefficient	Top	-1.4	-1.3
	Middle	-1.7	-0.8
	Side	-1.9	-1.3

7.2 Gust loading factor

Peak tensile forces in tie members were estimated in this study. The gust loading factors were determined by using the following equation:

$$G = \frac{\hat{F}}{q_H \times A \times C} \tag{7.2}$$

where $\hat{F}$ is the largest peak tensile force among all tie members, which estimated by pressure integration method in Chapter Five. The reference areas are 2 scaffold units, 4 scaffold units and 6 scaffold units and the design wind speed at the reference height (building top) is 21m/s. The aerodynamic force coefficient for entire scaffolding is 1.7 which is the largest value from the experimental data.

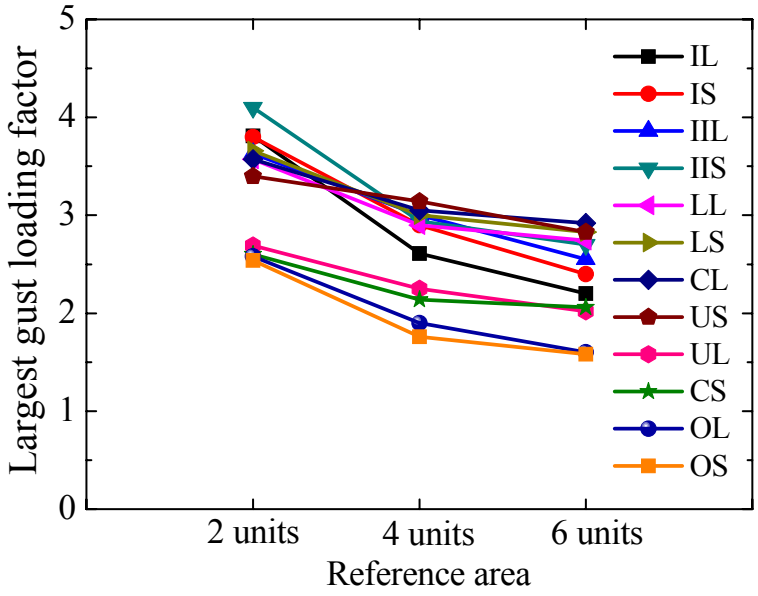

Fig. 7.1 Largest gust loading factor for different scaffolding geometries and reference areas.

For each scaffolding geometry, the largest gust loading factor is picked out among all wind directions and all building opening ratios as shown in Fig. 7.1. The largest gust loading factors for 2 scaffold units are always larger than for 4 and 6 scaffold units. The largest gust loading factor tends to be smaller when the reference area increases.

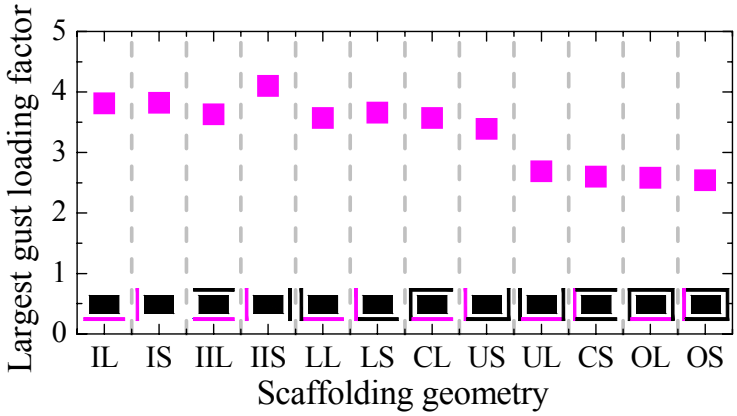

Fig. 7.2 Largest gust loading factor for different scaffolding geometries.

Fig. 7.2 shows the largest gust loading factor among all wind directions, all building opening ratios and all reference areas for different scaffolding geometry. As discussed in Fig. 7.1, the largest gust loading factors are always found for the reference area of 2 scaffold units. The largest value of all is 4.1 which is found for geometry IIS. The values for geometries UL, CS, OL and OS are quite small compare to other geometries, which are around 2.5~2.7. Geometries UL, CS, OL and OS have the same feature that both two side edges of the measured scaffolding are covered by the scaffolding placed at the adjacent building sides.

7.3 Interference factor

Interference effects of neighboring building on peak tensile forces in ties were studied, interference factors were determined (Chapter Six). For wind-resistant design consideration, the peak tensile forces in tie members should including interference effects by multiplying the interference factor (*IF*).The distributions of interference factors are shown in Fig 7.3, 7.4 and 7.5. The numbers nearby the dots are the values of *IF*.

Detailed interference effects were discussed in Chapter Four and Chapter Six.

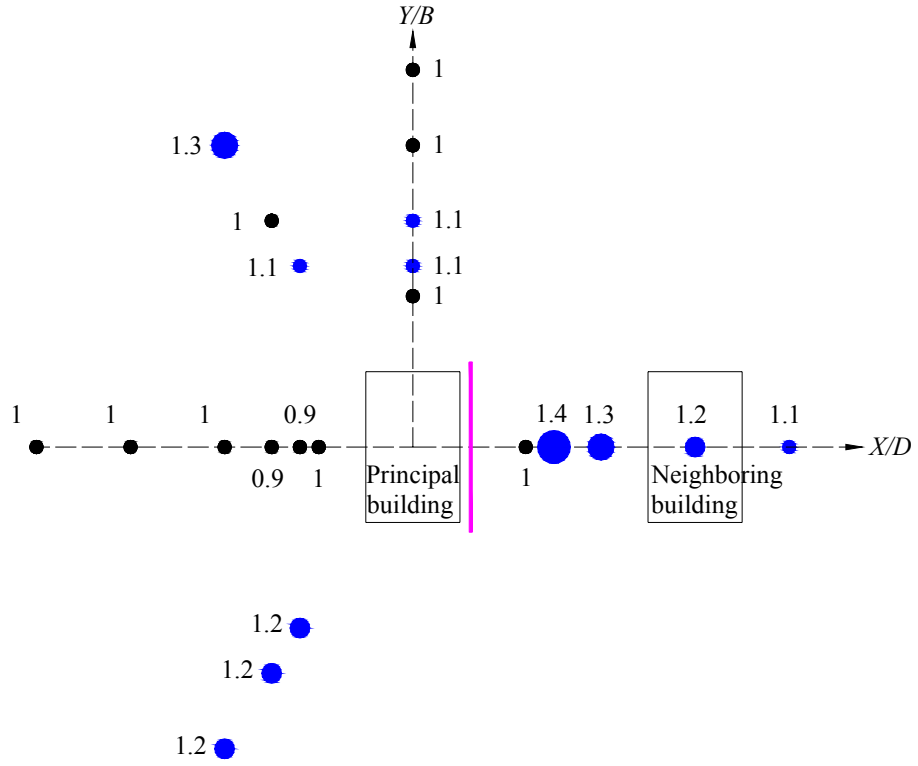

Fig. 7.3 Distributions of interference factors, geometry I.

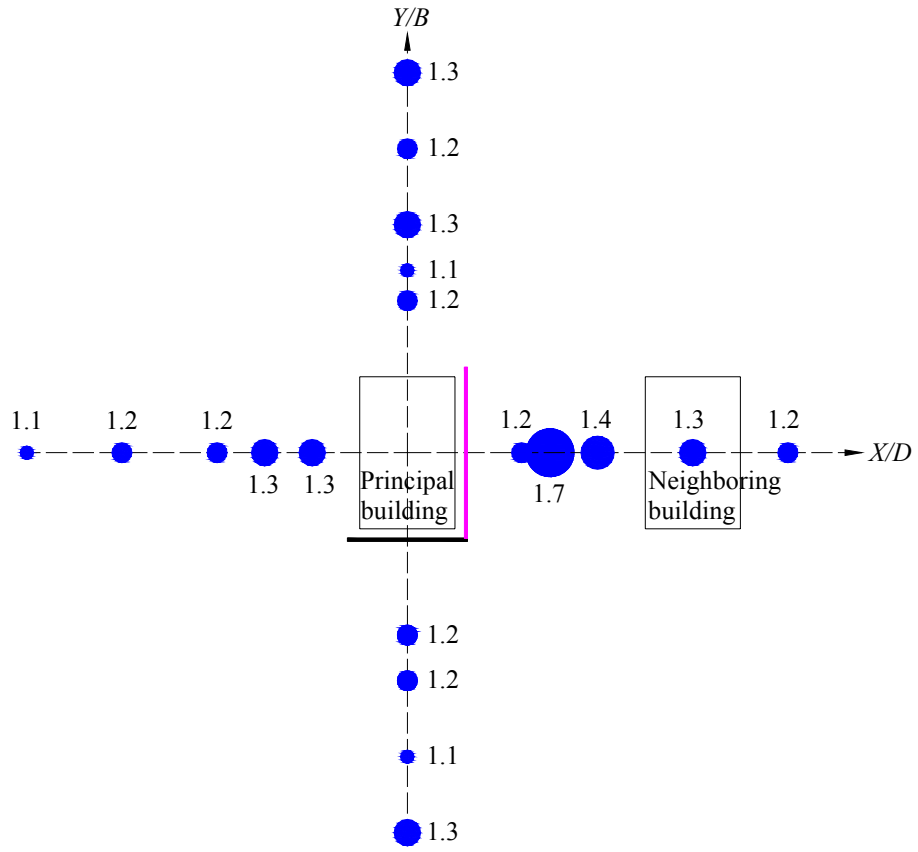

Fig. 7.4 Distributions of interference factors, geometry L.

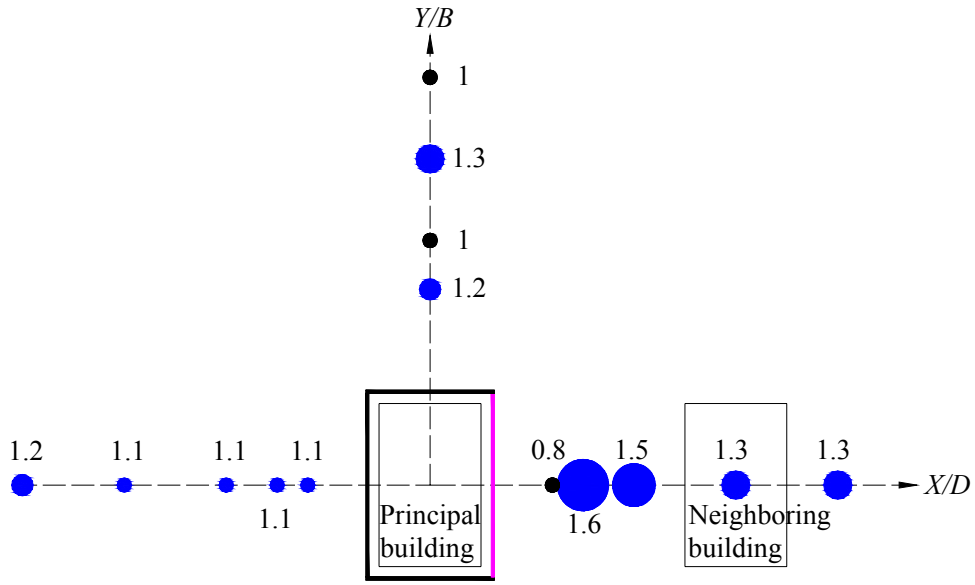

Fig. 7.5 Distributions of interference factors, geometry O.

CHAPTER VIII : CONCLUSIONS

A detailed and comprehensive study of aerodynamic characteristics of scaffolding with nonporous cladding has been carried out. The main objective of this dissertation was to wind loads acting on clad scaffolding and the interference effects of neighboring building on scaffolding. Extensive wind tunnel experiments have been conducted to measure wind pressures acting on scaffolding. Effects of building opening, scaffolding geometry, wind direction and turbulence intensity were investigated. Neighboring building induced interference effects on scaffolding were studied which never been discussed before. Base on experimental data and analytical results, comparisons with related design recommendations were made and wind-resistant design considerations were proposed.

(1)Building openings have almost no effect on pressures on the outer surfaces of scaffolding. However, wind pressures on the inner surfaces of scaffolding play an important role in wind loads on clad scaffolding. For most scaffolding geometries, the largest positive local peak net pressures tend to become smaller and the largest negative local peak net pressures tend to become larger when building building opening ratio increases. When scaffolding is placed on one or two sides of the building, local peak net pressures on the scaffolding are more sensitive to change of building openings.

(2)For each scaffolding geometry, the largest local peak net pressure coefficient

usually occurs in the upper region or side edge of scaffolding. The magnitude of both positive and negative peak pressures tend to be smaller when scaffolding is placed on more building sides, because they may interfere with each other. When scaffolding completely encloses the building, the negative mean and area-averaged wind force coefficients are quite small.

(3)The neighboring building has significant effects on wind loads acting on scaffolding. The negative force coefficients are larger when the neighboring building is located in front of scaffolding, and the shielding effects on positive force coefficients are significantly. When the neighboring building is located at left or right side of scaffolding, the positive force coefficients are greater than the isolated cases. When the neighboring building is adjoining with the principal building, both the positive and negative force coefficients are not larger than the isolated cases. The increment of the height ratio of neighboring building can intensifies the interference effects that continuous increasing or decreasing wind loads on scaffolding.

(4)The peak tensile forces acting on scaffolding were calculated in this study. Compare to building openings, scaffolding geometry has more remarkable effects on the peak tensile forces. IF both two sides of scaffolding are free (not connecting to other scaffolding which is placing at adjacent building sides), peak tensile force is the largest when the free zone of tie is quite small. When only one side of scaffolding is free, peak tensile force for a larger area is the greatest. When both two sides of scaffolding connecting to the scaffolding which located at adjacent building sides, peak tensile forces in ties are smaller than for other scaffolding geometries. For most scaffolding geometries, the largest peak tensile force presents the increasing trend when building opening ratio of principal building increases. High turbulence intensity results in larger peak tensile forces. For all scaffolding geometries, vertical tying pattern diminish the largest peak tensile force comparing to horizontal tying pattern. For different

scaffolding geometries, the largest interference factors are found when the neighboring building is located in front of scaffolding. Neighboring building has almost no effect on the wind direction which caused the largest peak tensile force. The height ratio of neighboring building affects the interference factor slightly. The largest peak tensile force among all tie members is usually occurs at the side edge of scaffolding.

(5) Based on the data of all experimental cases, the largest mean panel force coefficient is 1.7 which is larger than 1.3 recommended by BS EN 12811 and JGJ 128. In this study, the largest positive area-averaged wind force coefficient for the top zone is 1.6 larger than the value 1.3 recommended by SCEA recommendations. The largest negative area-averaged wind force coefficients for the top zone, side zone and middle zone are -1.4, -1.9 and -1.7 larger than the values -1.3, -1.3 and -0.8 recommended by SCEA recommendations, respectively.

(6) Wind-resistant design considerations are discussed in chapter seven, equivalent static wind load acting on scaffolding is proposed. Aerodynamic force coefficient, gust loading factor and interference factor are investigated. If the scaffolding is covered with nonporous cladding or high solidity ratio cladding, the tying pattern is better to be continuous vertical tying pattern rather than continuous horizontal tying pattern.

REFERENCES

[1] British Standards Institution, BS EN 12811-1, Temporary Works Equipment – Part 1: Scaffolds – Performance Requirements and General Design, 2003.

[2] Scaffolding and Construction Equipment Association of Japan, Safety technical guideline for scaffolding to wind loads (in Japanese), 1999.

[3] The Ministry of Construction of People's Republic of China, JGJ 128, Safety and technical code for frame scaffolding with steel tubules in construction (in Chinese), 2000.

[4] Ohdo, K., Takanashi, S., Hino, Y., Saito, K., Measurement of wind load acting on the scaffolds, Specific Research Reports of the National Institute of Industrial Safety, NIIS-SRR-NO.31(in Japanese), 2005.

[5] Yue, F., Yuan, Y., Li, G.Q., Ye, K.M., Chen, Z.M., Wang, Z.P., Wind Load on Integral-Lift Scaffolds for Tall Building Construction, Journal of Structural Engineering 131, 816-824, 2005.

[6] Charuvisit, S., Hino, Y., Ohdo, K., Maruta, E., Kanda, M., Wind tunnel experiment on wind pressures acting on the scaffolds in strong winds, Journal of Wind Engineering, JAWE 32, 1-10, 2007.

[7] Hino, Y., Phongkumsing, S., Study on the Estimation Method of Wind Pressure Acting on the temporary Scaffolds, Specific Research Reports of the National Institute of Industrial Safety, NIIS-SRR-NO.31(in Japanese), 2005.

[8] Irtaza, H., Beale, R.G., Godley, M.H.R., A wind-tunnel investigation into the pressure distribution around sheet-clad scaffolds, Journal of Wind Engineering and Industrial Aerodynamics 103, 86-95, 2012.

[9] Feng Wang, Yukio Tamura, Akihito Yoshida, Wind loads on clad scaffolding with different arrangements and building opening ratios, Journal of Wind Engineering and Industrial Aerodynamics, 120, 37–50, 2013.

[10] Maurizio Orlando, Wind-induced interference effects on two adjacent cooling towers,Engineering Structures, 23,979–992, 2001.

[11] Z. N. Xie, M. Gu, Simplified formulas for evaluation of wind-induced

interference effects among three tall buildings, Journal of Wind Engineering and Industrial Aerodynamics, 95, 31–52, 2007.

[12] K.M. Lam, M.Y. H. Leung, J.G. Zhao, Interference effects on wind loading of a row of closely spaced tall buildings, Journal of Wind Engineering and Industrial Aerodynamics, 96, 562–583, 2008.

[13] Wonsul Kim, Yukio Tamura, Akihito Yoshida, Interference effects on local peak pressures between two buildings, Journal of Wind Engineering and Industrial Aerodynamics, 99, 584–600,2011.

[14] Yi Hui, Yukio Tamura, Akihito Yoshida, Mutual interference effects between two high-rise building models with different shapes on local peak pressure coefficients, Journal of Wind Engineering and Industrial Aerodynamics, 104-106, 98–108, 2012.

[15] Architectural Institute of Japan (AIJ 2004). Chapter 6: Wind Loads, Recommendations for Loads on Buildings, 2004.

[16] Irwin, H.P.A.H., Cooper, K.R., Girard, R., Correction of distortion effects caused by tubing systems in measurements of fluctuating pressures. Journal of Wind Engineering and Industrial Aerodynamics 5, 93–107, 1979.

[17] T. V. Lawson, The design of cladding, Building and Environment 11, 37-38, 1976.

[18] Holmes, J.D., Equivalent time averaging in wind engineering. Journal of Wind Engineering and Industrial Aerodynamics 72, 411–419, 1997.

[19] Cook, N.J., Mayne, J.R., A refined working approach to the assessment of wind loads for equivalent static design. Journal of Wind Engineering and Industrial Aerodynamics 6, 125–137, 1979.

[20] British Standards Institution, BS EN 12810-1, Façade scaffolds made of prefabricated components – Part 1: Products specifications, 2003.

[21] The Ministry of Construction of People's Republic of China, JGJ 130, Technical code for safety of steel tubular scaffold with couplers in construction (in Chinese), 2011.

[22] Japan International Center for Occupational Safety and Health, Ordinance on Industrial Safety and Health (in Japanese), 2007.

[23] Daved T. Sandwell, Biharmonic spline interpolation of GEOS-3 and Seasat altimeter data, Geophysical research letters 14, 139-142, 1987.

[24] Yi Hui, Interference effects on local peak pressures between two highrise buildings—considering square and rectangular shapes. Ph.D. thesis, Tokyo Polytechnic University, 2012.

[25] Demetres Briassoulis, Antonis Mistriotis, Anastasios Giannoulis, Wind forces on porous elevated panels, Journal of Wind Engineering and Industrial Aerodynamics 98, 919–928, 2010.

[26] Li Guoqiang,Yue Feng,Yuan Yong,Ye Kemin,Research on wind-induced vibration coefficient of self-climbing scaffold attached to tall buildings in construction, Earthquake Engineering and Engineering vibration 24, 62-67, 2004.

[27] J. L. Peng, A. D. Pan, D. V. Rosowsky, W. F. Chen, T. Yen, S. L. Chan, High clearance scaffold systems during construction I-Structural modelling and modes of failure, Engineering Structures 18, 247-257, 1996.

[28] J. L. Peng, A. D. Pan, D. V. Rosowsky, W. F. Chen, T. Yen, S. L. Chan, High clearance scaffold systems during construction II- Structural analysis and development of design guidelines, Engineering Structures 18, 258-267, 1996.

[29] British Standards Institution, BS EN 12811-2, Temporary Works Equipment – Part 2: Information and materials, 2004.

[30] British Standards Institution, BS EN 12811-3, Temporary Works Equipment – Part 3: Load testing, 2002.

[31] British Standards Institution, BS EN 12810-2, Façade scaffolds made of prefabricated components – Part 2: Particular methods of structural design, 2003.

[32] American Society of Civil Engineers, ASCE-37, Design loads on structures during construction, 2002

[33] YUE Feng, YUAN Yong, LI Guo-qiang, YE Ke-ming, Wind Tunnel Test on the Self-climbing Scaffold Attached to Tall Buildings in Construction, Journal of Tongji University 29, 1220-1224 (in Chinese), 2001.

[34] Yue Feng, Li Guoqiang, yuan Yong, Ye keming, Calculation of winf load on self-climbing scaffold in high-rise building construction (part 1), Architecture Technology 35, 590-593 (in Chinese), 2004.

[35] Yue Feng, Li Guoqiang, yuan Yong, Ye keming, Calculation of winf load on self-climbing scaffold in high-rise building construction (part 2), Architecture Technology 35, 696-5698 (in Chinese), 2004.

[36] Ohdo, K., Hino Y., Phongkumsing, S., Hazard Evaluation of scaffolds againt wind loads using construction-environmental-simulator wind tunnel, Specific Research Reports of the National Institute of Industrial Safety, NIIS-SRR-NO.26(in Japanese), 2002.

[37] Katsutoshi Ohdo, Ahsan Kareem, Yozo Fujino, Study on wind induced accidents of civil structures during construction, Journal of Wind Engineering 81, 59-70 (in Japanese), 1999.

[38] 吉田 正邦， 真田 早敏，本郷 刚，中村 修，建設足場に設置された養生シートおよび防音パネルに作用する風荷重に関する実験的研究，日本建築学会大会学術講演梗概集，1980.